## General Disclaimer

## One or more of the Following Statements may affect this Document

- This document has been reproduced from the best copy furnished by the organizational source. It is being released in the interest of making available as much information as possible.

- This document may contain data, which exceeds the sheet parameters. It was furnished in this condition by the organizational source and is the best copy available.

- This document may contain tone-on-tone or color graphs, charts and/or pictures, which have been reproduced in black and white.

- This document is paginated as submitted by the original source.

- Portions of this document are not fully legible due to the historical nature of some of the material. However, it is the best reproduction available from the original submission.

Produced by the NASA Center for Aerospace Information (CASI)

NASA [redacted]

E7.6-10191
[redacted]
TMX-72961

"Made available under NASA sponsorship
in the interest of early and wide dissemination of Earth Resources Survey
Program information and without liability
for any use made thereof."

(E76-10191) OCEAN PROPERTIES Final Report N76-18612
(NASA) 98 p HC $5.00 CSCL 08J

Unclas
G3/43 00191

# FINAL REPORT FOR SKYLAB INVESTIGATION

## EPN 586 - OCEAN PROPERTIES

Principal Investigator:

C. Laurence Korb
Goddard Space Flight Center
Greenbelt, Maryland 20771

Co-Investigator

John F. Potter
Lockheed Electronic Corporatio
Houston, Texas

## Introduction

This report is divided into two major sections. The first section considers in some detail the problem of atmospheric interference on remotely sensed data. A program is described which allows the effects of atmospheric absorption and emission by carbon dioxide, water vapor, methane, nitrous oxide, carbon monoxide, and ozone to be determined so that correction techniques can be devised. The program covers the spectral region from 0.69 to 20μm and divides the atmosphere into up to thirty layers of equal optical mass. The theory needed to understand the program, the program description and operating instructions, and comparisons to test data are given in the first section of this report. A complete description of the program including a program listing, input card formats and sample data runs, and samples of the data used in the program are given in Appendix A of this report.

The second section of this report gives an analysis of ocean truth data and subsequent laboratory analyses which were performed in support of this study. Unfortunately, a coordinated analysis of Skylab acquired data could not be performed with associated ocean truth data as was planned

for our two different test sites. For test site 1 which was located in the Eastern Atlantic Ocean adjacent to the northwest coast of Africa the ocean truth data for this investigation was to be acquired and supplied to us by the Principal Investigator of EPN 518. Unfortunately, due to the shifting track of the Skylab spacecraft, EPN 518 was unable to acquire ocean truth in conjunction with a Skylab overpass and, thus, EPN 518 was unable to supply our investigation with the required ocean truth data. The second test site for this investigation was located in the Gulf of Mexico in the near coastal waters off the coast of Freeport, Texas. The actual location of this site shifted during the course of Skylab from the coastal waters of Freeport, Texas to those of Matagorda Bay, Texas, and finally to the offshore waters off the coast of Matagorda Bay, Texas. A total of four ocean truth expeditions were conducted beneath the Skylab spacetrack on 5/31/73, 6/5/73, 8/8/73, and finally on 9/16/73. Of these four expeditions, Skylab acquired data on only two occasions, namely 6/5/73 and 8/8/73. Of these two data sets, the data on 6/5/73 was badly contaminated by solar glitter[+], and the data from 8/8/73 was contaminated by approximately 95% cloud cover. Thus, since no Skylab data could be acquired with the required concomitant ocean truth data, the results of section two of this report are limited to a presentation and analysis of the ocean truth data obtained.

---

[+]The solar elevation angle on 6/5/73 was 82° and the maximum solar elevation angle required by the Investigation Requirement Document was 65°.

# ATMOSPHERE TRANSMISSION COMPUTER PROGRAM CP[1]

By D. E. Pitts, T. L. Barnett, C. L. Korb,
Walter Hanby,* and Alyce E. Dillinger*
Lyndon B. Johnson Space Center

## SUMMARY

All Earth resources remote-sensing techniques are affected, to some degree, by the atmosphere lying between the sensor and the test site. The computer program described herein allows the effects of atmospheric absorption and emission by carbon dioxide, water vapor, methane, nitrous oxide, carbon monoxide, and ozone to be assessed so that correction techniques can be devised and tables for atmospheric correction algorithms can be calculated. The absence of carbon monoxide data on the data tape, however, limits calculations to the remaining five gases. The program incorporates data from wavelengths of 0.69 to approximately 20 micrometers, generated by R. Calfee of the National Oceanic and Atmospheric Administration, but can incorporate other line-by-line data in the proper format. The atmosphere is divided into layers ($\leq 30$), each of equal mass, and is defined by significant levels of either radiosonde data or a model atmosphere. Both upwelling and downwelling emissions are calculated to enable simulation of both terrestrial and spaceborne measurements. The program is designed so that punched cards can be produced for use in other computer programs. Sample runs for both radiosonde data and laboratory data are provided in the appendixes.

## INTRODUCTION

The objectives of the NASA Earth Observations Program are to determine the performance capabilities of various sensors, to identify signature criteria of resources, to develop new sensors and systems, to devise analysis systems and procedures, and to demonstrate applications using these tools. The laboratory usually affords the best testing environment for a sensor, but the type of target, the conditions of the signal path, and other testing parameters are limited. Because the laboratory environment is usually restrictive, a successful laboratory test of the sensor is necessary but not sufficient to ensure proper operation of the sensor in the real environment. Therefore, much of the testing is performed in an environment that duplicates the conditions under which the instrument is expected to operate. The success of the testing under such conditions requires that the data concerning the environment between the instrument platform and the test site be as accurate as possible.

---

[1]This report was produced under Skylab EREP contracts EPN-582, 584, & 586.
*Lockheed Electronics Company, Inc.

The magnitude of the effect on the signal caused by interaction between the atmosphere and the signal depends on the type of sensor used, the wavelength employed, and the meteorological conditions prevailing at the time of the measurement. Furthermore, the atmosphere can cause large deleterious effects in some analysis systems (e.g., maximum-likelihood pattern recognition computer programs); thus, the analysis system as well as the sensor and electronics must be evaluated. Therefore, the output from the CP computer program has been arranged so that punched cards can be produced for use in other computer programs to predict the effect of the atmosphere or to correct the data for atmospheric effects for a data collection and analysis system.

The computer program described herein allows the calculation of atmospheric transmission due to carbon dioxide, water vapor, methane, nitrous oxide, ozone, and carbon monoxide. Because no data exist on the data tape for the last of these, however, carbon monoxide calculations are precluded. The program incorporates data from wavelengths of 0.69 to approximately 20 micrometers but can incorporate other line-by-line data in the proper format.

Appreciation is expressed to Dr. R. F. Calfee, who assisted the authors in using his model and data, and to David Anding, who kindly ran his band model for the Salem, Illinois, test case.

## SYMBOLS

**A** full width at half maximum for triangular slit function, $cm^{-1}$

**BOUND** distance from a line at which the wings of the line must be considered (usually approximately 12 $cm^{-1}$), $cm^{-1}$

**$C_1$, $C_2$** constants determined from the boundary conditions

**CAYBUR** dummy variable

**CONN** $= \frac{-M*g}{RO}$

**c** speed of light, $3.0 \times 10^{10}$ cm/sec

**DELV** the increment in $cm^{-1}$ for calculations of upwelling and downwelling intensity, $\leq \frac{A}{2}$; also distance the center of triangular slit is moved to make the next intensity calculation.

**DV** integration step within the triangular slit, $cm^{-1}$

$E_n(x)$ Kourganoff function, $\int_0^1 \mu^{n-2} e^{-x/\mu} d\mu$

$E''$ lower rotational energy level of the transition, $cm^{-1}$

$g$ acceleration due to gravity

$I_{b\nu}(T)$ black-body monochromatic intensity at $T$ and $\nu$, $W/(cm^2 \cdot sr \cdot \mu m)$

$I_{0\nu}$ monochromatic intensity of Sun or other source, $W/(cm^2 \cdot sr \cdot \mu m)$

$I_\nu^+(\tau_\nu, \mu)$ monochromatic upward-welling radiation (intensity or radiance), $W/(cm^2 \cdot sr \cdot \mu m)$

$I_\nu^-(\tau_\nu, \mu)$ monochromatic downward-welling radiation (intensity or radiance), $W/(cm^2 \cdot sr \cdot \mu m)$

$\bar{I}_{\nu_0}$ degraded intensity, $W/(cm^2 \cdot sr \cdot \mu m)$, averaged over frequency

$i$ atmospheric layer index

$J$ dummy variable representing atmospheric layers

$K_\nu$ monochromatic mass absorption coefficient, $(molecules/cm^2)^{-1}$

$$K_0 = \frac{S}{\alpha_d}\sqrt{\frac{\ln 2}{\pi}}$$

$k$ Boltzmann constant

$\ell$ number of integration steps from $\nu_1 - A$ to $\nu_1 + A$, which is equal to $\frac{2A}{DV}$

$M$ mass of molecule, g

$M^*$ molecular weight of the atmosphere, $g/(g \cdot mole)$

$m$ one interval in frequency

| | |
|---|---|
| NN | number of equal-mass layers in the atmosphere |
| n | monochromatic refractive index of the atmosphere |
| P | atmospheric pressure, atm |
| $P_i$ | ambient atmospheric pressure for layer i, atm |
| $P_0$ | 1 atmosphere pressure, atm (101 325 $N/m^2$, 1013.25 mbar) |
| R | radius of planet |
| RO | universal gas constant based on the carbon-12 atomic weight scale in ergs/(K g·mole) |
| r | variable factor in equation (19), exponent which is a function of the molecular species |
| S | line intensity at P and T, $cm^{-1}/(molecule \cdot cm^{-2})$ |
| $S_0$ | line intensity at $T_0$ and $P_0$: $cm^{-1}/(g \cdot cm^{-2})$ for water and $cm^{-1}/(molecule \cdot cm)$ for carbon dioxide and other gases |
| SAY | dummy variable |
| T | temperature of the atmosphere as a function of z, K |
| $T_0$ | base temperature for spectral lines = 296 K for Calfee data |
| $T_1$ | temperature of the target, K |
| $T_i$ | transmission for ith layer |
| $T_{i,mono}$ | transmission for all line-by-line calculations |
| t | dummy variable of optical depth |
| U | optical mass, $\int_0^z \rho(z)dz$, molecules/$cm^2$ |
| $U_i$ | water-vapor optical mass, molecules/$cm^2$ |
| $Wl_i$ | water-vapor partial pressure, atm |

$E_n(x)$ Kourganoff function, $\int_0^1 \mu^{n-2} e^{-x/\mu} d\mu$

$E''$ lower rotational energy level of the transition, $cm^{-1}$

$g$ acceleration due to gravity

$I_{b\nu}(T)$ black-body monochromatic intensity at $T$ and $\nu$, $W/(cm^2 \cdot sr \cdot \mu m)$

$I_{0\nu}$ monochromatic intensity of Sun or other source, $W/(cm^2 \cdot sr \cdot \mu m)$

$I_\nu^+(\tau_\nu, \mu)$ monochromatic upward-welling radiation (intensity or radiance), $W/(cm^2 \cdot sr \cdot \mu m)$

$I_\nu^-(\tau_\nu, \mu)$ monochromatic downward-welling radiation (intensity or radiance), $W/(cm^2 \cdot sr \cdot \mu m)$

$\bar{I}_{\nu_0}$ degraded intensity, $W/(cm^2 \cdot sr \cdot \mu m)$, averaged over frequency

$i$ atmospheric layer index

$j$ dummy variable representing atmospheric layers

$K_\nu$ monochromatic mass absorption coefficient, $(molecules/cm^2)^{-1}$

$$K_0 = \frac{S}{\alpha_d}\sqrt{\frac{\ln 2}{\pi}}$$

$k$ Boltzmann constant

$\ell$ number of integration steps from $\nu_1 - A$ to $\nu_1 + A$, which is equal to $\frac{2A}{DV}$

$M$ mass of molecule, g

$M^*$ molecular weight of the atmosphere, $g/(g \cdot mole)$

$m$ one interval in frequency

$W_d$ weighting function for downwelling intensity (unitless), derivative of transmission with respect to altitude times $\Delta z_i$

$W_u$ weighting function for upwelling intensity (unitless), derivative of transmission with respect to altitude times $\Delta z_i$

$w$ variable factor in equation (18)

$$X = \left| \frac{\nu - \nu_0 \sqrt{\ln 2}}{\alpha_d} \right|$$

$$x = -(t - \tau)$$

$$Y = \frac{\alpha_0 P}{\alpha_d P_0} \sqrt{\ln 2}$$

$z$ altitude, cm

$\alpha$ Lorentz half width at $P$ and $T$, $cm^{-1}$

$$\alpha_d = \nu_0 \sqrt{\frac{2kT \ln 2}{Mc^2}}$$

$\alpha_0$ Lorentz half width at $T_0$ and $P_0$, $cm^{-1}$

$\Delta z_i$ height of atmospheric layer $i$

$\Delta \mu_1$ zenith extent of Sun or other source

$\Delta \phi_1$ azimuthal extent of Sun or other source

$\bar{\varepsilon}$ gray-body emissivity assumed between $\nu_1$ and $\nu_2$

$\varepsilon_\nu$ monochromatic emissivity of target

$\theta$ zenith angle, rad

$\mu$ cos $\theta$ (unitless)

$\mu_1$ position of Sun or other source (unitless)

| | |
|---|---|
| $\mu_i$ | cos $\theta_i$, where $\theta_i$ = angle through ith layer |
| $\nu$ | frequency, $cm^{-1}$ |
| $\nu_0$ | frequency of line center, $cm^{-1}$ |
| $\nu_1$ | frequency at beginning of calculation interval, $cm^{-1}$ |
| $\nu_2$ | frequency at end of calculation interval, $cm^{-1}$ |
| $\rho$ | constituent gas density as a function of z, molecules/$cm^3$ |
| $\rho_\nu$ | monochromatic reflectivity of target |
| $\sigma(\nu)$ | normalized instrument function |
| $\sigma^*(\nu)$ | triangular instrument function |
| $\tau_{0\nu}$ | monochromatic optical depth of the entire atmosphere (dimensionless) |
| $\tau_\nu$ | monochromatic optical depth, $\int_0^z K_\nu \rho \, dz$ (dimensionless) |
| $\phi$ | azimuthal angle, rad |
| $\phi_1$ | azimuthal angle of Sun or other source, rad |
| $\Omega$ | plateau function |

## THEORY

In many remote-sensing applications through the Earth atmosphere in which scattering is not an important phenomenon and local thermodynamic equilibrium can be approximated because of the lack of rapid chemical reactions, the equations for radiative heat transfer can be written in the manner of Love (ref. 1), as indicated by the following equations and diagram.

$$\mu \frac{dI_\nu^+(\tau_\nu,\mu)}{d\tau_\nu} = -I_\nu^+(\tau_\nu,\mu) + n^2 I_{b\nu}(T) \tag{1}$$

$$-\mu \frac{dI_\nu^-(\tau_\nu,\mu)}{d\tau_\nu} = -I_\nu^-(\tau_\nu,\mu) + n^2 I_{b\nu}(T) \tag{2}$$

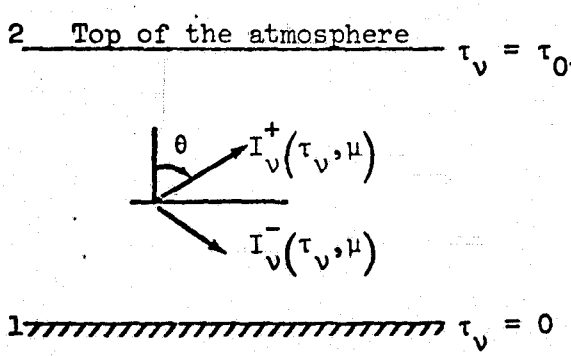


where $\mu = \cos\theta$

$\theta$ = zenith angle

$I_\nu^+(\tau_\nu,\mu)$ = monochromatic upward-welling radiation (intensity or radiance)

$I_\nu^-(\tau_\nu,\mu)$ = monochromatic downward-welling radiation (intensity or radiance)

$\tau_\nu$ = optical depth, $\int_0^z K_\nu \rho \, dz$

$\tau_{0\nu}$ = optical depth of the entire atmosphere

$K_\nu$ = monochromatic mass absorption coefficient

$\rho$ = constituent gas density as a function of altitude z

$\phi$ = azimuthal angle

n = refractive index

$I_{b\nu}(T)$ = black-body intensity at atmospheric temperature T

$\nu$ = frequency

The solutions to equations (1) and (2) for the case in which atmospheric temperature is a function of altitude require the use of an integrating factor.

$$I_\nu^+\left(\tau_\nu,\mu\right) = C_1 e^{\frac{-\tau_\nu}{\mu}} + n^2\int_0^{\tau_\nu} \frac{e^{\frac{t-\tau_\nu}{\mu}}}{\mu} I_{b\nu}(t)dt \tag{3}$$

$$I_\nu^-\left(\tau_\nu,\mu\right) = C_2 e^{\frac{\tau_\nu-\tau_{0\nu}}{\mu}} + n^2\int_{\tau_\nu}^{\tau_{0\nu}} \frac{e^{\frac{\tau-t}{\mu}}}{\mu} I_{b\nu}(t)dt \tag{4}$$

where $C_1$ and $C_2$ are constants determined from the boundary conditions and t is a dummy variable of optical depth. Assuming that the target is a diffuse reflector $\rho_\nu$ having an emissivity $\varepsilon_\nu$ and a temperature $T_1$ and located at $t_\nu = 0$, that $\rho_2 = 0$ and $I_{b2}(T_2) = 0$ at the top of the atmosphere ($t_\nu = \tau_{\nu 0}$), and that the Sun or other source is illuminating the top of the atmosphere with radiance $I_{0\nu}$ incident over the area represented by $\Delta\mu$ and $\Delta\phi$ at $\mu_1$ and $\phi_1$, respectively, the boundary conditions are as follows.

$$I_\nu^+(0,\mu) = \varepsilon_\nu I_{b\nu}\left(T_1\right) + \frac{\rho_\nu}{\pi}\int_0^{2\pi}\int_0^1 I^-(0,\mu')\mu'\, d\mu'\, d\phi' \tag{5}$$

$$I_\nu^-\left(\tau_{0\nu},\mu\right) = \Omega I_{0\nu} \tag{6}$$

# THEORY

In many remote-sensing applications through the Earth atmosphere in which scattering is not an important phenomenon and local thermodynamic equilibrium can be approximated because of the lack of rapid chemical reactions, the equations for radiative heat transfer can be written in the manner of Love (ref. 1), as indicated by the following equations and diagram.

$$\mu \frac{dI_\nu^+(\tau_\nu,\mu)}{d\tau_\nu} = -I_\nu^+(\tau_\nu,\mu) + n^2 I_{b\nu}(T) \tag{1}$$

$$-\mu \frac{dI_\nu^-(\tau_\nu,\mu)}{d\tau_\nu} = -I_\nu^-(\tau_\nu,\mu) + n^2 I_{b\nu}(T) \tag{2}$$

2 Top of the atmosphere $\tau_\nu = \tau_{0\nu}$

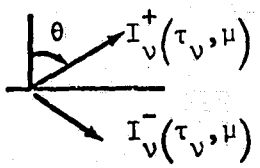


1 $\tau_\nu = 0$

where $\mu = \cos\theta$

$\theta$ = zenith angle

$I_\nu^+(\tau_\nu,\mu)$ = monochromatic upward-welling radiation (intensity or radiance)

$I_\nu^-(\tau_\nu,\mu)$ = monochromatic downward-welling radiation (intensity or radiance)

$\tau_\nu$ = optical depth, $\int_0^z K_\nu \rho \, dz$

$\tau_{0\nu}$ = optical depth of the entire atmosphere

$K_\nu$ = monochromatic mass absorption coefficient

$\rho$ = constituent gas density as a function of altitude z

$\phi$ = azimuthal angle

n = refractive index

$I_{b\nu}(T)$ = black-body intensity at atmospheric temperature T

$\nu$ = frequency

The solutions to equations (1) and (2) for the case in which atmospheric temperature is a function of altitude require the use of an integrating factor.

$$I_\nu^+\left(\tau_\nu,\mu\right) = C_1 e^{\frac{-\tau_\nu}{\mu}} + n^2\int_0^{\tau_\nu} \frac{e^{\frac{t-\tau_\nu}{\mu}}}{\mu} I_{b\nu}(t)dt \tag{3}$$

$$I_\nu^-\left(\tau_\nu,\mu\right) = C_2 e^{\frac{\tau_\nu-\tau_{0\nu}}{\mu}} + n^2\int_{\tau_\nu}^{\tau_{0\nu}} \frac{e^{\frac{\tau-t}{\mu}}}{\mu} I_{b\nu}(t)dt \tag{4}$$

where $C_1$ and $C_2$ are constants determined from the boundary conditions and t is a dummy variable of optical depth. Assuming that the target is a diffuse reflector $\rho_\nu$ having an emissivity $\varepsilon_\nu$ and a temperature $T_1$ and located at $t_\nu = 0$, that $\rho_2 = 0$ and $I_{b2}(T_2) = 0$ at the top of the atmosphere ($t_\nu \doteq \tau_{\nu 0}$), and that the Sun or other source is illuminating the top of the atmosphere with radiance $I_{0\nu}$ incident over the area represented by $\Delta\mu$ and $\Delta\phi$ at $\mu_1$ and $\phi_1$, respectively, the boundary conditions are as follows.

$$I_\nu^+(0,\mu) = \varepsilon_\nu I_{b\nu}\left(T_1\right) + \frac{\rho_\nu}{\pi}\int_0^{2\pi}\int_0^1 I^-(0,\mu')\mu'\, d\mu'\, d\phi' \tag{5}$$

$$I_\nu^-\left(\tau_{0\nu},\mu\right) = \Omega I_{0\nu} \tag{6}$$

where, when the plateau function $\Omega = 0$, $\phi > \phi_1 + \frac{\Delta\phi}{2}$, $\mu > \mu_1 + \frac{\Delta\mu}{2}$, $\phi < \phi_1 - \frac{\Delta\phi}{2}$, and $\mu < \mu_1 - \frac{\Delta\mu}{2}$ (i.e., the function is a rectangular box in the middle of the $(\phi,\mu)$ plane); $\Omega = 1$ otherwise.

Solving for $C_1$ and $C_2$ in equations (3) and (4) by using equations (5) and (6) gives the following solutions.

$$I_\nu^+(\tau_\nu,\mu) = \left\{\epsilon_\nu I_{b\nu}(T_1) + \frac{\rho_\nu}{\pi}\int_0^{2\pi}\int_0^1\left[\Omega I_0 e^{\frac{-\tau_{0\nu}}{\mu'}} + n^2\int_0^{\tau_{0\nu}} \frac{e^{\frac{\tau-t}{\mu'}}}{\mu'} I_{b\nu}(t)dt\right]\mu'\, d\mu'\, d\phi'\right\} e^{\frac{-\tau_\nu}{\mu}} + n^2\int_0^{\tau_\nu} \frac{e^{\frac{t-\tau}{\mu}}}{\mu} I_{b\nu}(t)dt \quad (7)$$

$$I_\nu^-(\tau_\nu,\mu) = \Omega I_{0\nu} e^{\frac{\tau_\nu-\tau_{0\nu}}{\mu}} + n^2\int_{\tau_\nu}^{\tau_{0\nu}} \frac{e^{\frac{\tau-t}{\mu}}}{\mu} I_{b\nu}(t)dt \quad (8)$$

The two most important cases of remote sensing through an atmosphere are covered by equations (7) and (8): sensing upwelling radiance (eq. (7)) reflected and/or emitted from a target using downward-looking sensors and sensing downwelling radiance (eq. (8)) from targets. In both cases, the equations are general and account for both monochromatic absorption and reradiation by the atmosphere for targets at any altitude in or above the atmosphere (arbitrarily called $\tau_\nu = 0$) and for sensors in or above the atmosphere.

Equation (7) can be simplified somewhat by integrating over the azimuthal direction.

$$I_\nu^+(\tau_\nu,\mu) = \epsilon_\nu I_{b\nu}(T_1)e^{\frac{-\tau_\nu}{\mu}} + \frac{I_0\rho_\nu\,\Delta\phi\, e^{\frac{-\tau_\nu}{\mu}}}{\pi}\int_{\mu_1-\frac{\Delta\mu}{2}}^{\mu_1+\frac{\Delta\mu}{2}} e^{\frac{-\tau_{0\nu}}{\mu'}}\mu'\,d\mu'$$

$$+ 2\rho_\nu n^2 e^{\frac{-\tau_\nu}{\mu}}\int_0^1\int_0^{\tau_{0\nu}} e^{\frac{\tau-t}{\mu'}} I_{b\nu}(t)d\mu'\,dt$$

$$+ n^2\int_0^{\tau_\nu}\frac{e^{\frac{t-\tau}{\mu}}}{\mu} I_{b\nu}(t)dt \qquad (9)$$

By taking the limit at small $\Delta\mu$ for the upper radiation source and introducing the exponential integral or Kourganoff function (ref. 2)

$$E_n(x) = \int_0^1 \mu^{n-2} e^{\frac{-x}{\mu}} d\mu \qquad (10)$$

where $x = -(t - \tau)$, equation (9) then can be written

$$I_\nu^+(\tau_\nu,\mu) = \epsilon_\nu I_{b\nu}(T_1)e^{\frac{-\tau_\nu}{\mu}} + \frac{I_{0\nu}\rho_\nu e^{\frac{-\tau_\nu}{\mu}} \Delta\phi \, e^{\frac{-\tau_{0\nu}}{\mu_1}} \mu_1 \, \Delta\mu_1}{\pi}$$

$$+ 2\rho_\nu n^2 e^{\frac{-\tau_\nu}{\mu}} \int_0^{\tau_{0\nu}} E_2(t - \tau) I_{b\nu}(t)dt$$

$$+ n^2 \int_0^{\tau_\nu} \frac{e^{\frac{t-\tau}{\mu}}}{\mu} I_{b\nu}(t)dt \qquad (11)$$

In the case of most natural targets, the value of $\epsilon_\nu$ is approximately 0.9 or higher for wavelengths of 4 to 20 micrometers and thus causes $\rho_\nu$ to be small. Thus, for remote-sensing measurements, the reflectance of atmospheric downwelling flux usually is negligible except when sensing is being attempted in or very near strongly absorbing bands from low-altitude platforms or when sensing is done at a very large angle from nadir, for which $\rho_\nu$ is much larger. Thus, the third term in equation (11)

$$2\rho_\nu n^2 e^{\frac{-\tau_\nu}{\mu}} \int_0^{\tau_{0\nu}} E_2(\tau - t) I_{b\nu}(t)dt$$

can usually be ignored. The second term in equation (11)

$$\frac{I_{0\nu}\rho_\nu e^{\frac{-\tau_\nu}{\mu}} \Delta\phi e^{\frac{-\tau_{0\nu}}{\mu_1}} \mu_1 \, \Delta\mu_1}{\pi}$$

is usually small as well, but is larger than the third term since the source considered is often the Sun. The second term should always be a strong candidate for inclusion at wavelengths <4 micrometers and should be included for specular reflectances at any wavelength.

For most purposes, it is therefore possible to simplify equation (11) to

$$I_\nu^+(\tau_\nu,\mu) = \varepsilon_\nu I_{b\nu}(T_1)e^{\frac{-\tau_\nu}{\mu}} + \frac{n^2}{\mu}\int_0^{\tau_\nu} e^{\frac{t-\tau_\nu}{\mu}} I_{b\nu}(t)dt \qquad (12)$$

## COMPUTER PROGRAM

### Program Development

The terms in equations (8) and (12) are calculated in finite difference form by assuming a refractive index of unity. The optical depth $\tau_\nu$ in finite difference form is

$$\tau_\nu = \sum_{i=1}^{NN} K_{\nu_i}\rho_i\,\Delta z_i \qquad (13)$$

where NN is the number of equal-mass layers i (usually NN $\geq$ 10). The monochromatic intensity transmitted through the atmosphere (where j is a dummy variable representing atmospheric layers and $\bar{\varepsilon}$ is gray-body emissivity assumed between $\nu_1$ and $\nu_2$ is

$$\varepsilon_\nu I_{b\nu}(T_1)e^{\frac{-\tau_\nu}{\mu}} = \bar{\varepsilon}I_{b\nu}(T_1)\prod_{j=1}^{NN} e^{\frac{-\left(K_{\nu_j}\rho_j\,\Delta z_j\right)}{\mu_j}} \qquad (14)$$

The upward-emitted intensity, designated in the printout (appendixes A and B) as "INT UP TOTAL" (for the NN-layer printout) is

$$n^2 \sum_{i=1}^{NN} \frac{I_{b\nu i}}{\mu_i} \prod_{j=i}^{NN} e^{\frac{-\left(K_{\nu_j} \rho_j \Delta z_j\right)}{\mu_j}} \tag{15}$$

and the downward-emitted intensity, designated in the printout (appendixes A and B) as "INT DOWN TOTAL" (for the NN-layer printout), is

$$n^2 \sum_{i=1}^{NN} \frac{I_{b\nu i}}{\mu_i} \prod_{j=1}^{i} e^{\frac{-\left(K_{\nu_j} \rho_j \Delta z_j\right)}{\mu_j}} \tag{16}$$

Thus, the terms in equations (8) and (12) can be calculated for the Lorentz broadening of the line shape, where

$$K_\nu = \frac{S\alpha}{\pi\left[\left(\nu - \nu_0\right)^2 + \alpha^2\right]} \tag{17}$$

where

$$S = S_0\left(\frac{T_0}{T}\right)^w \exp\left[\frac{-E''\left(T_0 - T\right)}{kT_0T}\right] \tag{18}$$

$$\alpha = \alpha_0\left(\frac{P}{P_0}\right)\left(\frac{T_0}{T}\right)^r \tag{19}$$

where $k$ is the Boltzmann constant, $T_0 = 296$ K, and $P_0 = 1$ atmosphere = $1013.25 \times 10^2$ N/m$^2$ (1013.25 millibars); $r$ is 0.62, 0.58, 0.5, 0.5, 0.5, and 0.5, and $w$ is 1.5, 1.0, 1.5, 1.5, 1.0, and 1.5, for water, carbon dioxide, ozone, nitrous oxide, carbon monoxide, and methane, respectively; $E''$ is the

lower rotational energy level of the transition; $S_0$ is the line intensity in $cm^{-1}/(molecule \cdot cm^{-2})$; $\alpha_0$ is the Lorentz half width; and $\nu_0$ is the frequency at a line center. These last four parameters are obtained from a magnetic tape containing data for carbon dioxide, water, nitrous oxide, ozone, and methane (ref. 3). These data, a sample of which is shown in appendix C, are obtainable from the authors of this report on request. Other data can be used just as easily with the program, provided that the format and parametric units are the same or that statement 151 of the main program can be changed to accommodate other data tape formats (ref. 4). The relationships between the units for optical mass U, for $K_0(\nu)$, and for S indicated in the list of symbols in this document and the older units are given in table I, taken from reference 5.

Because the absorption at any frequency $\nu$ results not only from lines near that frequency but also from the wings of nearby lines, the absorption coefficient must include contributions from these sources. This procedure is accomplished by summing all values of $K_\nu$ for $\nu_0 \pm$ BOUND, where BOUND is the distance from a line at which the wings of the line must be considered.

$$K_\nu = \frac{1}{\pi} \sum_{\nu'=\nu_0-\text{BOUND}}^{\nu'=\nu_0+\text{BOUND}} \frac{S_{\nu_0} \alpha_{\nu'}}{(\nu - \nu')^2 + \alpha_{\nu'}^2} \tag{20}$$

For low pressures, the predominant broadening effect is caused by the motion of the molecules (Doppler broadening). To account for this effect and for the transition between Lorentz and Doppler broadening, the Voigt profile (refs. 6 and 7) is used to calculate the absorption coefficient ($K_\nu$) when $\frac{P}{P_0} < 0.25$, $X < 25.0$, and $Y < 5.0$.

$$K_\nu = \frac{K_0 Y}{\pi} \int_{-\infty}^{\infty} \frac{e^{-t}}{Y^2 + (X - t)^2} \, dt \tag{21}$$

where $X = \left| \frac{(\nu - \nu_0)\sqrt{\ln 2}}{\alpha_d} \right|$

$$Y = \frac{\alpha_0 P}{\alpha_d P_0} \sqrt{\ln 2}$$

$$\alpha_d = \nu_0 \sqrt{\frac{2kT \ln 2}{Mc^2}}$$

$$K_0 = \frac{S}{\alpha_d} \sqrt{\frac{\ln 2}{\pi}}$$

c = speed of light

M = mass of the molecule

For very low pressures, equation (21) approaches Doppler broadening; for higher pressures, it approaches Lorentz broadening.

Because remote sensing is accomplished with instruments of finite bandwidth, equations (14) to (16) are integrated over a triangular instrument function $\sigma^*(\nu) = A - |\nu_i - \nu|$, where $\nu_i - A \le \nu \le \nu_i + A$, as indicated by the following diagram, in which A is one-half the width of the slit triangle base, DV is the integration step with the triangular slit, and DELV is the step between printouts.

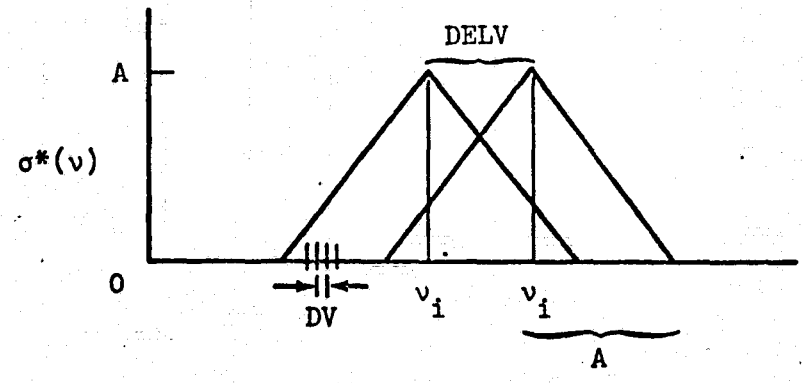


For example, to find the degraded intensity $\bar{I}_{\nu 0}$ through the atmosphere (ref. 3)

$$\bar{I}_{\nu_0} = \frac{\int_{\nu_i - A}^{\nu_i + A} I_\nu \sigma^*(\nu) d\nu}{\int_{\nu_i - A}^{\nu_i + A} \sigma^*(\nu) d\nu} \qquad (22)$$

where the normalized instrument function $\sigma(\nu)$ is defined by

$$\sigma(\nu) = \frac{\sigma^*(\nu)}{\int_{\nu_i - A}^{\nu_i + A} \sigma^*(\nu)d\nu} = \frac{\sigma^*(\nu)}{A^2} \tag{23}$$

and this step is performed for each $\nu_0$ value from $\nu_1$ to $\nu_2$ so that

$$\bar{I}_{\nu_0} = \int_{\nu_i - A}^{\nu_i + A} I_\nu \sigma(\nu)d\nu \tag{24}$$

Thus, the average intensity transmitted upward through the atmosphere plus that emitted for one position of the filter function at $\nu_k$ will be

$$\overline{I^+_{\nu_k}(\tau_\nu, \mu)} = \frac{\Delta\nu\varepsilon}{A^2}\sum_{m=1}^{m=\ell} I_b(T_1) \prod_{j=1}^{NN} e^{\frac{-\left(K_{m_j}\rho_j\,\Delta z_j\right)}{\mu_j}}$$

$$+ \frac{\Delta\nu n^2}{A^2}\sum_{m=1}^{m=\ell}\sum_{i=1}^{NN} \frac{I_{bm}}{\mu_i} \prod_{j=i}^{NN} e^{\frac{-\left(K_{m_j}\rho_j\,\Delta z_j\right)}{\mu_j}} \tag{25}$$

For a target of intensity $I_0$ in or above the atmosphere, the average intensity transmitted through the atmosphere plus that emitted downward for one position of the filter function at $\nu_k$ will be

$$\overline{I^-_{\nu_k}(\tau_\nu,\mu)} = \frac{\Delta\nu}{A^2}\sum_{m=1}^{m=\ell} I_{Om} \prod_{j=1}^{NN} e^{\frac{-\left(K_{m_j}\rho_j\,\Delta z_j\right)}{\mu_j}} + \frac{\Delta\nu n^2}{A^2}\sum_{m=1}^{m=\ell}\sum_{i=1}^{NN} \frac{I_{bm}}{\mu_i} \prod_{j=1}^{i} e^{\frac{-\left(K_{m_j}\rho_j\right)}{\mu_j}} \qquad (26)$$

where NN = number of layers chosen for the atmosphere, i = one layer in the atmosphere, $\ell$ = number of integration steps from $\nu_i - A$ to $\nu_i + A$, $\frac{2A}{DV}$, and m = one interval in frequency.

Thus, equations (25) and (26) describe the degraded intensities $\bar{I}^+_{\nu_0}$ and $\bar{I}^-_{\nu_0}$, which are upwelling and downwelling intensities, respectively, for a gray body with emissivity $\varepsilon$ and temperature $T_1$.

$$\overline{I^+_{\nu_k}(\tau_\nu,\mu)} = \varepsilon\,\overline{I_{b\nu}(T_1)e^{\frac{-\tau_\nu}{\mu}}} + \int_0^{\tau_\nu} \frac{e^{\frac{t-\tau}{\mu}}}{\mu} I_{b\nu}(t)dt \qquad (27)$$

$$\overline{I^-_{\nu_k}(\tau_\nu,\mu)} = \Omega\,\overline{I_{O\nu}e^{\frac{\tau_\nu-\tau_{O\nu}}{\mu}}} + \int_{\tau_\nu}^{\tau_{O\nu}} \frac{e^{\frac{\tau-t}{\mu}}}{\mu} I_{b\nu}(t)dt \qquad (28)$$

The two terms in each equation are calculated in finite difference form and are printed and punched out by the computer program. To enable the

calculation of equations (25) and (26), two computer programs were integrated. One of these (ref. 3) is used to calculate a monochromatic atmospheric transmission spectrum for one layer of the atmosphere and then to degrade this spectrum to the desired wavelength resolution as it might be observed with a spectrometer. The other program (ref. 8) affords a self-consistent method for calculating the state of the atmosphere on a refracted path through a spherical atmosphere, between two specified points, on the basis of radiosonde data or model atmosphere data (ref. 9).

The combination of the two programs, using a layered atmosphere ($\leq$30 layers), produces high-resolution[2] transmission and emission over any path by using realistic model atmospheres that can then be degraded to the appropriate resolution. The model can be used to correct upward-, sideward-, or downward-looking instruments of either high or low spectral resolution in the frequency range of 0.742 to $1.4415 \times 10^4$ $cm^{-1}$. The data include 15 250 lines of carbon dioxide, water vapor, ozone, nitrous oxide, and methane. Moreover, the model includes all significant levels of water vapor and as many as 30 layers of differing concentrations of carbon dioxide, ozone, nitrous oxide, carbon monoxide, and methane. Furthermore, this computer program is not restricted to the Earth atmosphere. Any atmosphere for which any of the five constituent gases is appropriate may be studied by changing the molecular weight of the gas M*, the radius of the planet R, the acceleration of gravity g, and CONN, which equals $\frac{-M^*g}{RO}$ where RO is the universal gas constant, to the appropriate planetary values in the main program data statement.

Another calculation added was that of weighting functions for downwelling intensity (which is the derivative of transmission with respect to altitude times $\Delta z_i$)

$$\overline{W_i d} = \frac{e^{\frac{\overline{t-\tau}}{\mu}}}{\mu} dt = \frac{\Delta\nu n^2}{\mu_i A^2} \sum_{m=1}^{m=\ell} \left[ \prod_{j=1}^{i-1} e^{\frac{-\left(K_{m_j} \rho_j\right)}{\mu_j}} - \prod_{j=1}^{i} e^{\frac{-\left(K_{m_j} \rho_j\right)}{\mu_j}} \right] \qquad (29)$$

[2]Resolution should not be pushed beyond 2 or 3 $cm^{-1}$ because Calfee compresses the lines within each 1-$cm^{-1}$ interval into one or two equivalent "compressed" lines for each species.

and for upwelling intensity

$$\overline{W_i u} = \overline{\frac{e^{\frac{\tau - t}{\mu}}}{\mu}\, dt} = \frac{\Delta\nu n^2}{\mu_i A^2} \sum_{m=1}^{m=\ell} \left[ \prod_{j=1}^{NN} e^{\frac{-\left(K_{m_j} \rho_j\right)}{\mu_j}} - \prod_{j=i-1}^{NN} e^{\frac{-\left(K_{m_j} \rho_j\right)}{\mu_j}} \right] \tag{30}$$

These functions are required for inputs to inversion routines that derive temperature structure from the upwelling radiance in the 14- to 15-micrometer wavelength region and water-vapor specific humidity structure from the upwelling radiance at wavelengths of 6.3 to 7.0 micrometers and a knowledge of the temperature structure. Chahine (ref. 10), Barnett (ref. 11), and Smith (ref. 12) have shown that it is necessary to have weighting functions for a class of atmospheric conditions near the solution to ensure rapid convergence.

## Continuum

The wave number region between 800 and 1250 per centimeter encompasses the continuum absorption due to water vapor. Calfee has used the continuum absorption coefficient given by Burch (ref. 13) for this region. First, he uses the optical mass of water vapor ($U_i$ in molecules/cm$^2$) to calculate the partial pressure due to water vapor ($Wl_i$) for the ith layer.

$$Wl_i = \frac{U_i T \mu_i}{\Delta z_i * 7.349 \times 10^{21}} \tag{31}$$

$$PH_i = -Wl_i + 0.005 * \left(P_i + Wl_i\right) \tag{32}$$

$$CAYBUR = -0.0665335 \times 10^{-29}\, \nu^3 + 0.3721108 \times 10^{-26} \nu^2 - 0.5971389 \times 10^{-23}\, \nu + 0.3113485 \times 10^{-20} \tag{33}$$

$$SAY = U_i * \left(CAY + CAYBUR * PH_i\right) \tag{34}$$

$$T_i = T_{i,mono} * \exp\left(-SAY\right) \tag{35}$$

where $T_i$ = transmission for ith layer

$T_{i,mono}$ = transmission for all line-by-line calculations

$\nu$ = frequency, $cm^{-1}$

CAYBUR = dummy variable

SAY = dummy variable

$P_i$ = ambient atmospheric pressure for layer i, atm

$U_i$ = molecules/$cm^2$ of water vapor

$\Delta z_i$ = vertical path length through ith layer

$\mu_i$ = cos $\theta_i$, where $\theta_i$ = angle through ith layer

$Wl_i$ = water-vapor partial pressure, atm

## Program Description and Operating Instructions

The CP program uses a Univac 1108 computer with four tape drives. The program tape is on unit C, the data tape is on unit A, and the scratch tape is on unit B. A tape drive is also used to produce microfilm plot results on a General Dynamics 4060 plotter. If plot results are not desired or if the required hardware is not available, FORTRAN statements 335 to 348 should be removed. An option is available for producing results on punched cards, if desired.

The program is written in FORTRAN 5 language and, with storage, requires approximately 44K words. Only standard library routines compatible with FORTRAN 4 are used. No overlays are used. The subroutines MODATM, ATMOS3, INPUT, REFRAC, PATH, COSINV, SININV, Q, ALTITU, PRES, E,.R, and F are routines used to describe the atmospheric properties. These routines are described in reference 8. All these routines are usually used by MODATM, which is the subroutine called by the main program CP. The purpose of each of these subprograms and its arguments are also defined in comment cards placed in the subroutine.

The computer function XK (which is called by the main program CP) calculates the Voigt spectrum line profile (eq. (21)) by means of the routines XK1, XK2, and XK3. The arguments of XK, X and Y, are defined in equation (21).

For detailed calculations involving the solar intensity reflection or the reflection of atmospheric emission as shown in equation (11), multiple

and for upwelling intensity

$$\overline{W_i u} = \overline{\frac{e^{\frac{\tau - t}{\mu}}}{\mu} dt} = \frac{\Delta\nu n^2}{\mu_i A^2} \sum_{m=1}^{m=\ell} \left[ \prod_{j=1}^{NN} e^{\frac{-\left(K_{m_j} \rho_j\right)}{\mu_j}} - \prod_{j=i-1}^{NN} e^{\frac{-\left(K_{m_j} \rho_j\right)}{\mu_j}} \right] \tag{30}$$

These functions are required for inputs to inversion routines that derive temperature structure from the upwelling radiance in the 14- to 15-micrometer wavelength region and water-vapor specific humidity structure from the upwelling radiance at wavelengths of 6.3 to 7.0 micrometers and a knowledge of the temperature structure. Chahine (ref. 10), Barnett (ref. 11), and Smith (ref. 12) have shown that it is necessary to have weighting functions for a class of atmospheric conditions near the solution to ensure rapid convergence.

## Continuum

The wave number region between 800 and 1250 per centimeter encompasses the continuum absorption due to water vapor. Calfee has used the continuum absorption coefficient given by Burch (ref. 13) for this region. First, he uses the optical mass of water vapor ($U_i$ in molecules/cm$^2$) to calculate the partial pressure due to water vapor ($Wl_i$) for the ith layer.

$$Wl_i = \frac{U_i T \mu_i}{\Delta z_i * 7.349 \times 10^{21}} \tag{31}$$

$$PH_i = -Wl_i + 0.005 * \left(P_i + Wl_i\right) \tag{32}$$

$$CAYBUR = -0.0665335 \times 10^{-29} \nu^3 + 0.3721108 \times 10^{-26} \nu^2 - 0.5971389 \times 10^{-23} \nu + 0.3113485 \times 10^{-20} \tag{33}$$

$$SAY = U_i * \left(CAY + CAYBUR * PH_i\right) \tag{34}$$

$$T_i = T_{i,mono} * \exp\left(-SAY\right) \tag{35}$$

where $T_i$ = transmission for ith layer

$T_{i,mono}$ = transmission for all line-by-line calculations

$\nu$ = frequency, $cm^{-1}$

CAYBUR = dummy variable

SAY = dummy variable

$P_i$ = ambient atmospheric pressure for layer i, atm

$U_i$ = molecules/$cm^2$ of water vapor

$\Delta z_i$ = vertical path length through ith layer

$\mu_i$ = cos $\theta_i$, where $\theta_i$ = angle through ith layer

$Wl_i$ = water-vapor partial pressure, atm

## Program Description and Operating Instructions

The CP program uses a Univac 1108 computer with four tape drives. The program tape is on unit C, the data tape is on unit A, and the scratch tape is on unit B. A tape drive is also used to produce microfilm plot results on a General Dynamics 4060 plotter. If plot results are not desired or if the required hardware is not available, FORTRAN statements 335 to 348 should be removed. An option is available for producing results on punched cards, if desired.

The program is written in FORTRAN 5 language and, with storage, requires approximately 44K words. Only standard library routines compatible with FORTRAN 4 are used. No overlays are used. The subroutines MODATM, ATMOS3, INPUT, REFRAC, PATH, COSINV, SININV, Q, ALTITU, PRES, E, .R, and F are routines used to describe the atmospheric properties. These routines are described in reference 8. All these routines are usually used by MODATM, which is the subroutine called by the main program CP. The purpose of each of these subprograms and its arguments are also defined in comment cards placed in the subroutine.

The computer function XK (which is called by the main program CP) calculates the Voigt spectrum line profile (eq. (21)) by means of the routines XK1, XK2, and XK3. The arguments of XK, X and Y, are defined in equation (21).

For detailed calculations involving the solar intensity reflection or the reflection of atmospheric emission as shown in equation (11), multiple

executions of the program are necessary. A separate run is required to calculate equations (14) to (16) for each required path through the atmosphere.

The triangular instrument function is adequate for narrow-band spectrometers; for instruments of wider band pass, it is necessary to place a P in column 1 of card type 1. This step results in punching of two types of cards. The first type will punch $\nu$ ($cm^{-1}$), transmission, and transmitted radiance 1X, F9.2, E13.3, and E13.3. The second type will punch $\nu$ ($cm^{-1}$), downwelling-emitted radiance, and upwelling-emitted radiance 1X, F9.2, E13.3, and E13.3. These cards can then be used with the appropriate filter functions for calculations of the wide-band response of instruments to various concentrations of gases and various model atmospheres.

A source code listing of all required software is given in appendix A. The listing comprises 1355 FORTRAN cards. A detailed flow chart of the CP program is shown in figure 1. The number of input cards required varies from as few as 20 that might be used in a 10-layer prediction of laboratory transmission for one spectral region (5160 to 5200 $cm^{-1}$) (appendix B, section 2) to approximately 35 that might be encountered when using a 10-layer prediction of atmospheric transmission through a radiosonde-specified atmosphere for three spectral regions (1150 to 1300, 550 to 700, and 700 to 850 $cm^{-1}$) (appendix B, section 3). Sample runs are provided in these same sections of appendix B for the input cards shown, and the generalized input format is presented in appendix B, section 1.

A small section of the 15 250 lines of data stored on the data tape is presented in appendix C. A typical run of a 10-layer model using radiosonde data for three 150-$cm^{-1}$ spectral regions will require approximately 10 minutes of computer time. However, run time is a function of the number of spectral lines in the chosen spectral interval, and some runs have required as many as 45 minutes on the Univac 1108 computer. The number of pages usually produced is approximately 50 per spectral interval chosen, provided weighting functions are printed. If weighting functions are not printed out, approximately 10 pages would be printed. Because the program is cyclic and returns to read additional spectral interval cards, the terminating conditions usually result from an attempt to read an end-of-file card.

## COMPARISONS TO TEST DATA AND LIMITATIONS OF THE MODEL

Comparisons were made with laboratory spectra to perform necessary but insufficient tests of the model. The model reproduces Calfee original water-transmission data (ref. 3) well for 0.01 and 0.1 centimeter of precipitable water at 1 atmosphere pressure at frequencies between 5182 and 5193 per centimeter (figs. 2 and 3). For low pressure, the model underestimated the ozone absorption by a factor of approximately 2 at wave numbers between 940 and

1120 per centimeter (fig. 4). The CP model reproduces carbon dioxide data well for pressures of 1.00, 0.0857, and 0.02053 atmosphere except at wave numbers between 600 and 660 $cm^{-1}$ for the lower pressures (figs. 5 to 7). One set of carbon dioxide lines at wave numbers between 640 and 650 $cm^{-1}$ is evidently missing from the data in figure 7. The comparison of spectra taken from an RB-57F aircraft flying over the Gulf of Mexico to CP predictions from the Lake Charles, Louisiana, radiosonde on April 30, 1970, is shown in figure 8. A comparison of Skylab S191 spectra of Monroe Reservoir to those predicted by the CP program using radiosonde data from nearby Salem, Illinois, for June 10, 1973, is shown in figure 9. Because the amount of ozone in the atmosphere is unknown, test cases were run for optical masses of both 0.0144 and 0.144 atm·cm.

The results of Kunde and others (ref. 19) afford a comparison of a line-by-line model to Nimbus 4 interferometer data of 5 percent in the 425- to 550-per-centimeter water continuum and the 750- to 1200-per-centimeter atmospheric window and 5 to 10 percent in the 667-per-centimeter carbon dioxide absorption region. The absolute accuracy was 5 to 10 percent for each of the parameters: measured radiances, in situ measurements, and atmospheric transmittances. The conclusion was that it is not possible to uniquely determine the error arising from each source and that it is, therefore, very difficult to improve atmospheric transmittances (predicted by a computer program) through the radiance comparison technique. The results shown in figure 9 indicate a comparison within 5 percent for the atmospheric window, but reveal larger errors outside this region. Whether these errors arise from the CP program or the S191 spectrometer or from both is unknown. Some off-band contamination of the 6- to 9- and 13.0- to 15.5-micrometer regions of the S191 data has been identified that causes radiance of these regions to be excessively high. The amount of this correction is currently being determined by the sensor performance personnel at the NASA Lyndon B. Johnson Space Center.

## CONCLUDING REMARKS

The results of testing the CP program indicate that the best results can be obtained in the near-infrared water bands. The absorption due to water vapor and carbon dioxide in the thermal infrared band appeared to be less reliable in comparison to spacecraft-acquired data and band models; however, neither of these tests is sufficient. Comparisons of laboratory carbon dioxide transmission in the thermal infrared band show good agreement except in regions where lines are known to be missing. The comparison of ozone transmission at a wavelength of 9.6 micrometers to laboratory data showed unexpectedly large differences.

No testing has been done for the nitrous oxide or methane transmissions. At present, the data used in the program are probably better known for carbon dioxide, nitrous oxide, and water vapor than for ozone and methane. Although tests for all molecules and spectral regions have not been performed, the tests have been sufficient to ensure that the program mechanics are sound and work well on the Univac 1108 computer. Conversion to FORTRAN 4 for CDC or IBM

computers will no doubt require new tape read-and-write software. However, the necessary changes should be simple, few, and obvious, because most FORTRAN coding used here did not involve sophisticated FORTRAN 5 logic.

Lyndon B. Johnson Space Center
National Aeronautics and Space Administration
Houston, Texas, December 27, 1974
951-16-00-00-72

## REFERENCES


1. Love, Tom J.: Radiative Heat Transfer. C. E. Merrill Pub. Co., 1968.

2. Kourganoff, V.: Basic Methods in Transfer Problems; Radiative Equilibrium and Neutron Diffusion. Rev. ed., Dover Pub., Inc., 1963.

3. Deutschmann, E. M.; and Calfee, R. F.: Two Computer Programs to Produce Theoretical Absorption Spectra of Water Vapor and Carbon Dioxide. ESSA Technical Report IER 31-ITSA 31, Apr. 1967.

4. McClatchey, R. A.; Benedict, W. S.; Clough, S. A.; Burch, D. E.; Calfee, R. F.; Fox, K.; Rothman, L. S.; and Garing, J. S.: AFCRL Atmospheric Absorption Line Parameters Compilation. AFCRL-TR-73-0096, Jan. 1973.

5. Calfee, R. F.: A Note on Terminologies Used in Gaseous Absorption Processes. NOAA Technical Report ERL 211-WPL 15, Aug. 1971.

6. Korb, C. Laurence; Hunt, Robert H.; and Plyler, Earle K.: Measurement of Line Strengths at Low Pressures - Application to the 2-0 Band of Carbon Monoxide. J. Chem. Phys., vol. 48, no. 9, 1968, pp. 4252-4260.

7. Young, C.: Calculation of the Absorption Coefficient for Lines with Combined Doppler and Lorentz Broadening. J. Quant. Spectr. Radiat. Transfer (GB), vol. 5, no. 3, May-June 1965, pp. 549-552.

8. Pitts, David E.; and Kyle, Kirby D.: A Model Atmosphere for Earth Resources Applications. NASA TM X-58033, 1969.

9. U.S. Committee on Extension to the Standard Atmosphere (COESA): U.S. Standard Atmosphere Supplements. U.S. GPO, 1966.

10. Chahine, Moustafa T.: Determination of the Temperature Profile in an Atmosphere from its Outgoing Radiance. NAS-NRC Atmospheric Exploration by Remote Probes, vol. 2, Jan. 1969, pp. 453-464.

11. Barnett, Thomas L.: Application of a Nonlinear Least-Squares Method to Atmospheric Temperature Sounding. J. Atm. Sci., vol. 26, no. 3, May 1969, pp. 457-461.

12. Smith, W. L.: Iterative Solution of the Radiative Transfer Equation for the Temperature and Absorbing Gas Profile of an Atmosphere. J. Appl. Opt., vol. 9, 1970, pp. 1993-1999.

13. Burch, Darrell E.: Radiative Properties of the Windows. Conference on Atmospheric Radiation, Aug. 7-9, 1972, Ft. Collins, Colorado. Am. Meteorol. Soc., 1972.

14. McCaa, D. J.; and Shaw, J. H.: The Infrared Absorption Bands of Ozone. Ohio State Univ. Research Foundation Contractor Report, AFCRL-67-0137, Sci. Rept. no. 2, 1967.

15. Drayson, S. R.; and Young, C.: The Frequencies and Intensities of Carbon Dioxide Absorption Lines Between 12 and 18 Microns. The Univ. of Mich. Dept. of Engr. (Ann Arbor, Mich.), Rept. 08183-1-T, Nov. 1967.

16. Drayson, S. R.; Li, S. Y.; and Young, C.: Atmospheric Absorption by Carbon Dioxide, Water Vapor and Oxygen. Univ. of Mich. High Altitude Engr. Lab. Rept. 08183-2-F, 178068, Feb. 1968.

17. Burch, Darrell E.; Singleton, Edgar B.; Williams, Dudley; and Gryvnak, David: Infrared Absorption by Carbon Dioxide, Water Vapor, and Minor Atmospheric Constituents. AFCRL-62-698, July 1962.

18. Hamilton, J. N.; Rowe, J. A.; and Anding, D.: Atmospheric Transmission and Emission Program. SAMSO, AF Systems Command, Contract No. F04701-72-C-0073, June 1973.

19. Kunde, V. G.; Conrath, B. J.; Hanel, R. A.; Maguire, W. C.; Prabhakara, C.; and Salomonson, V. V.: The Nimbus 4 Infrared Spectroscopy Experiment. 2: Comparison of Observed and Theoretical Radiance from 425-1450 cm(MINUS 1). NASA TM X-66275, 1973.

TABLE I.- SUMMARY OF UNIT RELATIONSHIPS[a]

[1 precipitable centimeter water = 1 $g \cdot cm^{-2}$ water]

| Symbol and previous unit | Multiplying factor (b) | Current unit |
|---|---|---|
| U, atm·cm STP | $1.219 \times 10^{-2} \times \frac{M}{\theta}$ | $g \cdot cm^{-2}$ |
| U, $g/cm^2$ | $82.06 \times \frac{273}{M}$ | atm·cm STP |
| U, atm·cm STP | $2.689 \times 10^{19}$ | $molecule \cdot cm^{-2}$ |
| U, $g/cm^2$ water | $3.34 \times 10^{22}$ | $molecule \cdot cm^{-2}$ |
| $K_0(\nu)$, $(atm \cdot cm)^{-1}$ STP | $82.06 \frac{\theta}{M}$ | $(g \cdot cm^{-2})^{-1}$ |
| $K_0(\nu)$, $(g \cdot cm^{-2})^{-1}$ | $1.219 \times 10^{-2} \frac{M}{273}$ | $(atm \cdot cm)^{-1}$ STP |
| $K_0(\nu)$, $(atm \cdot cm)^{-1}$ STP | $3.72 \times 10^{-20}$ | $(molecule \cdot cm^{-2})^{-1}$ |
| $K_0(\nu)$, $(g \cdot cm^{-2})^{-1}$ | $\frac{A}{M}$ | $(molecule \cdot cm^{-2})^{-1}$ |
| $K_0(\nu)$, $(atm \cdot cm)^{-1}$ STP | $356.3 \frac{\theta}{M}$ | $dB/(g \cdot cm^{-2})$ |
| $K_0(\nu)$, $(atm \cdot cm)^{-1}$ STP | 4.343 | dB/(atm·cm) STP |
| $K_0(\nu)$, $(g \cdot cm^{-2})^{-1}$ | 4.343 | $dB/(g \cdot cm^{-2})$ |
| S, $\frac{cm^{-1}}{atm \cdot cm}$ STP | $82.06 \frac{\theta}{M}$ | $\frac{cm^{-1}}{g \cdot cm^{-2}}$ |
| S, $\frac{cm^{-1}}{g \cdot cm^{-2}}$ | $1.219 \times 10^{-2} \frac{M}{273}$ | $\frac{cm^{-1}}{atm \cdot cm}$ STP |
| S, $\frac{cm^{-1}}{atm \cdot cm}$ STP | $3.72 \times 10^{-20}$ | $\frac{cm^{-1}}{molecule \cdot cm^{-2}}$ |
| S, $\frac{cm^{-1}}{g \cdot cm^{-2}}$ | $\frac{M}{A}$ | $\frac{cm^{-1}}{molecule \cdot cm^{-2}}$ |

[a]Data from reference 5.

[b]$\theta$ = temperature, K, M = molecular weight, A = Avogadro's number.



REPRODUCIBILITY OF THE
ORIGINAL PAGE IS POOR

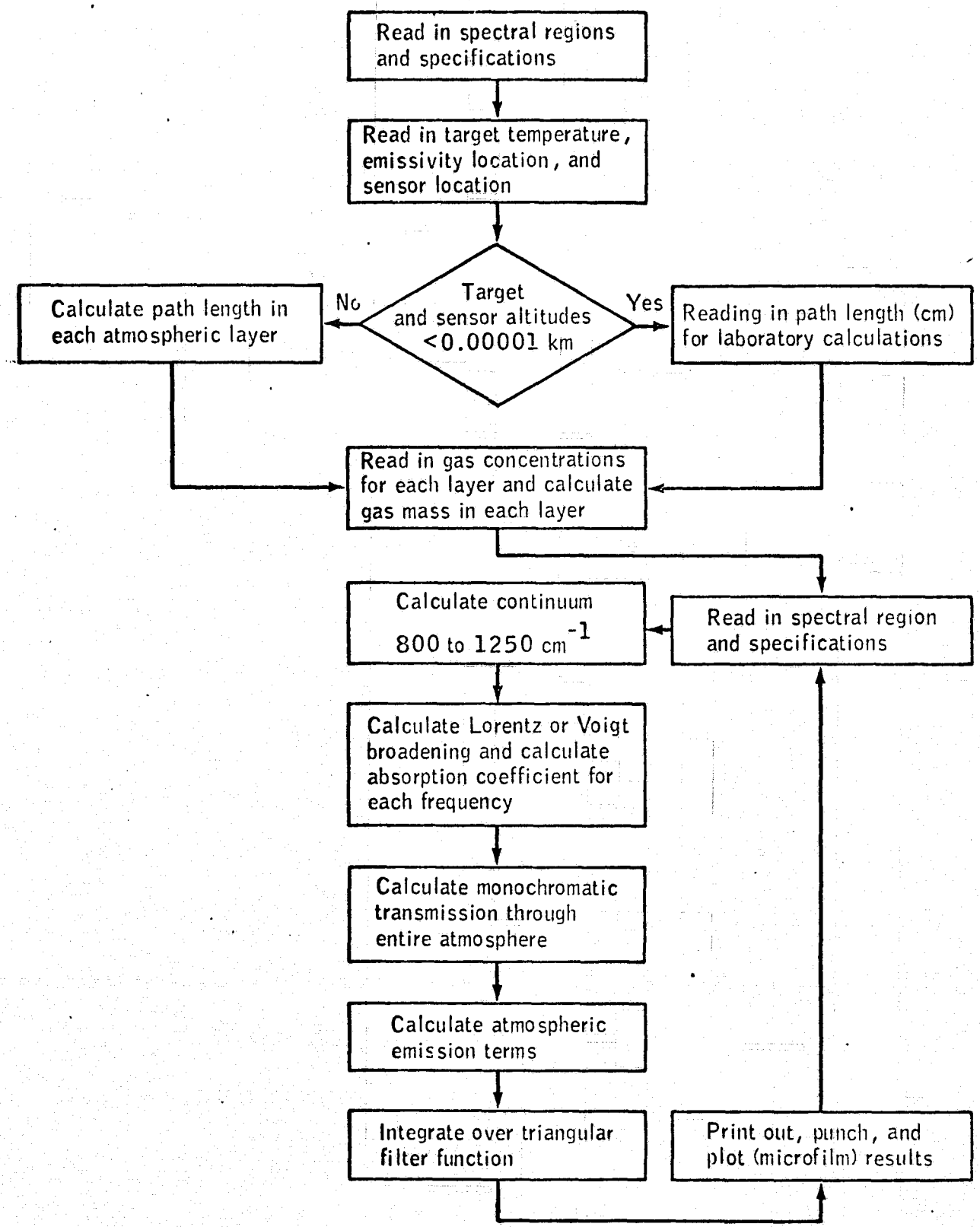


**Figure 1.- Flow chart of the CP program.**

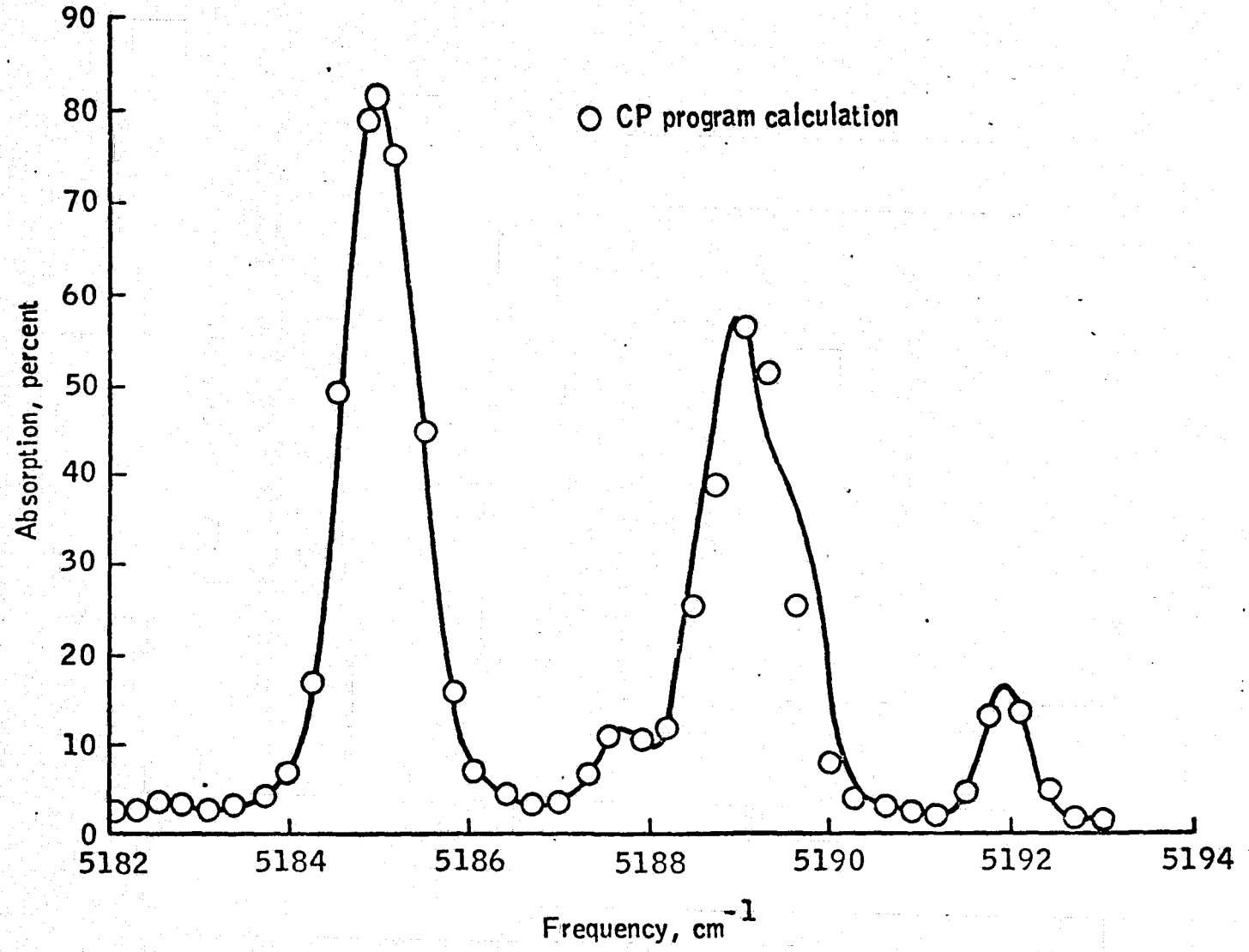


Figure 2.- Comparison of the predicted absorption for program CP with the original Deutschmann and Calfee (ref. 3) single-layer water-vapor-absorption spectrum for the frequency range 5182 to 5193 per centimeter at a pressure of 1.0 atmosphere, at a concentration of 0.01 centimeter of precipitable water vapor for a temperature of 287.7 K, and for a spectral slit width $\alpha$ of 0.5 cm$^{-1}$.

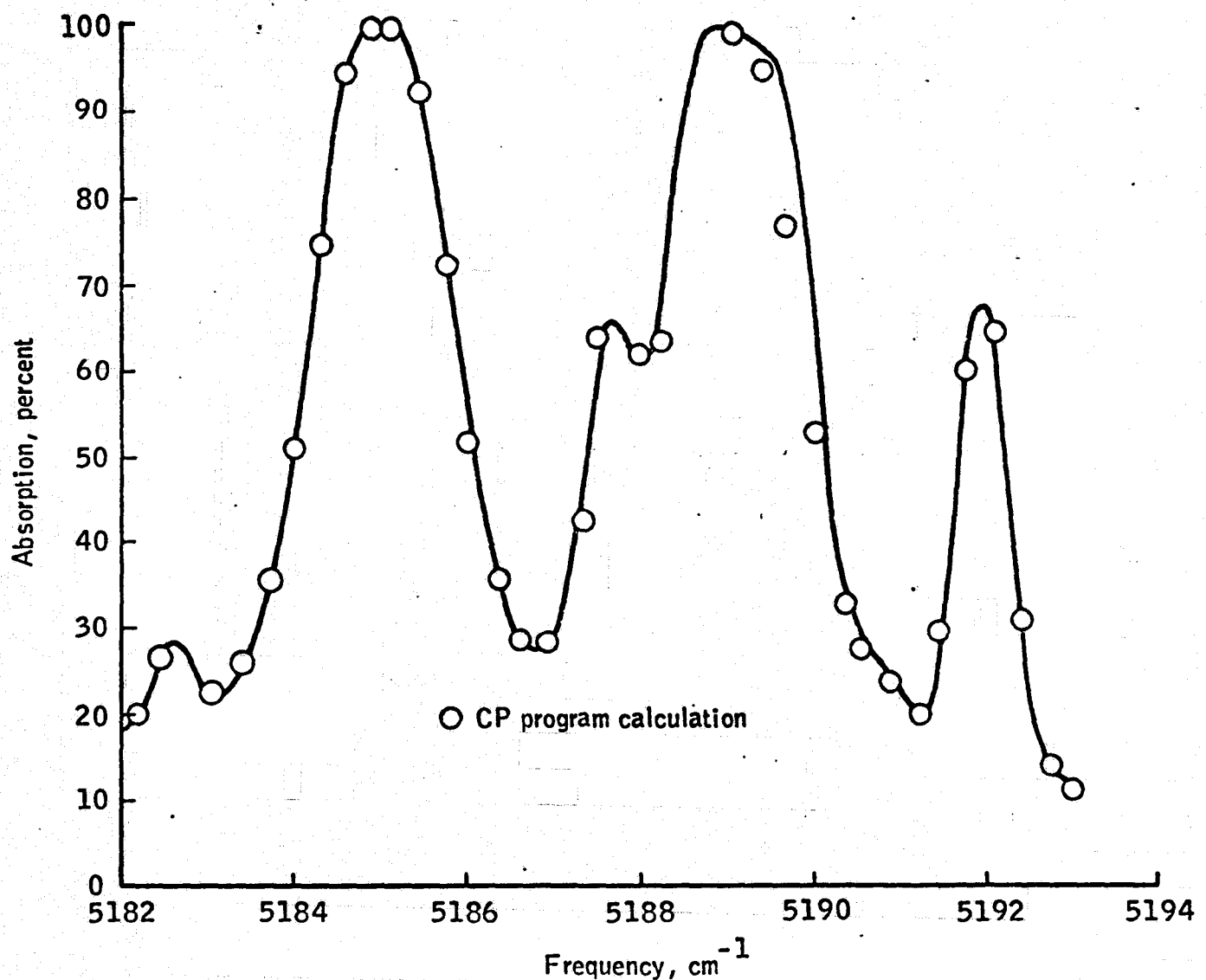


**Figure 3.-** Comparison of the predicted absorption for program CP with the original Deutschmann and Calfee (ref. 3) single-layer water-vapor-absorption spectrum for the frequency range 5182 to 5193 per centimeter at a pressure of 1.0 atmosphere, at a concentration of 0.1 centimeter of precipitable water vapor for a temperature of 287.7 K, and for a spectral slit width $a$ of 0.5 $cm^{-1}$.

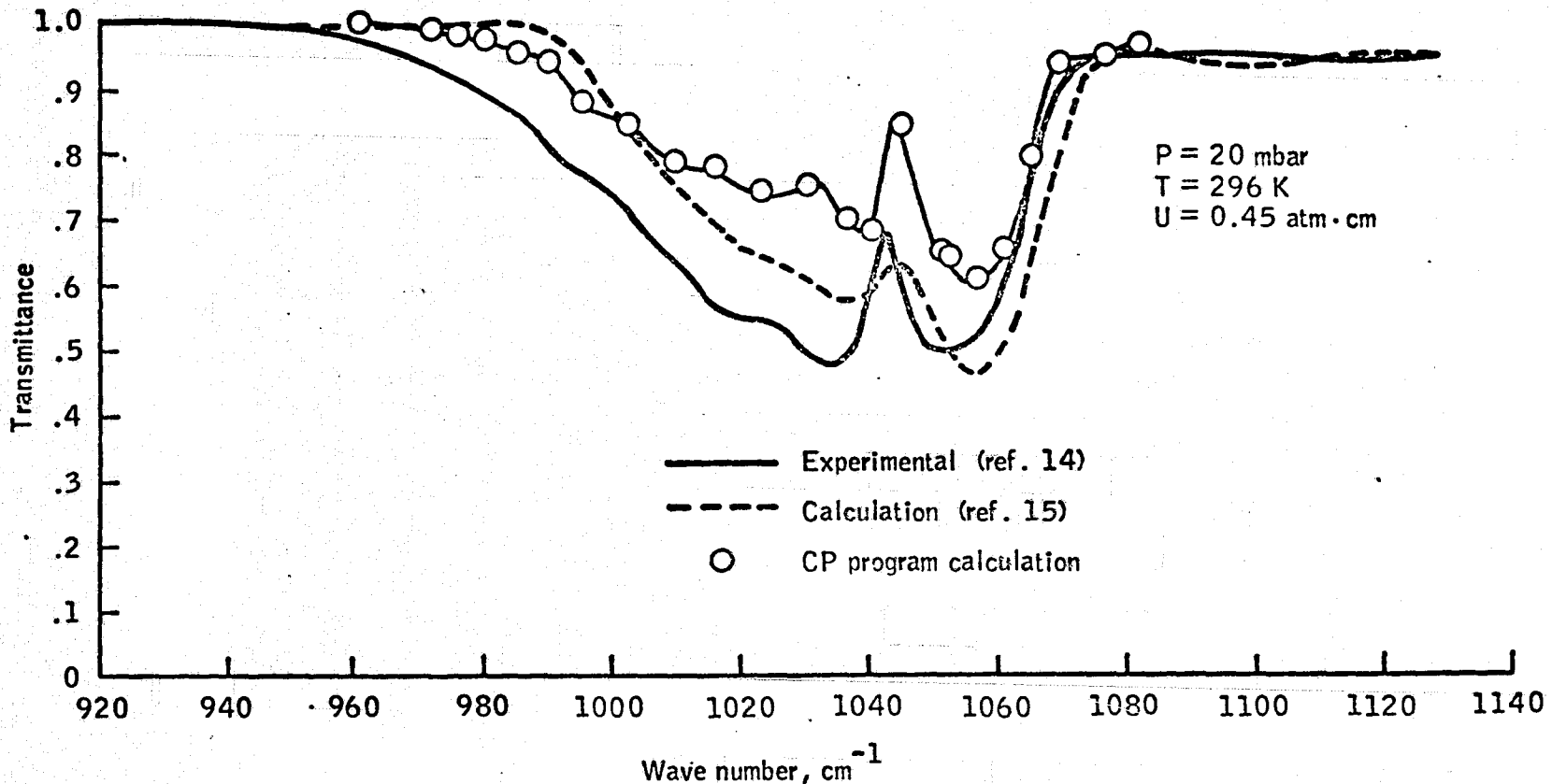


Figure 4.- Comparison of experimental and calculated absorption in the 1042-$cm^{-1}$ ozone band.

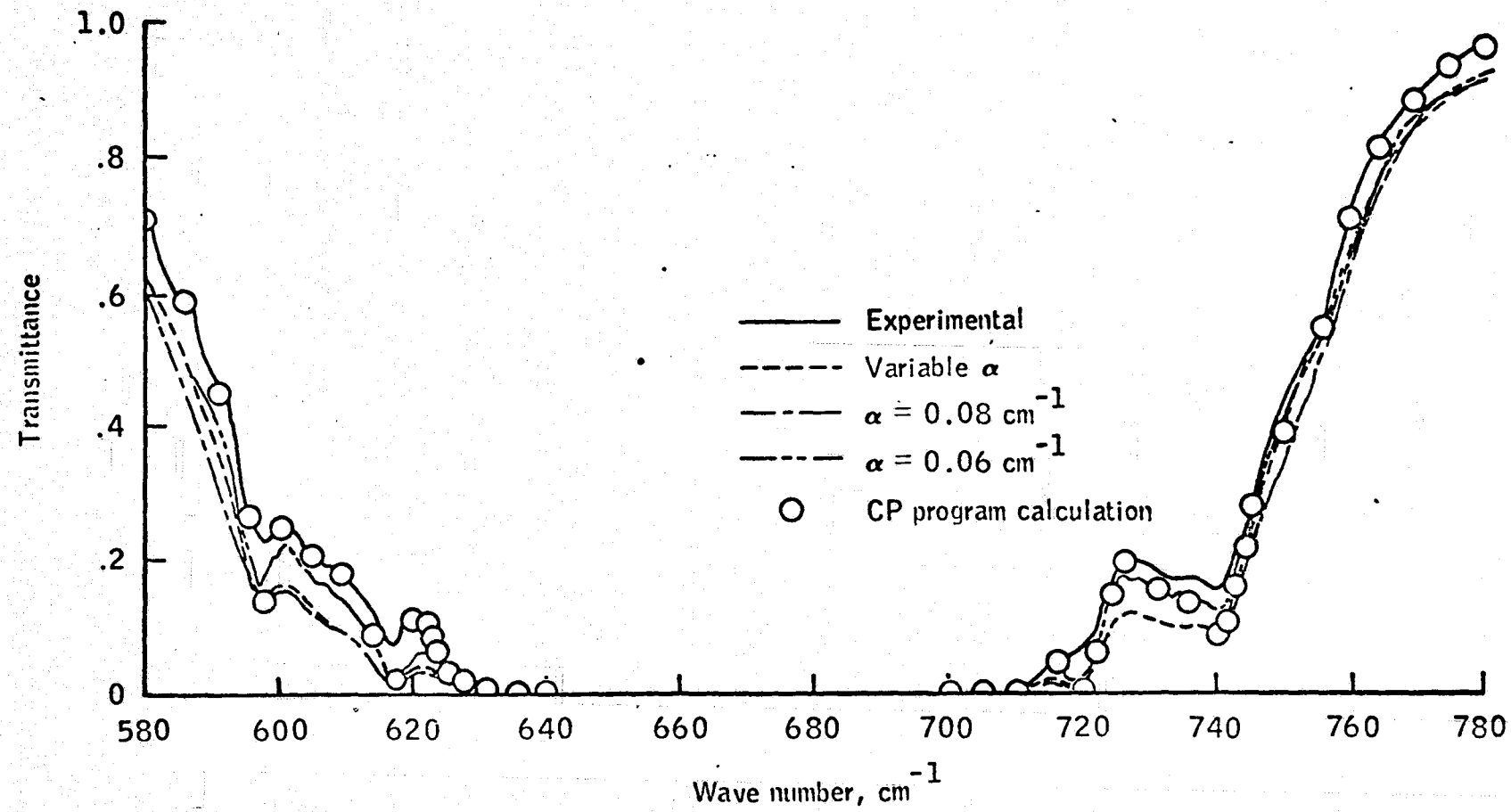


Figure 5.- Comparison of predicted transmission for program CP with the carbon dioxide transmission of Drayson and others (ref. 16) for an equivalent pressure of 1.00 atmosphere and an optical mass of 106.2 $atm \cdot cm_{300\ K}$.

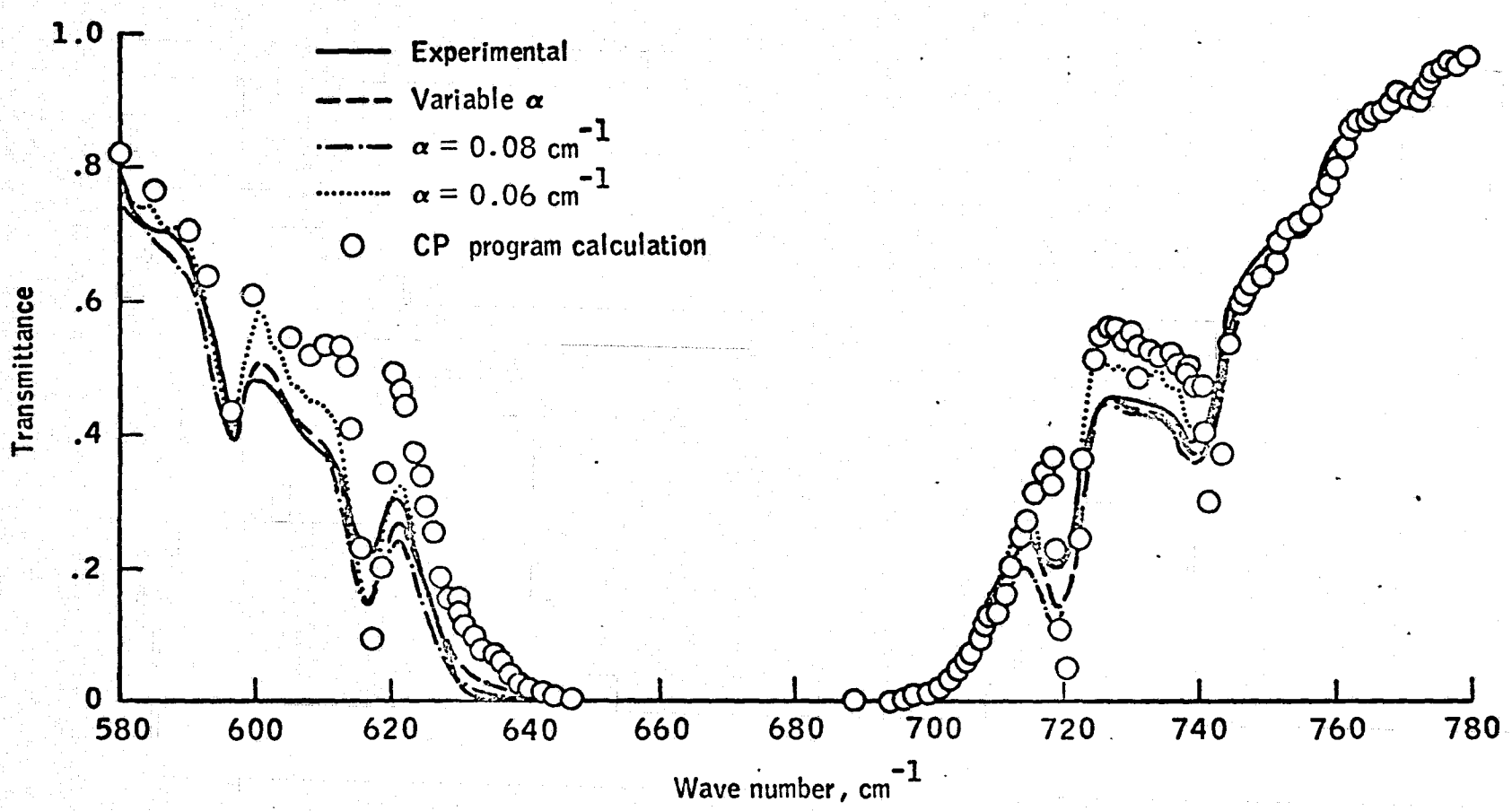


Figure 6.- Comparison of predicted transmission for program CP with the carbon dioxide transmission of Drayson and others (ref. 16) for an equivalent pressure of 0.0857 atmosphere and an optical mass of 212.1 atm·cm$_{300\ K}$.

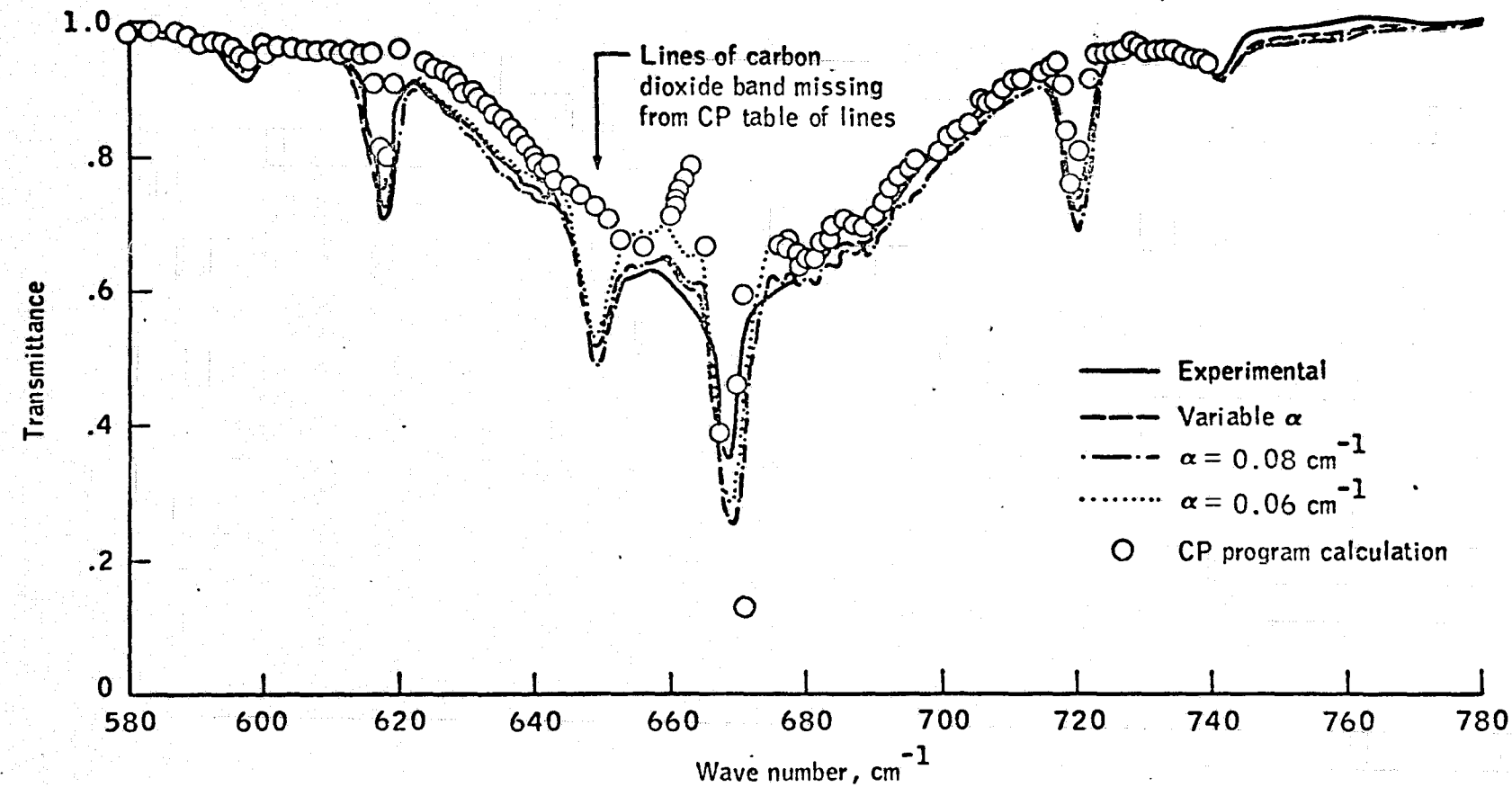


Figure 7.- Comparison of low-resolution spectra (ref. 17) with theoretical calculations of Drayson and others (ref. 16) and CP program for an equivalent pressure of 0.02053 atmosphere and an optical mass of 6.30 atm·cm$_{300\ K}$.

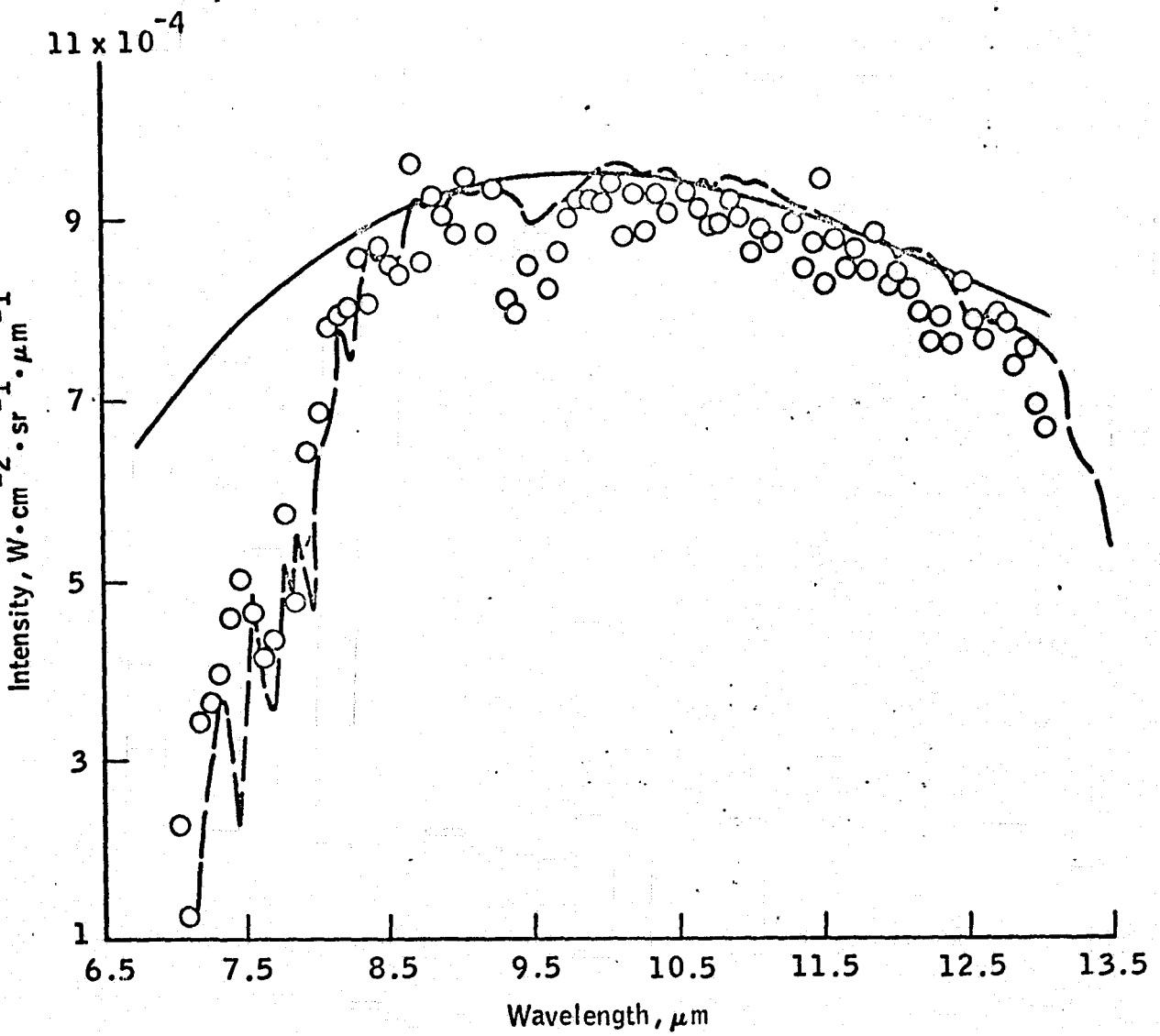


○ Intensity from the filter-wheel spectrometer obtained by using preflight and postflight calibrations

—— Nonlinear least-squares-fit black-body temperature = 297.1966 K

– – Predicted intensity upwelling from the Gulf of Mexico (T = 298.5 K) accounting for transmission and emission of the atmosphere using radiosonde data from Lake Charles, Louisiana, April 30, 1970, at 00:00 G.m.t.

Figure 8.- Calibration performed on April 30, 1970, using the Gulf of Mexico as a source and accounting for the intervening atmospheric transmission and emission.

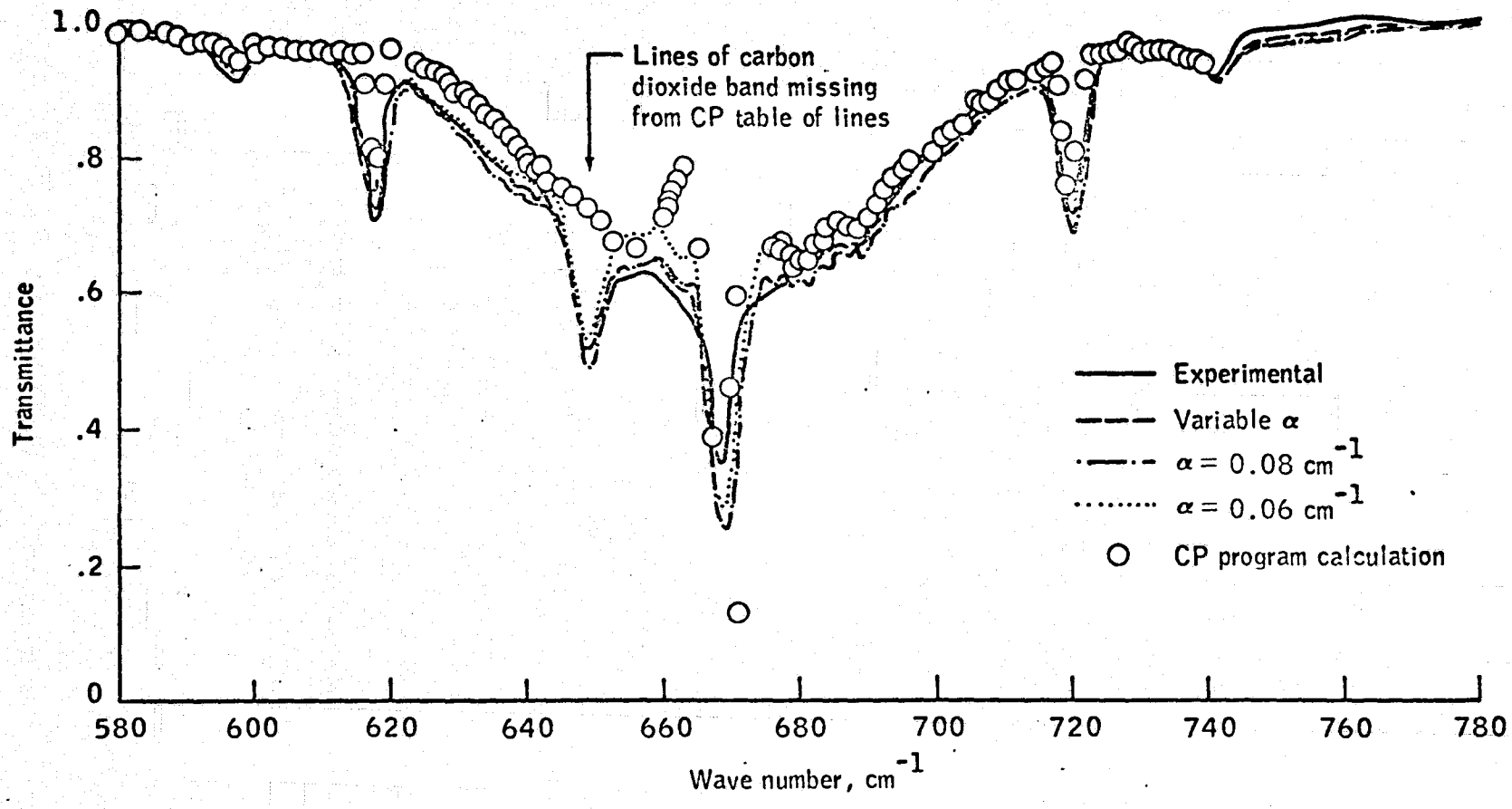


Figure 7.- Comparison of low-resolution spectra (ref. 17) with theoretical calculations of Drayson and others (ref. 16) and CP program for an equivalent pressure of 0.02053 atmosphere and an optical mass of 6.30 $atm \cdot cm_{300\ K}$.

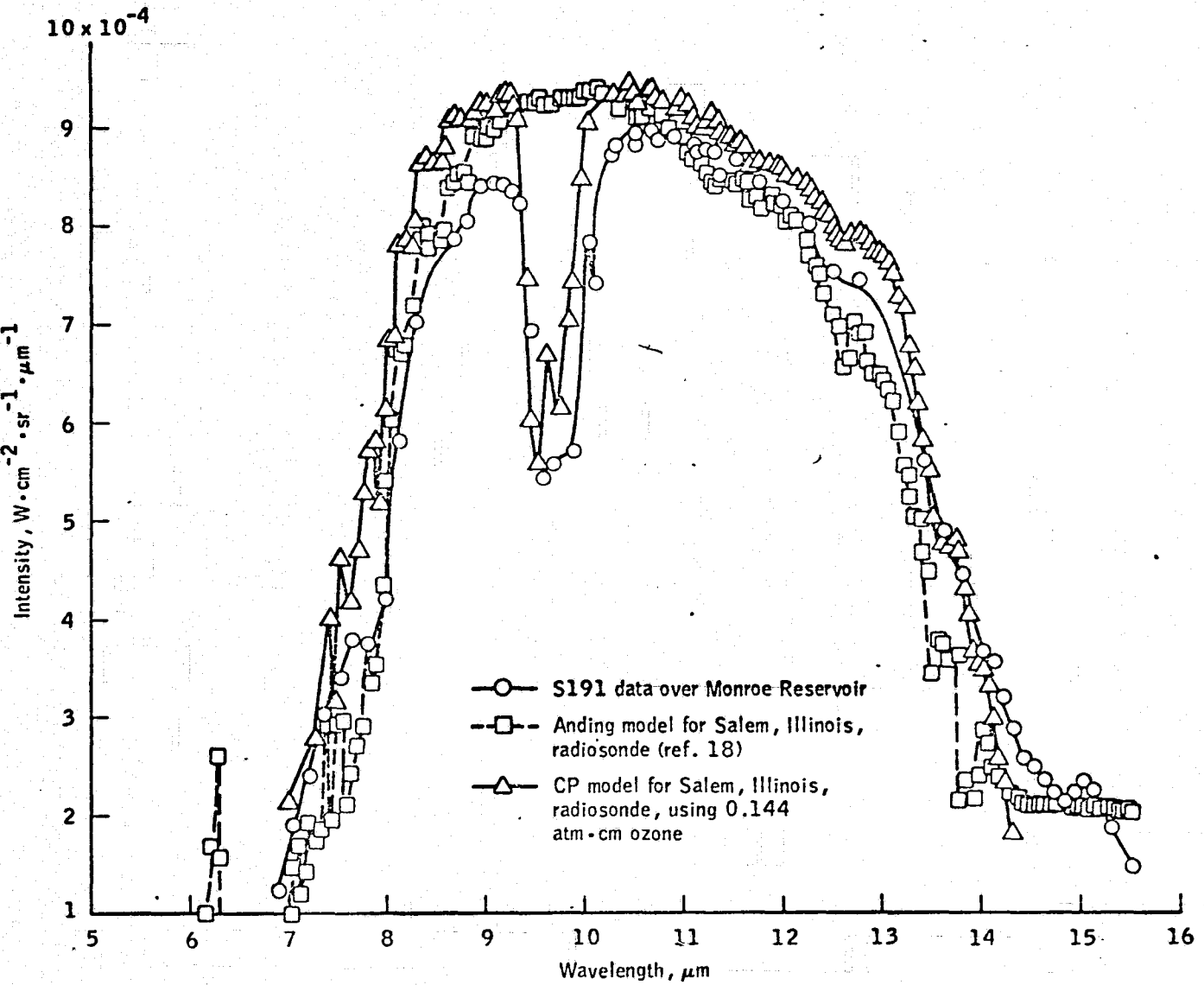


Figure 9.- Comparison of S191 sensor output data for Monroe Reservoir with CP model and Anding model radiosonde data from Salem, Illinois, on June 10, 1973.

# MEASUREMENT OF OCEAN PARAMETERS IN SUPPORT OF SKYLAB MISSIONS IN THE GULF OF MEXICO OFF THE TEXAS COAST

C. Laurence Korb,* and John F. Potter**

## INTRODUCTION

A series of four separate ocean truth missions were conducted to obtain the ground truth data necessary to support this investigation. The first mission was conducted on 5/31/73 from Freeport, Texas along a line extending southeasterly from Freeport, Texas at 28°55'N, 95°18'W to approximately 15 miles offshore at a 28°45'N, 95°09'W. The data obtained included measurements of chlorophyll concentration, turbidity, water temperature, water samples, and an attempt to measure incident spectral solar irradiance. Skylab data was not obtained for this mission and no laboratory spectral analysis was performed on the water samples which were taken.

The second mission was conducted on 6/5/73 from Port O'Connor, Texas and consisted of data taken in Matagorda Bay in the vicinity of 28°27'30"N, 96°21'30"W and coastal data taken along a line extending nearly due east to approximately 28°23'40"N, 95°55'30"W. The data taken included measurements of chlorophyll concentration, turbidity, water temperature, water samples, equivalent Lambert reflectance of the ocean, and solar photometer measurements.

* Goddard Space Flight Center
**Lockheed Electronics Corporation

A Skylab data-take was obtained for this mission. Unfortunately, the data take was at a solar elevation angle of 82° and thus the data was badly contaminated by solar glitter from the ocean. Extreme problems were also encountered in attempts to measure the spectral reflectance of the ocean from shipboard due to specular reflection by the ocean. The difficulties of these reflectance measurements were further compounded by ship motion.

The third mission was conducted on 8/8/73 from Freeport, Texas along the same line that was used for the first mission. The data obtained was limited to collecting water samples and measurements of water temperature since the vessel being used for data collection experienced a total power failure early in the mission, rendering all auxilliary instrumentation that required power unuseable. After returning to dockside later in the day, however, measurements of chlorophyll concentration and turbidity were performed using the water samples that had been collected. The weather during this third mission was extremely poor. The weather was dominated by thunderstorms early in the morning, and scattered rains and heavy cloud cover during the time of the Skylab overpass. A Skylab data-take was obtained for this mission, but the data was of no value for oceanography due to the presence of the heavy cloud cover.

The fourth ocean truth mission was conducted on 9/16/73 in the vicinity of 120 nm off the coast of Port O'Connor Texas along a line nearly due west from 27°15'N, 94°35'W

to 27°19'N, 94°54'W, and then along a second line extending northeast to 28°04'N, 95°52'W. The data obtained from this mission included measurements of chlorophyll concentration, turbidity, water temperature, water samples, equivalent Lambert reflectance of the ocean, solar photometer measurements, and extinction of the ocean over a one meter path at various depths. The weather for this mission was excellent with clear skies, winds in the 5 mph range, and a solar elevation angle of 45° at the time of the scheduled Skylab overpass at 10:45. Unfortunately, a Skylab data-take was not performed due to a weather forecast which predicted poor weather for the test site area.

## RESULTS AND DISCUSSION

The data acquired on Missions 2 and 4 covers the range of ocean parameters encountered in bay, coastal, and offshore studies and is presented in this section.

Table I gives the latitude, longitude, and time associated with each site for which measurements were made in the vicinity of Matagorda Bay and the associated coastal offshore waters on June 5, 1973.

Table II gives the measured values of turbidity, chlorphyll concentration, and water temperature which were found at these sites. The value of chlorophyll concentration were measured

47

TABLE 1

SITE NUMBER, LONGITUDE, LATITUDE, AND TIME FOR GROUND TRUTH DATA COLLECTION ON JUNE 5, 1973, IN THE VICINITY OF MATAGORDA BAY

| SITE | LONGITUDE | LATITUDE | TIME |
|---|---|---|---|
| 1 | 96°21'40" | 28°27'40" | 9.15 |
| 2 | 96°21'30" | 28°27'40" | 9.20 |
| 3 | 96°21'30" | 28°27'30" | 9.35 |
| 4 | 96°20'40" | 28°26'20" | 10.15 |
| 5 | 96°19'30" | 28°25'00" | 10.25 |
| 6 | 96°19'00" | 28°24'20" | 10.30 |
| 7 | 96°15'00" | 28°24'20" | 10.50 |
| 8 | 96°13'00" | 28°24'20" | 11.10 |
| 9 | 96°11'10" | 28°24'20" | 11.30 |
| 10 | 96° 8'10" | 28°24'10" | 11.50 |
| 11 | 96° 1'10" | 28°23'50" | 12.20 |
| 12 | 95°55'30" | 28°23'40" | 14.20 |
| 13 | 95°56'50" | 28°24'20" | 14.30 |
| 14 | 95°58'50" | 28°25'20" | 14.44 |
| 15 | 96°00'30" | 28°26'20" | 14.55 |
| 16 | 96°02'10" | 28°27'10" | 15.13 |
| 17 | 96°04'10" | 28°28'00" | 16.00 |
| 18 | 96°09'30" | 28°28'40" | 16.25 |
| 19 | 96°11'50" | 28°27'20" | 16.30 |
| 20 | 96°13'00" | 28°27'40" | 16.40 |
| 21 | 96°14'30" | 28°26'50" | 16.55 |
| 22 | 96°15'10" | 28°26'40" | 17.05 |
| 23 | 96°15'10" | 28°26'40" | 17.10 |
| 24 | 96°17'10" | 28°25'30" | 17.25 |
| 25 | 96°17'50" | 28°23'00" | 17.35 |
| 26 | 96°19'30" | 28°24'50" | 17.50 |
| 27 | 96°19'30" | 28°25'00" | 17.55 |
| 28 | 96°20'10" | 28°25'50" | 18.00 |
| 29 | 96°21'40" | 28°27'00" | 18.10 |
| 30 | 96°20'50" | 28°27'50" | 18.20 |

TABLE II

TURBIDITY, CHLOROPHYLL, AND TEMPERATURE OF OCEAN GROUND TRUTH SITES IN THE VICINITY OF MATAGORDA BAY, JUNE 5, 1973

| SITE | TURBIDITY (JTU) | CHLOROPHYLL ($mg/m^3$) | TEMPERATURE ($^oK$) |
|---|---|---|---|
| 1 | 17.0 | 6.9 | - |
| 2 | 19.0 | 5.0 | - |
| 3 | 13.0 | 6.9 | - |
| 4 | 19.0 | 7.5 | 27.7 |
| 5 | 23.0 | 6.2 | - |
| 6 | 16.0 | 7.1 | 27.7 |
| 7 | 12.0 | 5.9 | 27.5 |
| 8 | 5.5 | 1.2 | - |
| 9 | 5.0 | - | 26.9 |
| 10 | 4.0 | 2.5 | 26.7 |
| 11 | 2.4 | 1.0 | 26.7 |
| 12 | 0.9 | 1.2 | 27.1 |
| 13 | 1.4 | 1.8 | - |
| 14 | 1.7 | 1.8 | - |
| 15 | 1.5 | 2.4 | 26.9 |
| 16 | 3.5 | 4.0 | 26.9 |
| 17 | 2.6 | 3.9 | 27.1 |
| 18 | 5.5 | 5.4 | 27.7 |
| 19 | 6.5 | 5.4 | 29.2 |
| 20 | 25 | 7.7 | 28.3 |
| 21 | 22 | 13.0 | 28.3 |
| 22 | 20 | 14.5 | 28.4 |
| 23 | 7.5 | 9.0 | 28.4 |
| 24 | 6.5 | 9.0 | 28.4 |
| 25 | 6.5 | 6.0 | - |
| 26 | 16 | 8.2 | 28.4 |
| 27 | 15 | 8.2 | 28.3 |
| 28 | 11 | 7.1 | 28.3 |
| 29 | 9.5 | 6.9 | 28.3 |
| 30 | 9.0 | 11.2 | 28.6 |

using a Turner fluorometer. The fluorometer was calibrated periodically during the course of each mission using distilled water to determine zero offset readings. The relation between chlorophyll concentration and calibrated fluorometer readings was established by laboratory analysis of water samples by Texas A&M University. The measurements of turbidity were likewise made in situ using a Hach Laboratory Turbidemeter, Model 2100, which measured the intensity of light scattered by a sample of ocean water at an angle of $90^{o}$ relative to the direction of evidence. The turbidity readings were calibrated relative to a sample of Formazin solution and the calibrated measurements are given in Jackson Turbidity Units (JTU). The measurements of water temperature were made using a calibrated thermometer and the bucket method.

As may be seen from Table II, the values of chlorophyll found were in the range of 1.0 to 14.5 $mg/m^3$ which indicates a very high level of phytoplankton activity. The associated values of turbidity range from as low as 0.9 to as high as 25.0 JTU. The range of ocean temperatures found varied from a low of $26.9^{o}$ to a high of $29.2^{o}C$. It may be noted, however, that the effect of solar heating during the day accounted for about a $0.6^{o}C$ change in ocean temperature.

It may also be seen from Table II that trends occur in both the levels of chlorophyll and turbidity. The levels of chlorophyll and turbidity associated with sites 1 thru 7 are very high. These sites start in Matagorda Bay and move

into the waters adjacent to Matagorda Peninsula. The values of chlorophyll and turbidity then decrease as the sites move further offshore (sites 8 thru 11) and a minimum value of turbidity is found at site 12 which is the farthest point from landfall. The values of chlorophyll and turbidity then slowly increase as one approaches site 17 (4.5nm from the Peninsula), and then have a large increase in value in the vicinity of site 20 through 22 which lie only about 1.5nm off the coast of the Peninsula.

The high levels of turbidity which are associated with Matagorda Bay and the coastal waters within 2nm of the coast of the Peninsula may be understood as naturally occuring in shallow waters due to runoff from the shore and also perhaps due to mud and silt. It is also important to note, however, that high values of turbidity and high values of chlorophyll have a tendency to go together. The relationship between turbidity and chlorophyll was investigated by plotting (Figure 1) the values of turbidity vs. chlorophyll for each of the data sites in Table II. When a correlation coefficient was calculated for this data, it was found to be 0.68. This value indicates a correlation between the data significant at a confidence level of greater than 99%.

One would not a priori hypothesize a relationship such as that found in Table II and shown in Figure 1. It is reasonable on a physical basis that such a relationship might occur, however, since high or low turbidity is

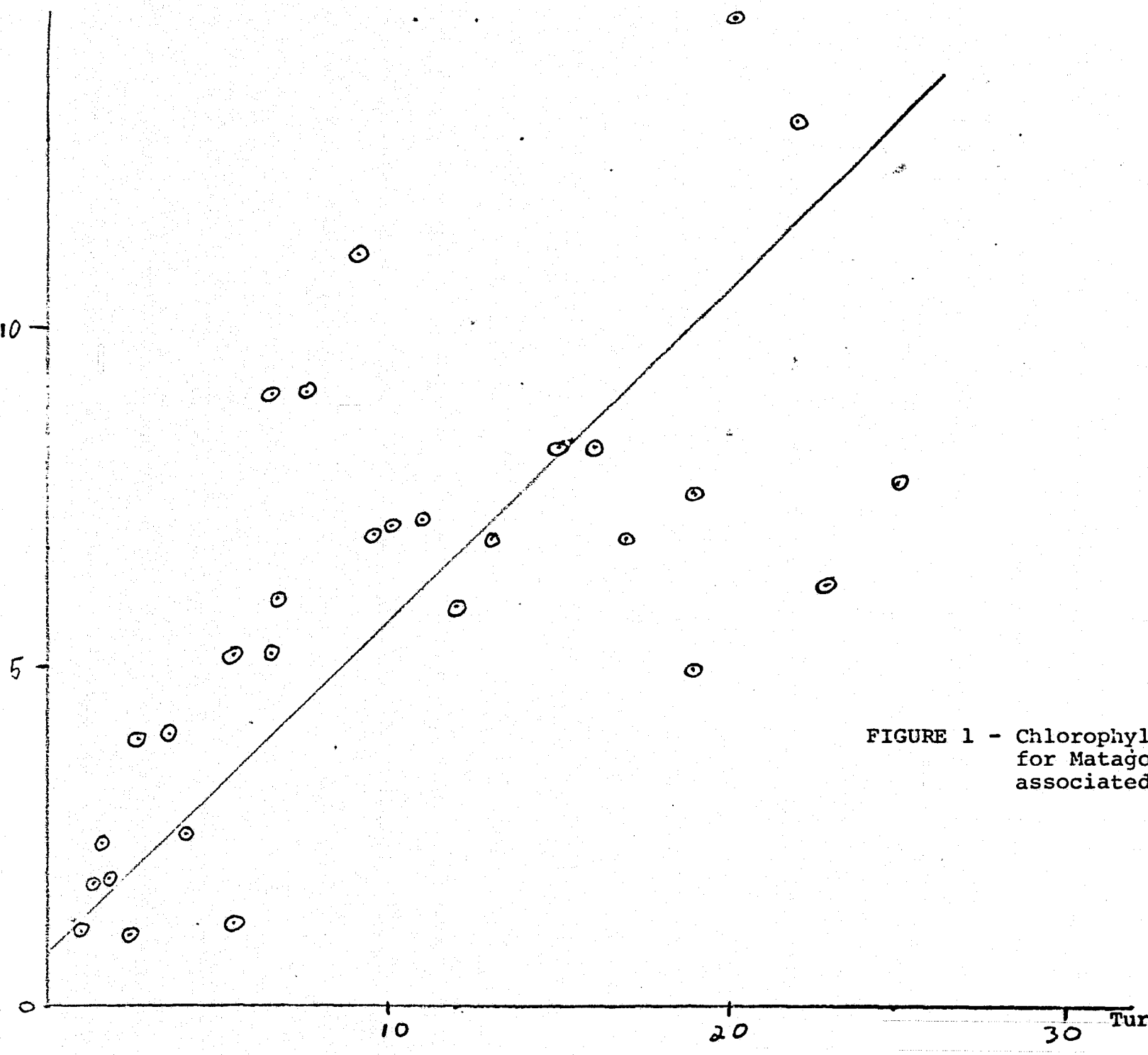


FIGURE 1 - Chlorophyll vs. turbidity for Matagorda Bay and associated coastal water.

associated with correspondingly high or low values of nutrients in the coastal waters. The high level of nutrients provide favorable conditions for high rates of photosynthesis and thus of chlorophyll.

Water samples were collected at each site during mission 2 and these samples were returned for laboratory spectral analysis. This analysis consisted of measuring the spectral transmittance of a 10 cm sample of ocean water using a Cary-14 spectroradiometer. The results of these laboratory measurements are shown in Figures A1 through A27. In order to eliminate the effects of absorption by the cell windows, reflection losses at the cell interface, and absorption due to the molecular absorption bands of liquid water, the transmission measurements were made relative to a reference cell containing a 10 cm path of distilled water.

As is shown in Figures A1 through A27, the resultant spectra generally show a nearly linear relationship between transmission and wavelength over the spectral region from 4000 to 8000 A° with higher values of transmittance at the longer wavelengths. The prime feature of these spectral curves is the shift in the overall level of transmitted energy between sites. At a wavelength of 4500A° the transmission varies from a low value of about 18% for site 2 in Matagorda Bay to a high value of 95% for the offshore coastal waters. The overall shape of the transmitted spectrum is consistent with the effects of large particles Mie scattering.

Figures A1 through A27

The ratio of the energy transmitted by a 10 cm sample of ocean water to that transmitted by an equal path length of distilled water as a function of wavelength for the spectral region from 4000 to 8000 A°.

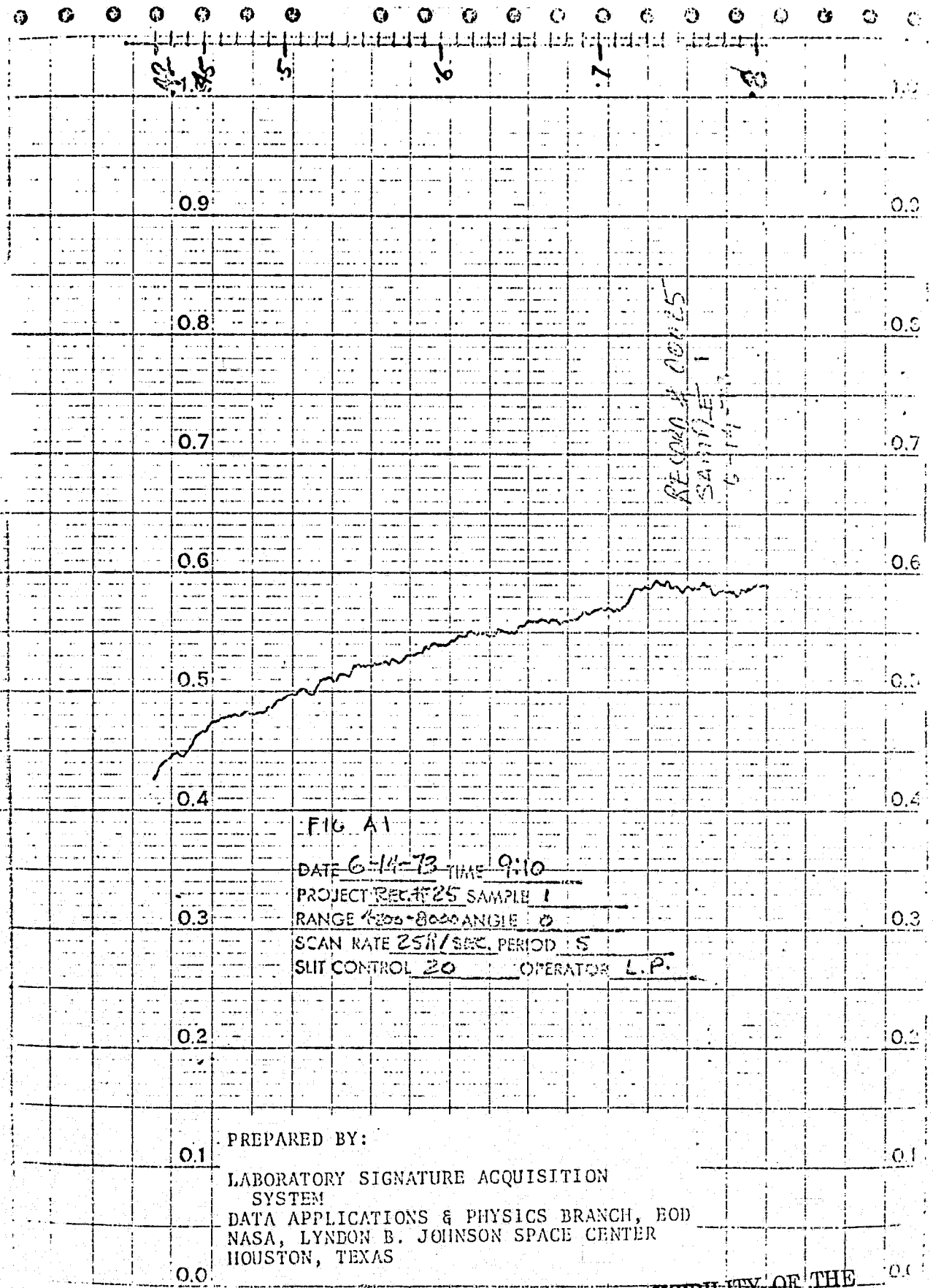


FIG A1

DATE 6-14-73 TIME 9:10
PROJECT RELAT25 SAMPLE 1
RANGE 4200-8000 ANGLE 0
SCAN RATE 25A/SEC. PERIOD 5
SLIT CONTROL 20 OPERATOR L.P.

PREPARED BY:

LABORATORY SIGNATURE ACQUISITION SYSTEM
DATA APPLICATIONS & PHYSICS BRANCH, EOD
NASA, LYNDON B. JOHNSON SPACE CENTER
HOUSTON, TEXAS

REPRODUCIBILITY OF THE ORIGINAL PAGE IS POOR

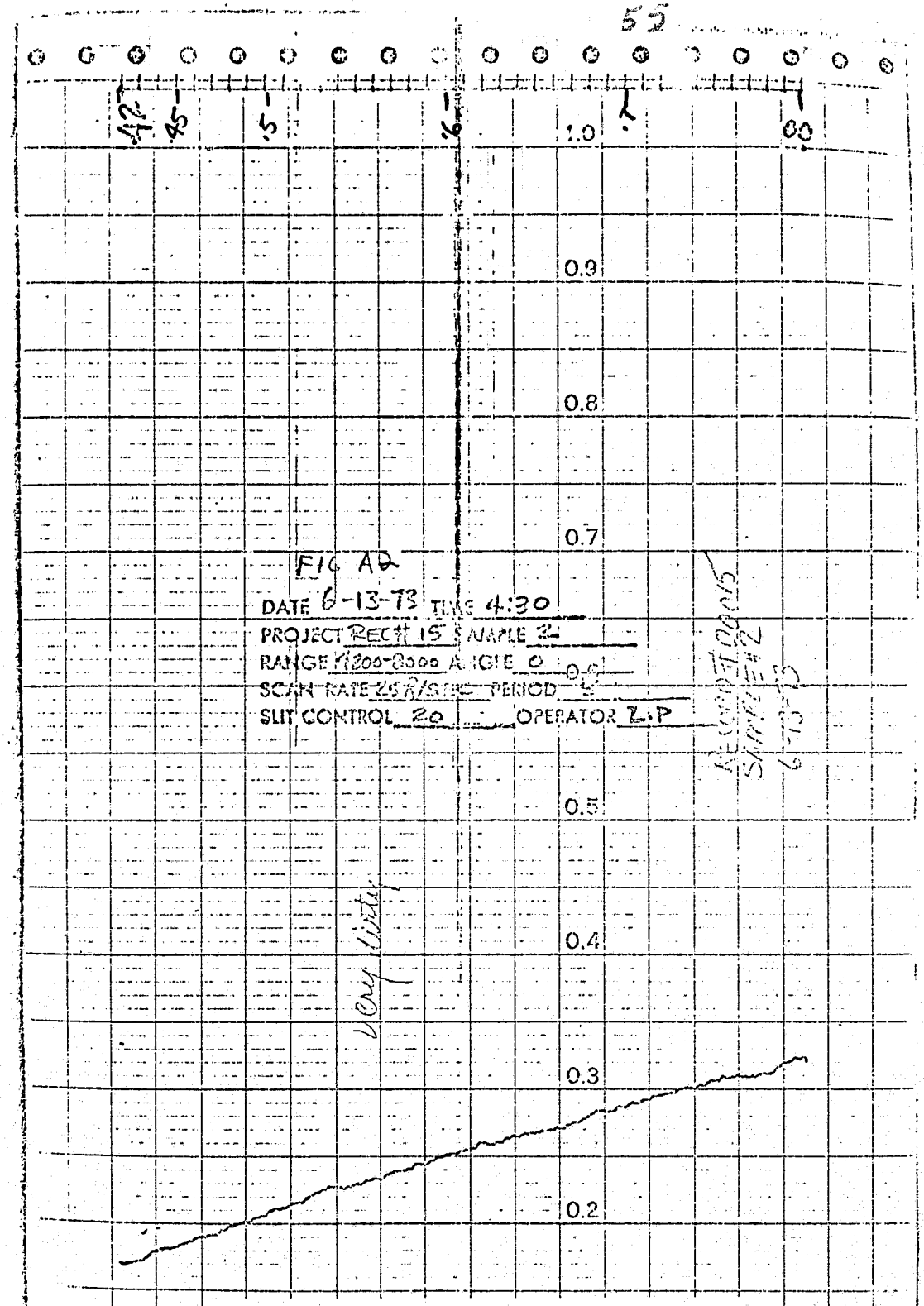


PREPARED BY:

LABORATORY SIGNATURE ACQUISITION SYSTEM
DATA APPLICATIONS & PHYSICS BRANCH, EOD
NASA, LYNDON B. JOHNSON SPACE CENTER
HOUSTON, TEXAS

ORIGINAL PAGE IS
OF POOR QUALITY

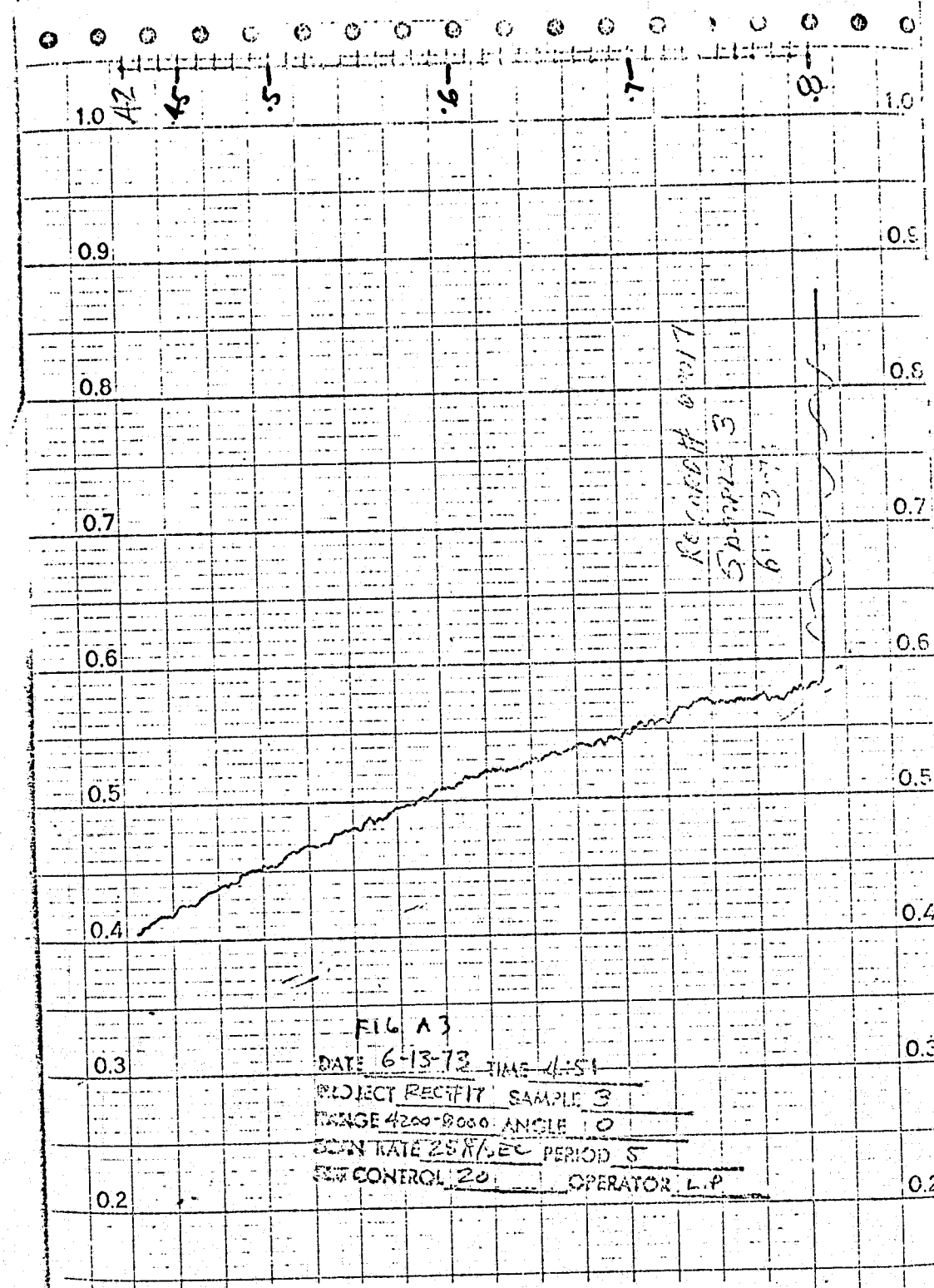


ORIGINAL PAGE IS
OF POOR QUALITY

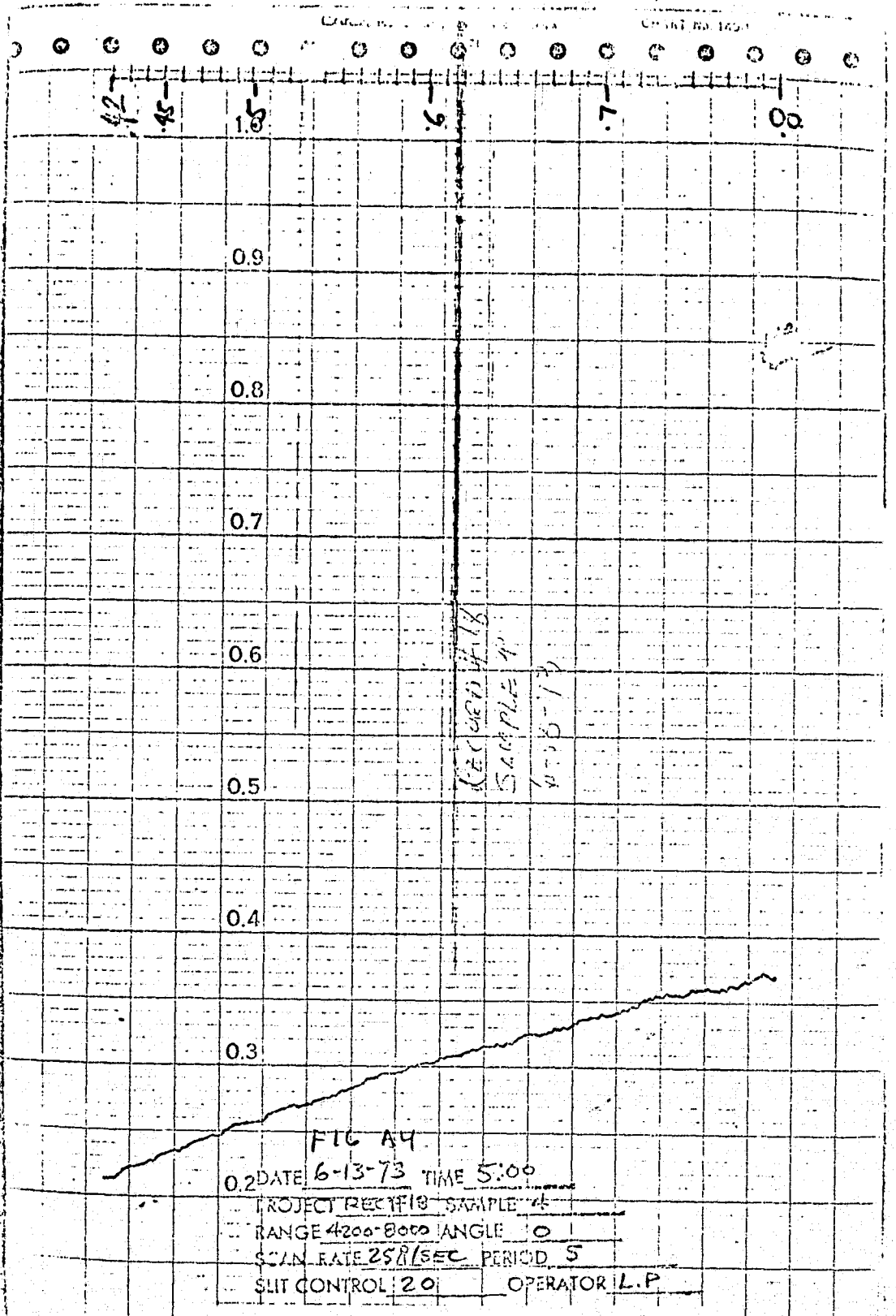


FIG A4

DATE 6-13-73 TIME 5:00

PROJECT RECTIFIED SAMPLE 4

RANGE 4200-8000 ANGLE 0

SCAN RATE 25Å/SEC PERIOD 5

SLIT CONTROL 20 OPERATOR L.P

PREPARED BY:

LABORATORY SIGNATURE ACQUISITION SYSTEM
DATA APPLICATIONS & PHYSICS BRANCH, EOD
NASA, LYNDON B. JOHNSON SPACE CENTER
HOUSTON, TEXAS

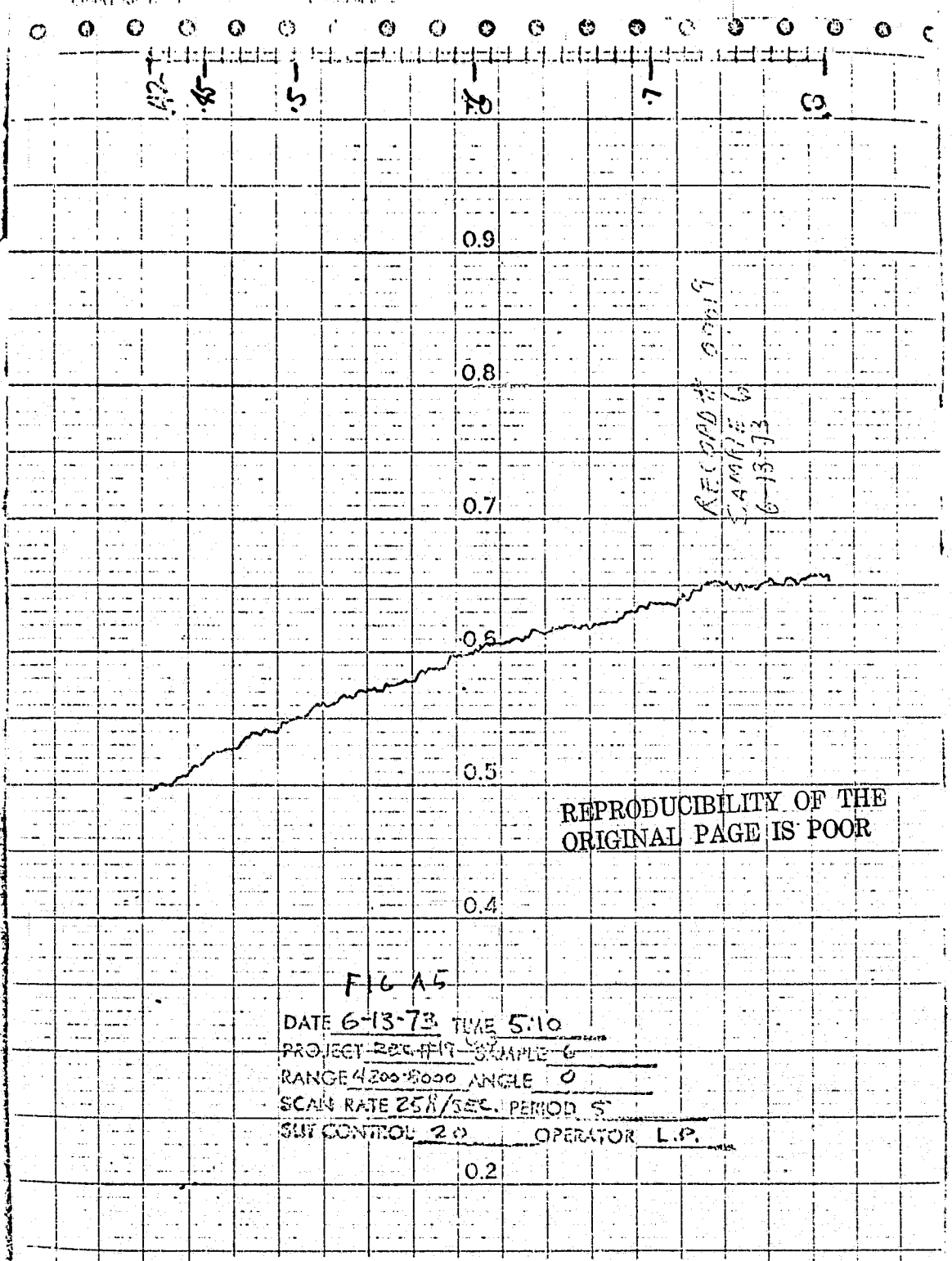


REPRODUCIBILITY OF THE ORIGINAL PAGE IS POOR

F16A5

DATE 6-13-73 TIME 5:10

PROJECT REC #19 SAMPLE 6

RANGE 4200-8000 ANGLE 0

SCAN RATE 25A/SEC. PERIOD 5

SUT CONTROL 20 OPERATOR L.P.

PREPARED BY:

LABORATORY SIGNATURE ACQUISITION SYSTEM
DATA APPLICATIONS & PHYSICS BRANCH, EOD
NASA, LYNDON B. JOHNSON SPACE CENTER
HOUSTON, TEXAS

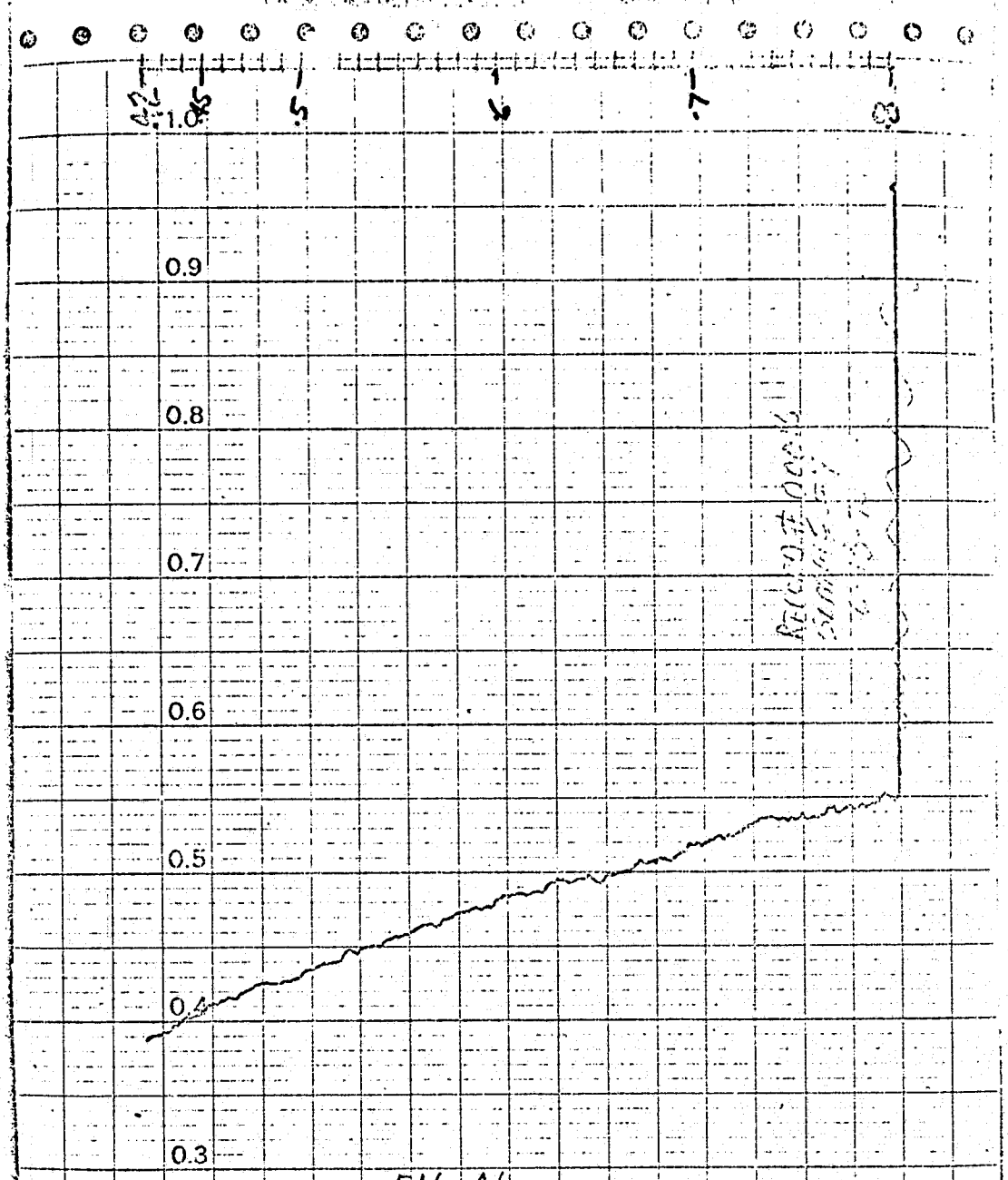


FIG A4

DATE 6-13-73 TIME 4:10

PROJECT RECAP 13 SAMPLE 7

RANGE 4200-8000 ANGLE 0

SCAN RATE 25N/SEC. PERIOD 5

SLIT CONTROL 20 OPERATOR L.P.

PREPARED BY:

LABORATORY SIGNATURE ACQUISITION SYSTEM
DATA APPLICATIONS & PHYSICS BRANCH, EOD
NASA, LYNDON B. JOHNSON SPACE CENTER
HOUSTON, TEXAS

60

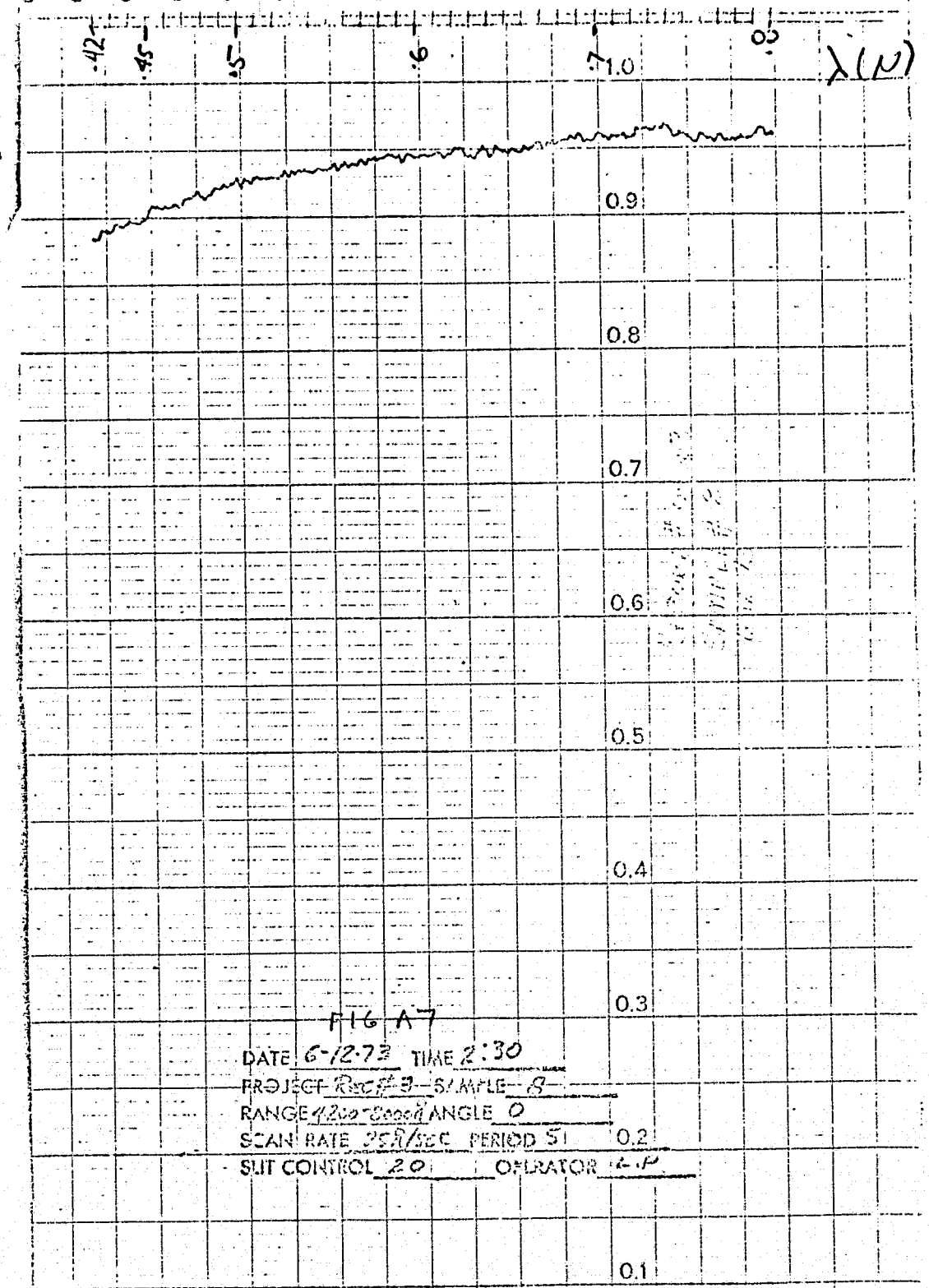


F16 A-7

DATE 6-12-73 TIME 2:30

PROJECT Ref #3 SAMPLE 8

RANGE 4.2 to 2.6 ANGLE 0

SCAN RATE 25A/SEC PERIOD 51

SLIT CONTROL 20 OPERATOR L.P

PREPARED BY:

LABORATORY SIGNATURE ACQUISITION SYSTEM
DATA APPLICATIONS & PHYSICS BRANCH, EOD
NASA, LYNDON B. JOHNSON SPACE CENTER
HOUSTON, TEXAS

CHART No. 1400

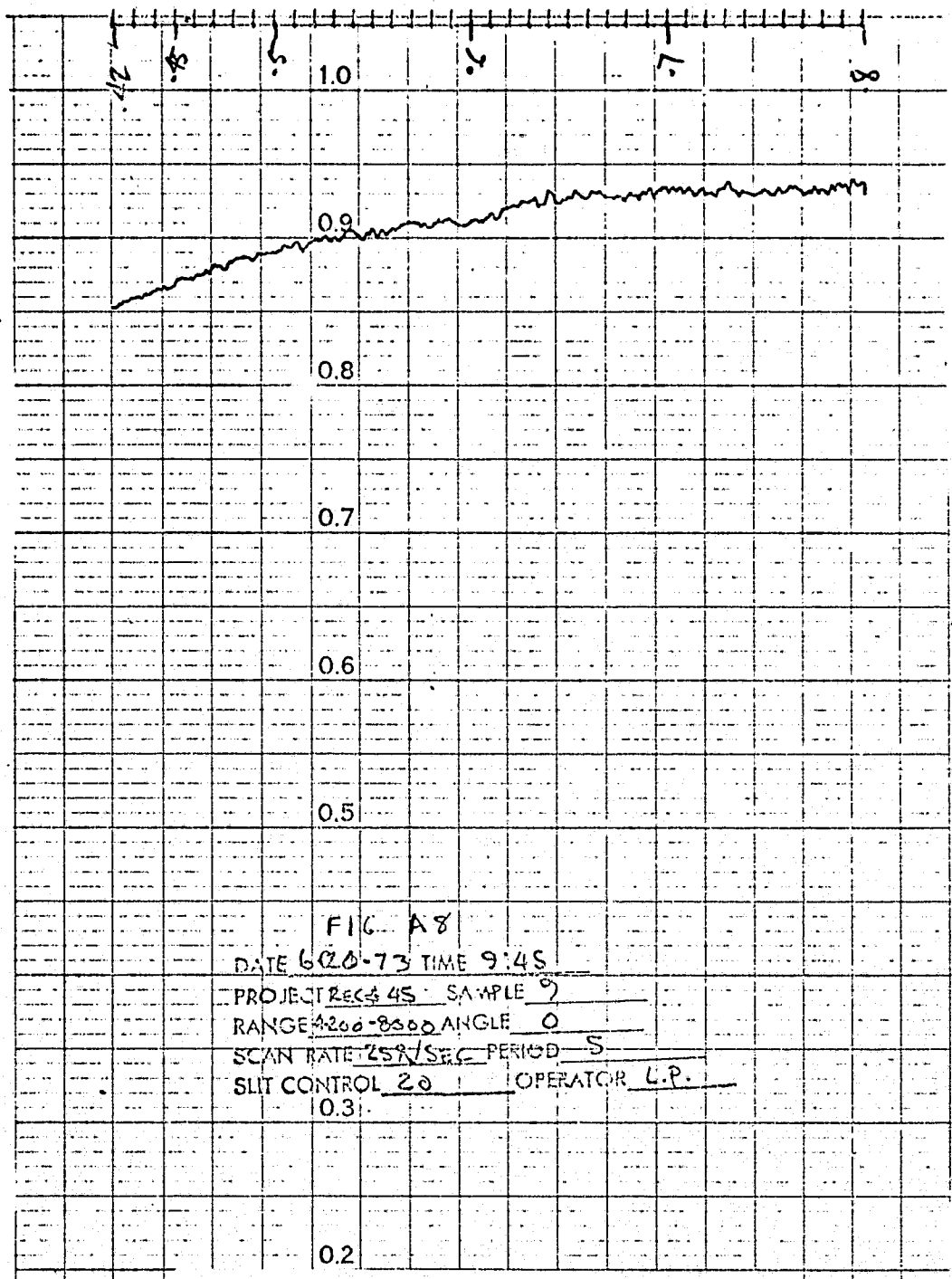


FIG A8

DATE 6-20-73 TIME 9:45

PROJECT Recs 45 SAMPLE 9

RANGE 4200-8500 ANGLE 0

SCAN RATE 25Å/SEC PERIOD 5

SLIT CONTROL 20 OPERATOR L.P.

PREPARED BY:

LABORATORY SIGNATURE ACQUISITION SYSTEM
DATA APPLICATIONS & PHYSICS BRANCH, EOD
NASA, LYNDON B. JOHNSON SPACE CENTER
HOUSTON, TEXAS

REPRODUCIBILITY OF THE ORIGINAL PAGE IS POOR

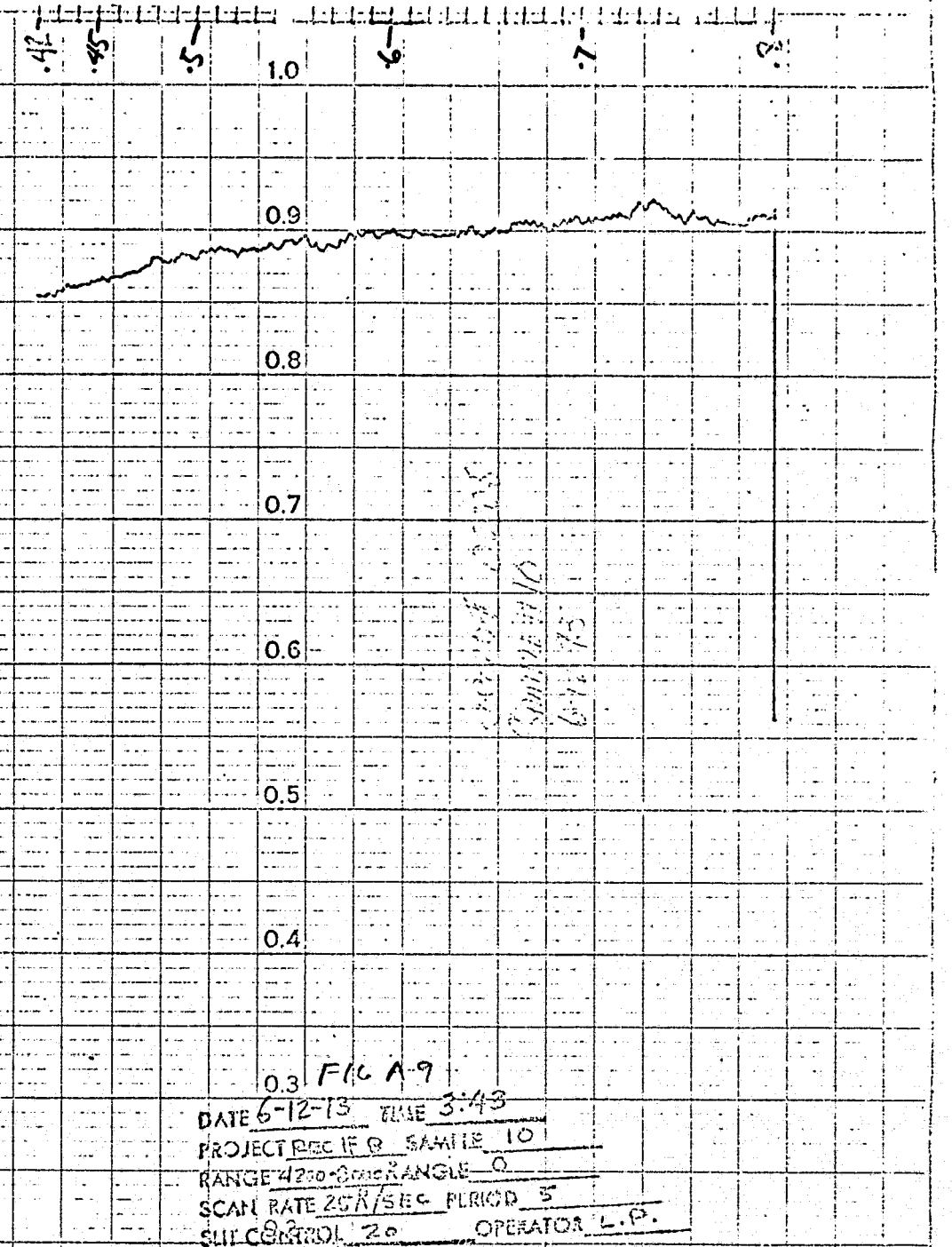


FIG A-9

DATE 6-12-13 TIME 3:43
PROJECT REC IF 8 SAMPLE 10
RANGE 4250-8000 RANGE 0
SCAN RATE 25 R/SEC PERIOD 5
SLIT CONTROL 20 OPERATOR L.P.

PREPARED BY:

LABORATORY SIGNATURE ACQUISITION SYSTEM
DATA APPLICATIONS & PHYSICS BRANCH, EOD
NASA, LYNDON B. JOHNSON SPACE CENTER
HOUSTON, TEXAS

ORIGINAL PAGE IS
OF POOR QUALITY

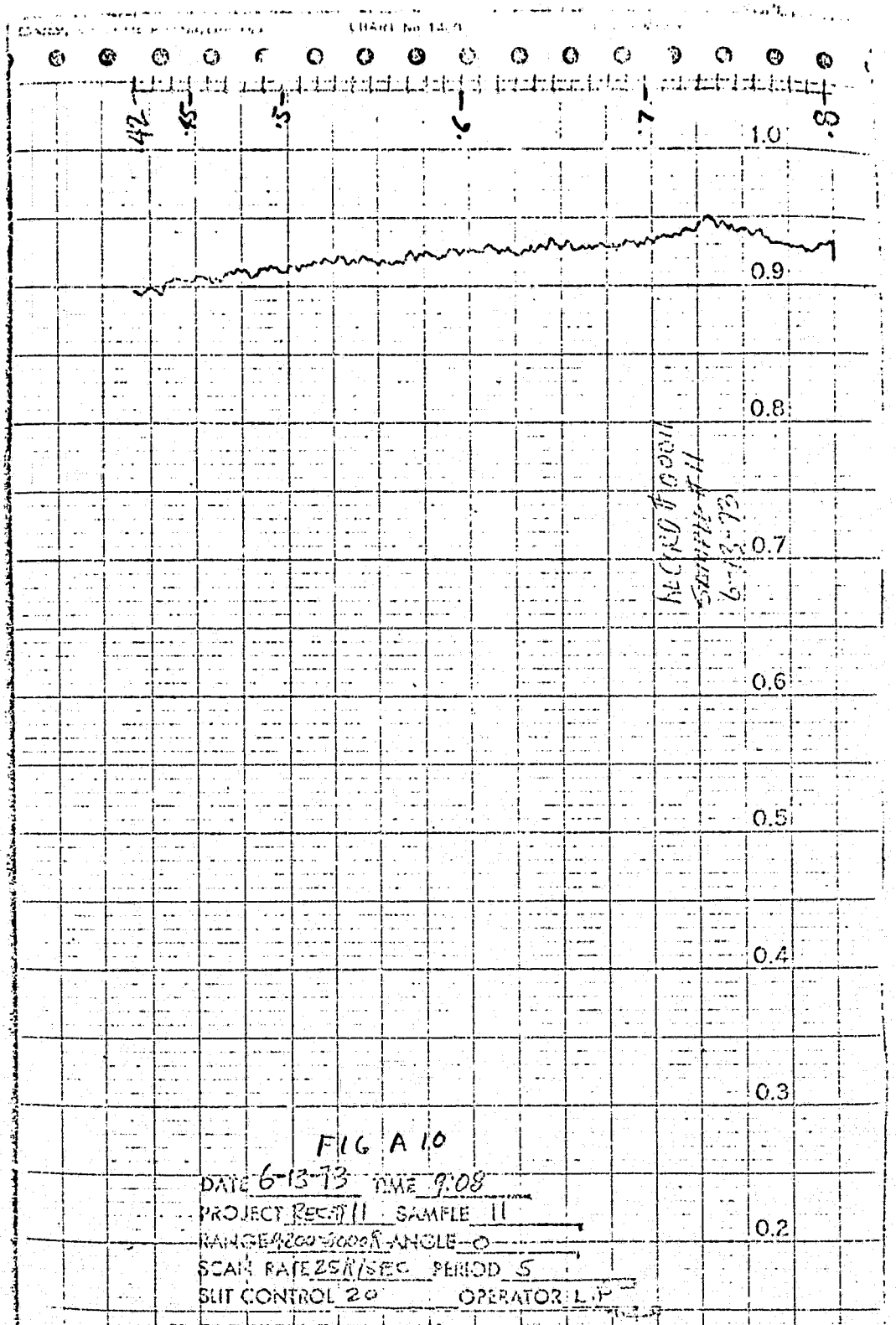


FIG A 10

DATE 6-13-73 TIME 9:08

PROJECT Recall SAMPLE 11

RANGE 2000-3000Å ANGLE 0

SCAN RATE 25Å/SEC PERIOD 5

SLIT CONTROL 20 OPERATOR L.P

PREPARED BY:

LABORATORY SIGNATURE ACQUISITION SYSTEM
DATA APPLICATIONS & PHYSICS BRANCH, EOD
NASA, LYNDON B. JOHNSON SPACE CENTER
HOUSTON, TEXAS

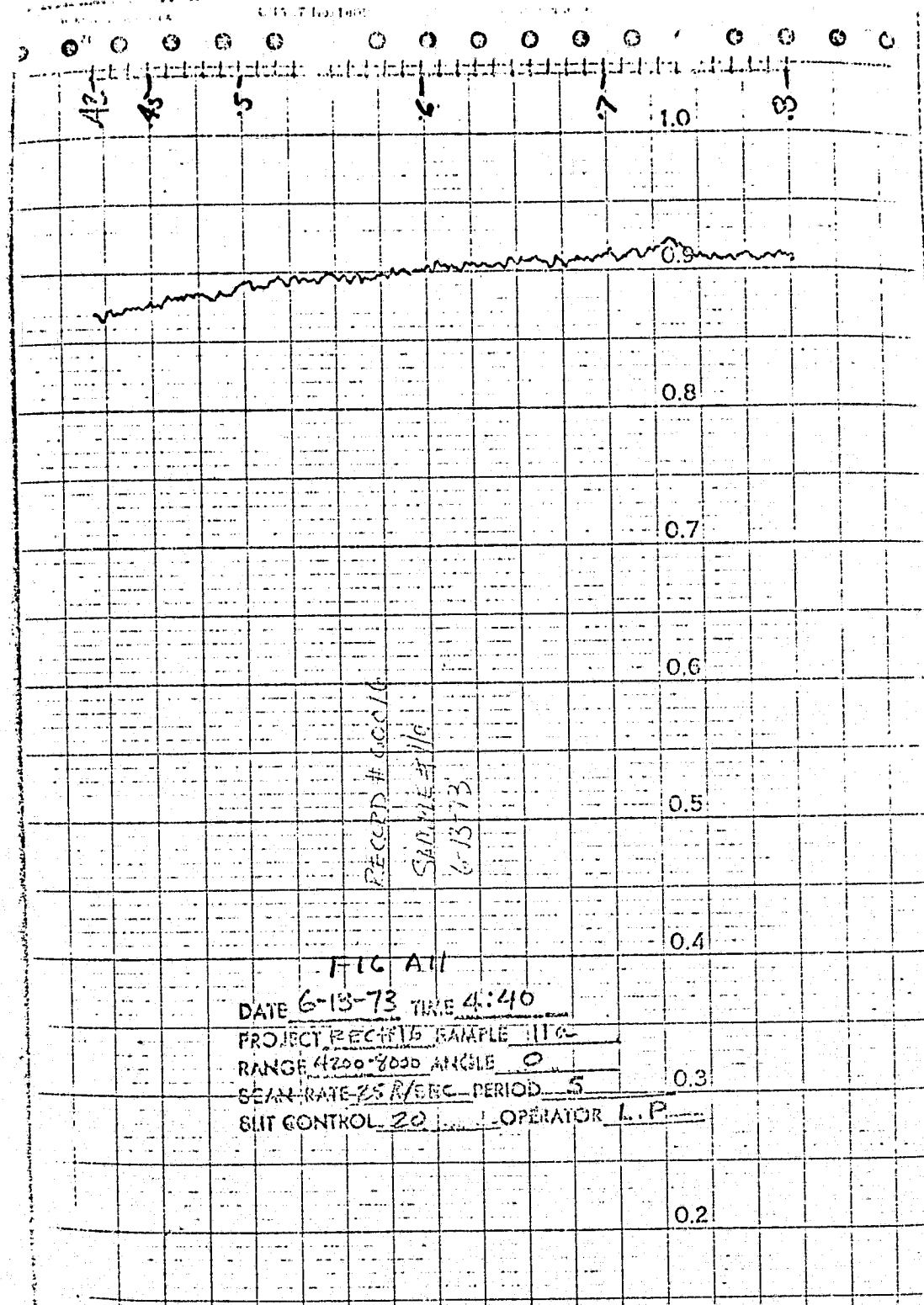


PREPARED BY:

LABORATORY SIGNATURE ACQUISITION SYSTEM
DATA APPLICATIONS & PHYSICS BRANCH, EOD
NASA, LYNDON B. JOHNSON SPACE CENTER
HOUSTON, TEXAS

ORIGINAL PAGE IS
OF POOR QUALITY

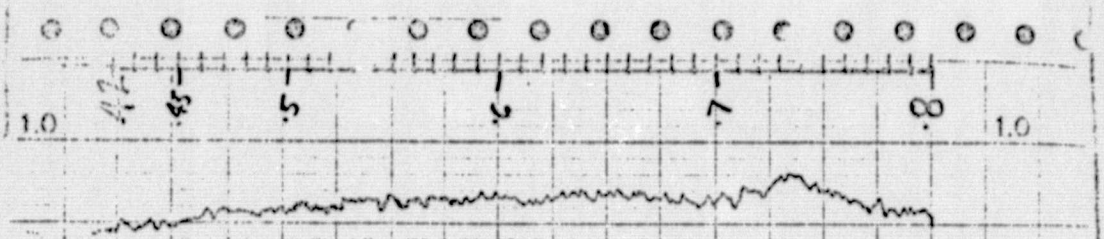


1.0 0.9 0.8 0.7 0.6 0.5 0.4 0.3 0.2 0.1 0.0

RECORD #12
SAMPLE 12
6-13-73

FIG A12

DATE 6-13-73 TIME 9:20
PROJECT REC #12 SAMPLE 12
RANGE 4000-8000 ANGLE 0
SCAN RATE 2SW/SEC PERIOD 5
SLIT CONTROL 20 OPERATOR L.P.

PREPARED BY:

LABORATORY SIGNATURE ACQUISITION SYSTEM
DATA APPLICATIONS & PHYSICS BRANCH, EOD
NASA, LYNDON B. JOHNSON SPACE CENTER
HOUSTON, TEXAS

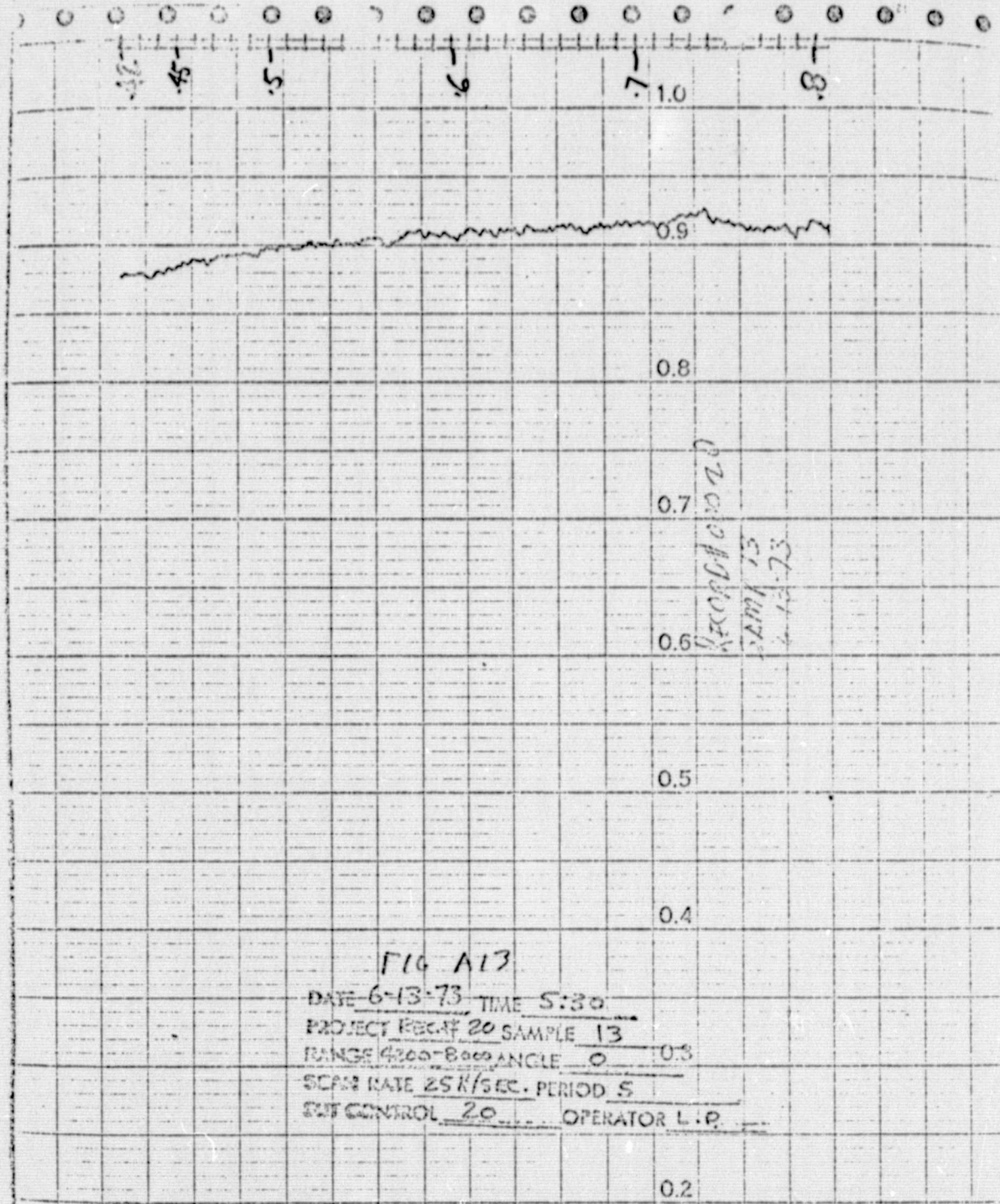


PREPARED BY:

LABORATORY SIGNATURE ACQUISITION SYSTEM
DATA APPLICATIONS & PHYSICS BRANCH, EOD
NASA, LYNDON B. JOHNSON SPACE CENTER
HOUSTON, TEXAS

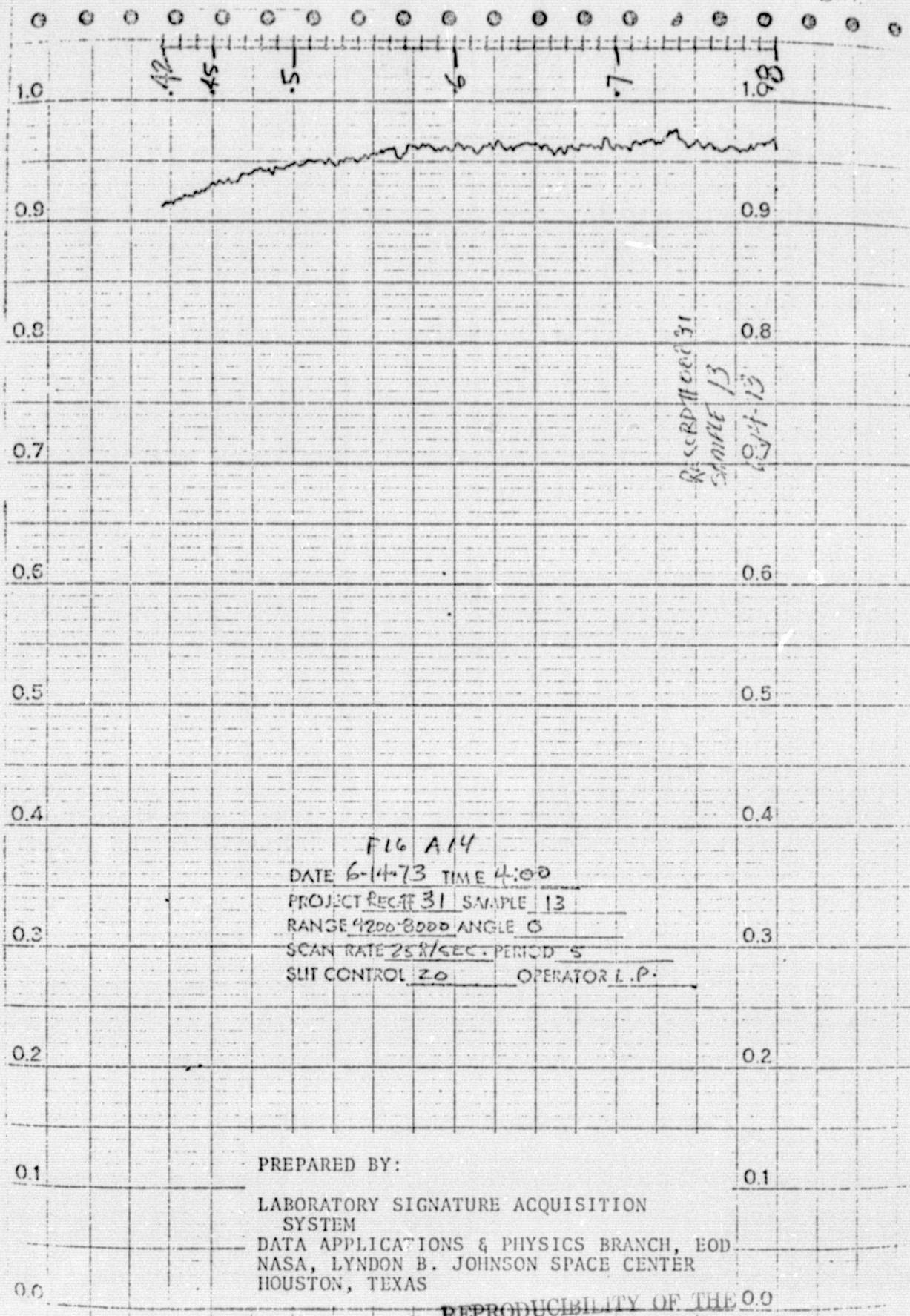


FIG A14

DATE 6-14-73 TIME 4:00
PROJECT Rec# 31 SAMPLE 13
RANGE 9200-8000 ANGLE 0
SCAN RATE 25 K/SEC. PERIOD 5
SLIT CONTROL 20 OPERATOR L.P.

PREPARED BY:

LABORATORY SIGNATURE ACQUISITION SYSTEM
DATA APPLICATIONS & PHYSICS BRANCH, EOD
NASA, LYNDON B. JOHNSON SPACE CENTER
HOUSTON, TEXAS

REPRODUCIBILITY OF THE ORIGINAL PAGE IS POOR

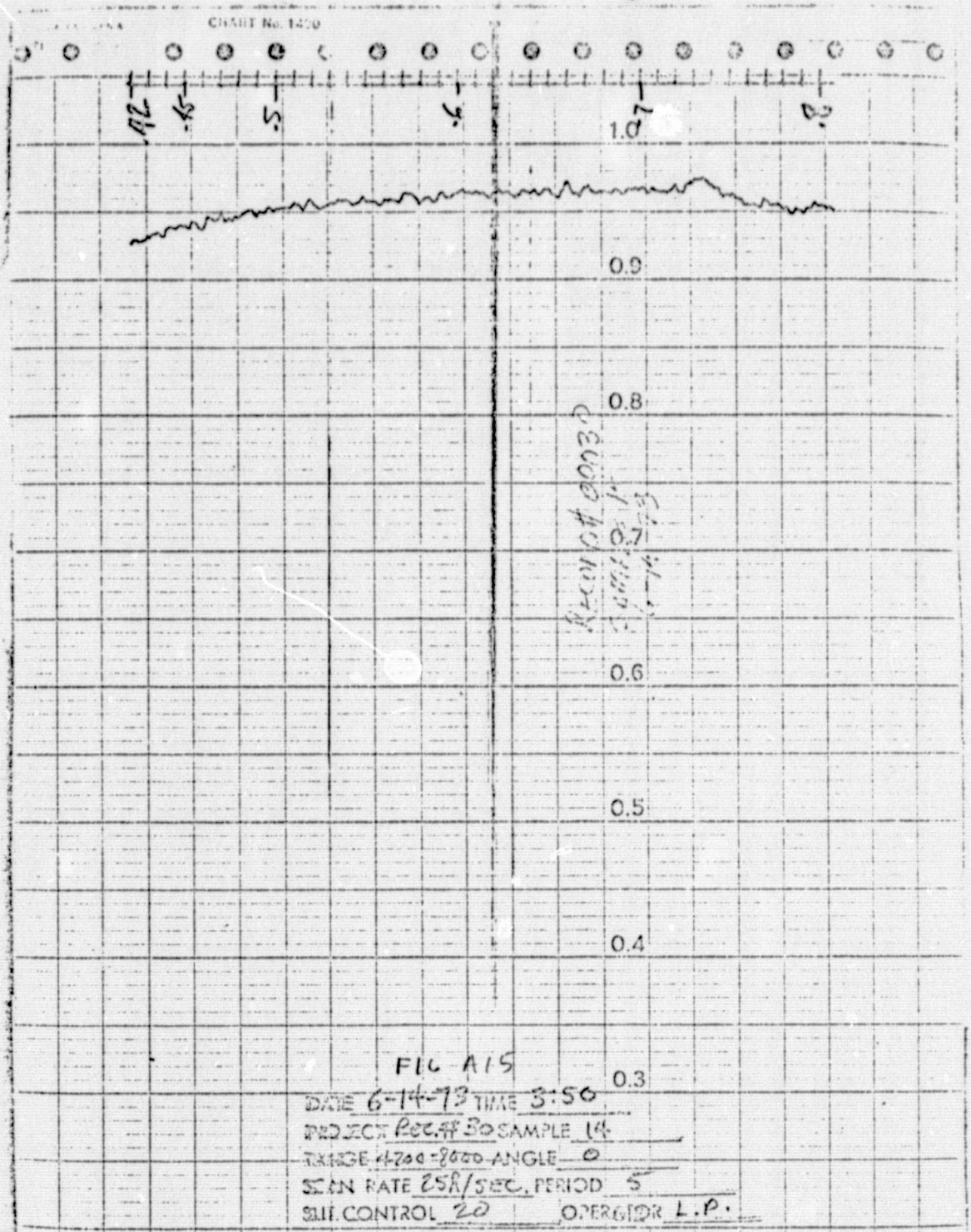


FIG A15

DATE 6-14-73 TIME 3:50
PROJECT Rec.# 30 SAMPLE 14
RANGE 4700-8000 ANGLE 0
SCAN RATE 25A/SEC. PERIOD 5
SIG. CONTROL 20 OPERATOR L.P.

PREPARED BY:

LABORATORY SIGNATURE ACQUISITION SYSTEM
DATA APPLICATIONS & PHYSICS BRANCH, EOD
NASA, LYNDON B. JOHNSON SPACE CENTER
HOUSTON, TEXAS

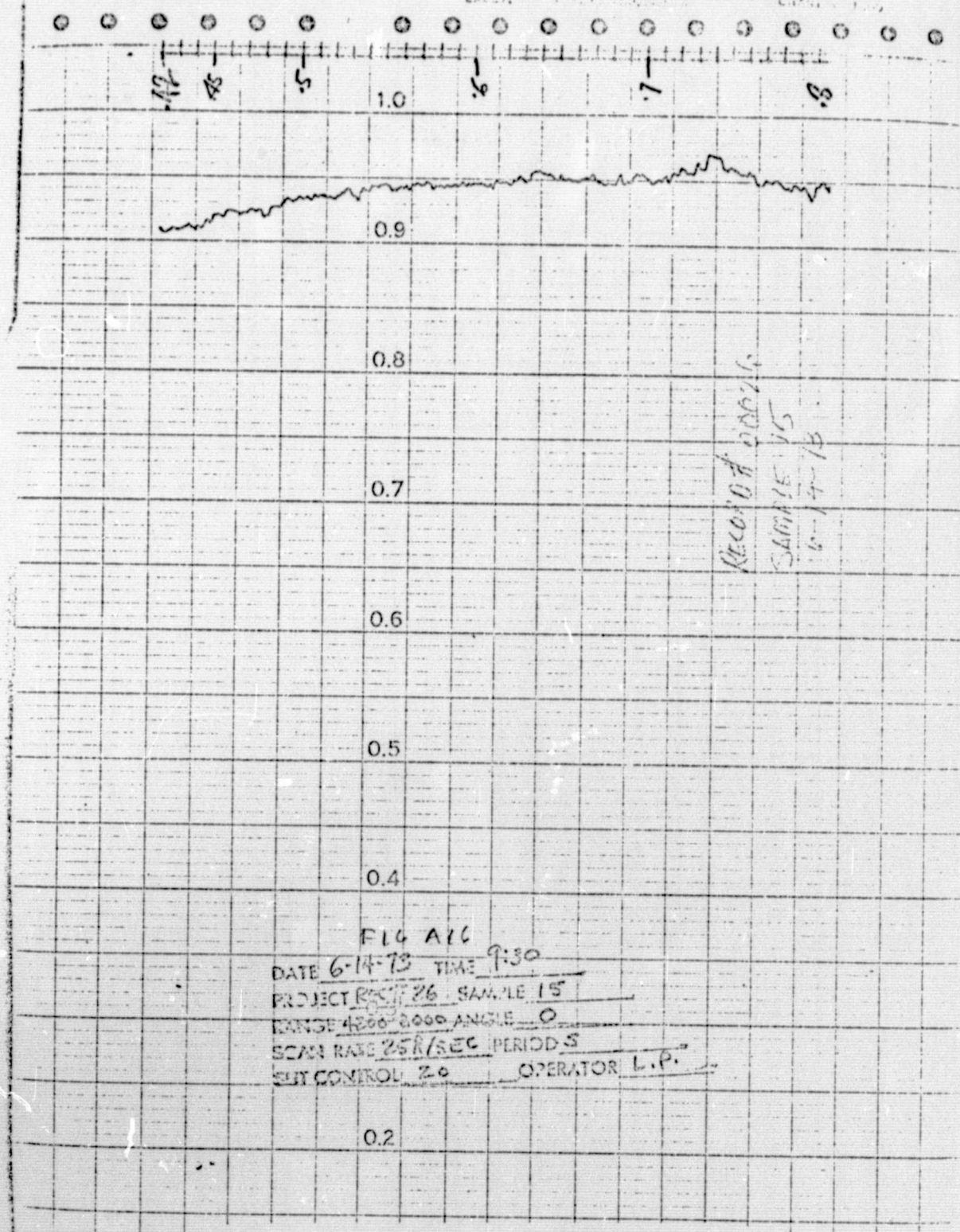


FIG A11

DATE 6-14-73 TIME 9:30
PROJECT RSCF 26 SAMPLE 15
RANGE 4000-8000 ANGLE 0
SCAN RATE 25 R/SEC PERIOD 5
SUN CONTROL 20 OPERATOR L.P.

PREPARED BY:

LABORATORY SIGNATURE ACQUISITION SYSTEM
DATA APPLICATIONS & PHYSICS BRANCH, EOD
NASA, LYNDON B. JOHNSON SPACE CENTER
HOUSTON, TEXAS

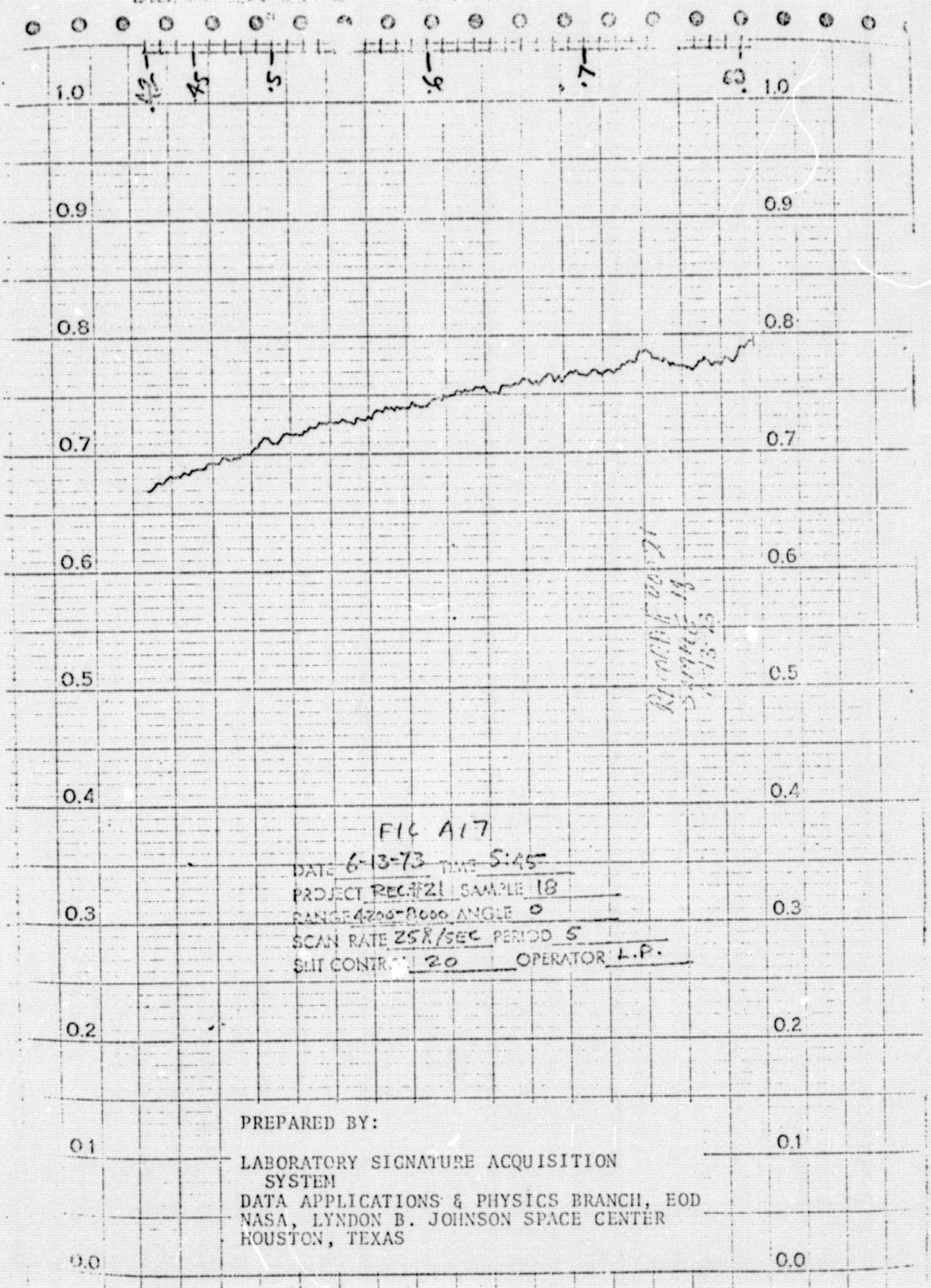


FIG A17

DATE 6-13-73 TIME 5:45

PROJECT REC #21 SAMPLE 18

RANGE 4200-8000 ANGLE 0

SCAN RATE 25R/SEC PERIOD 5

SLIT CONTROL 20 OPERATOR L.P.

PREPARED BY:

LABORATORY SIGNATURE ACQUISITION SYSTEM
DATA APPLICATIONS & PHYSICS BRANCH, EOD
NASA, LYNDON B. JOHNSON SPACE CENTER
HOUSTON, TEXAS

REPRODUCIBILITY OF THE
ORIGINAL PAGE IS POOR

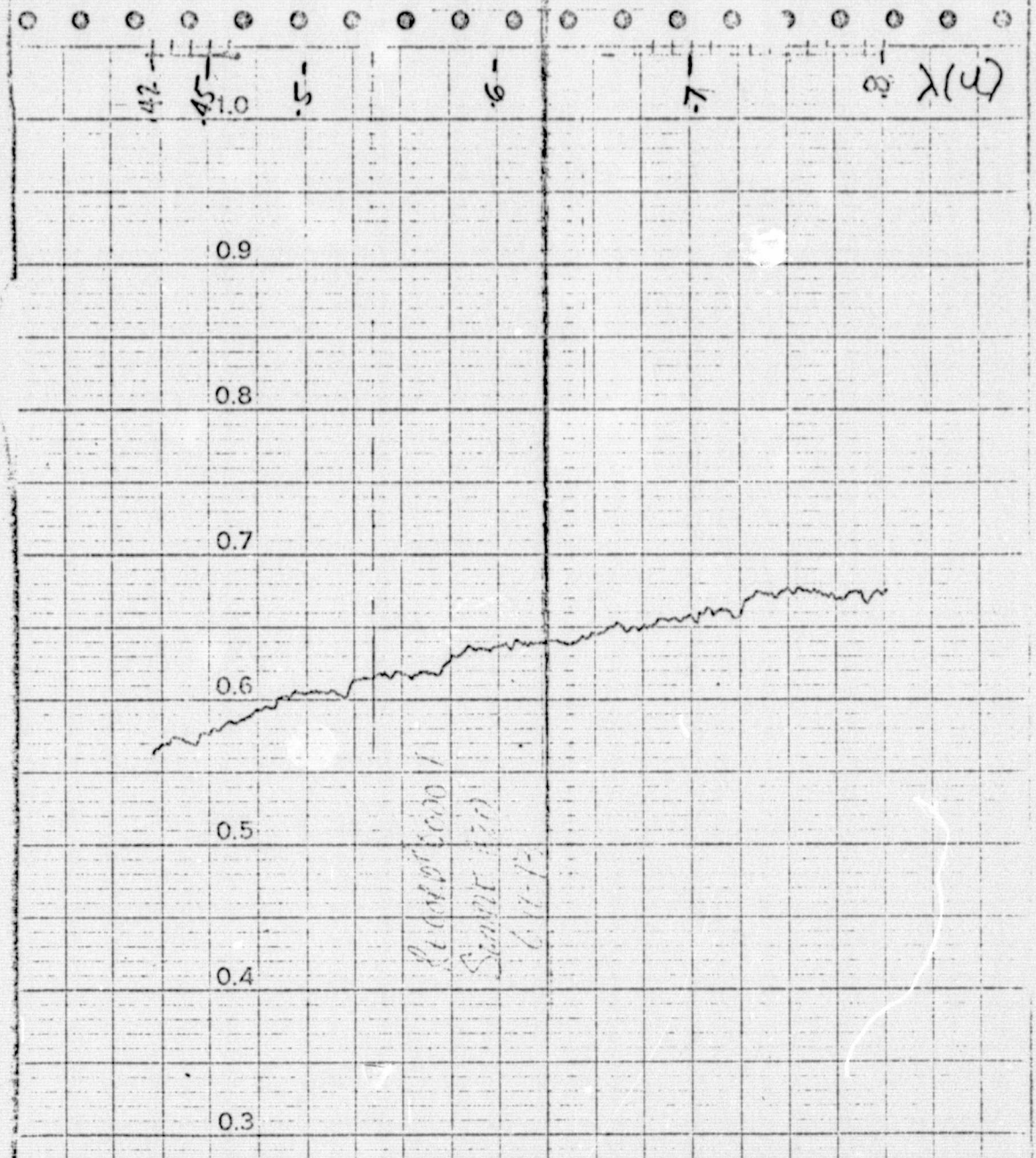


FIG A18

DATE 6-12-73 TIME 3:35
PROJECT REC 47 SAMPLE 20
RANGE 4300-2000Å ANGLE 0
SCAN RATE 25Å/SEC PERIOD 5
SLIT CONTROL 20 OPERATOR L.P.

PREPARED BY:

LABORATORY SIGNATURE ACQUISITION SYSTEM
DATA APPLICATIONS & PHYSICS BRANCH, EOD
NASA, LYNDON B. JOHNSON SPACE CENTER
HOUSTON, TEXAS

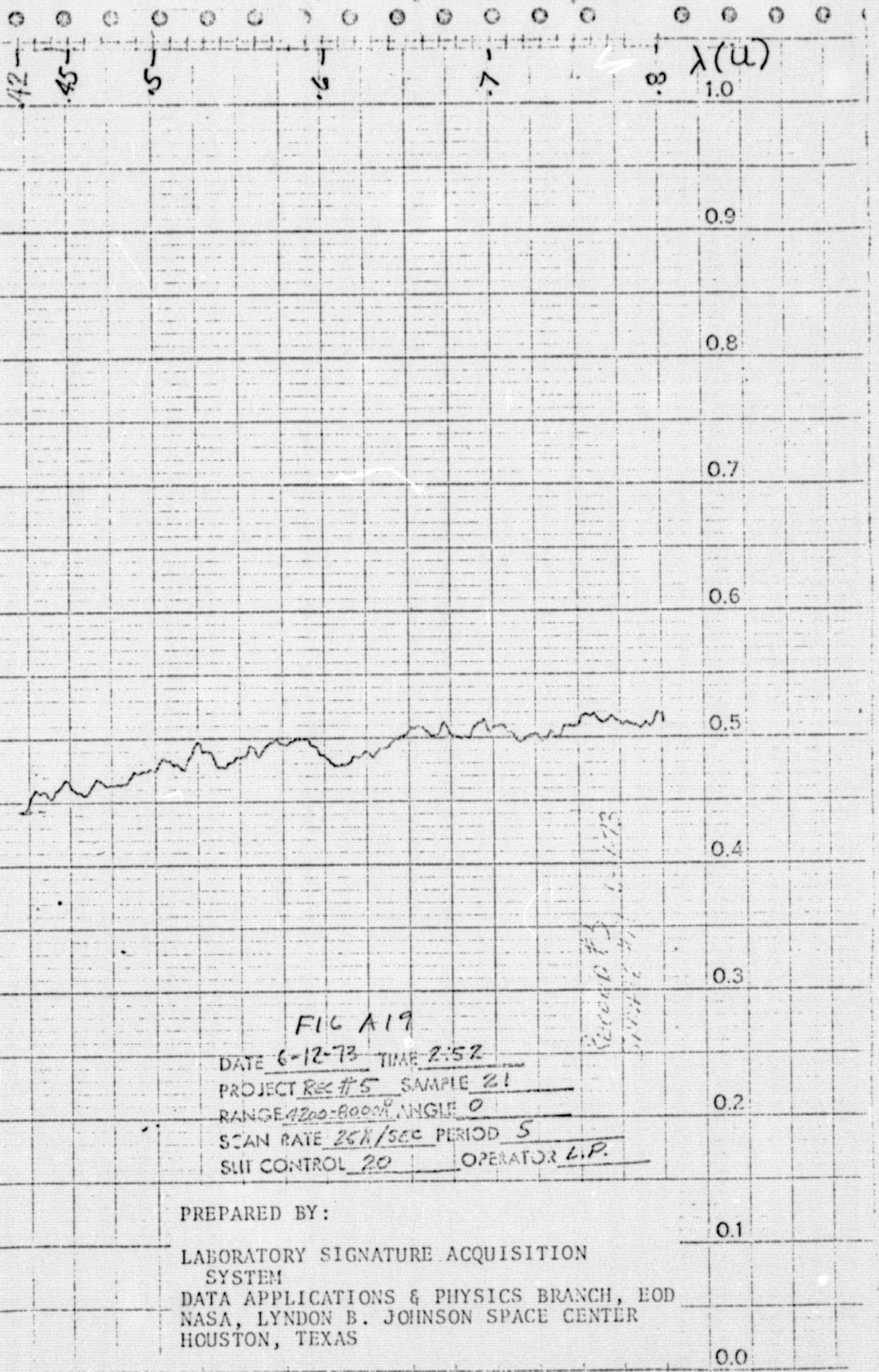


FIG A19

DATE 6-12-73 TIME 2:52
PROJECT Rec #5 SAMPLE 21
RANGE 4200-8000Å ANGLE 0
SCAN RATE 25Å/sec PERIOD 5
SLIT CONTROL 20 OPERATOR L.P.

PREPARED BY:

LABORATORY SIGNATURE ACQUISITION SYSTEM
DATA APPLICATIONS & PHYSICS BRANCH, EOD
NASA, LYNDON B. JOHNSON SPACE CENTER
HOUSTON, TEXAS

REPRODUCIBILITY OF TH
ORIGINAL PAGE IS POOR

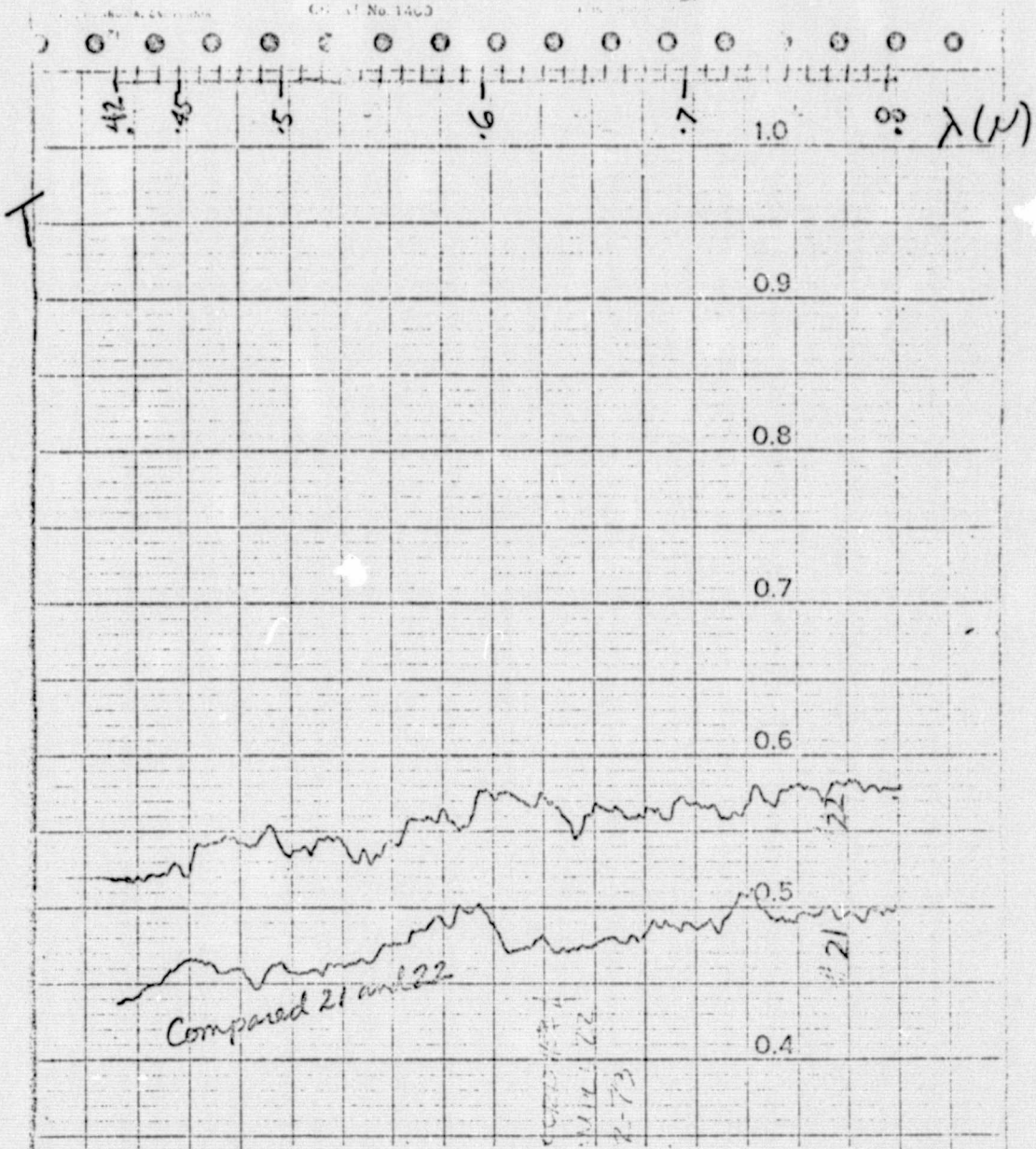


PREPARED BY:

LABORATORY SIGNATURE ACQUISITION SYSTEM
DATA APPLICATIONS & PHYSICS BRANCH, EOD
NASA, LYNDON B. JOHNSON SPACE CENTER
HOUSTON, TEXAS

FIG. A 20

DATE 6-12-73 TIME 2:37
PROJECT Rec #4 · SAMPLE 22
RANGE 4,000-700 ANGLE 0
SCAN RATE [illegible] OD 5
SUI CONTROL 20 [illegible] OPERATOR L.P.

74

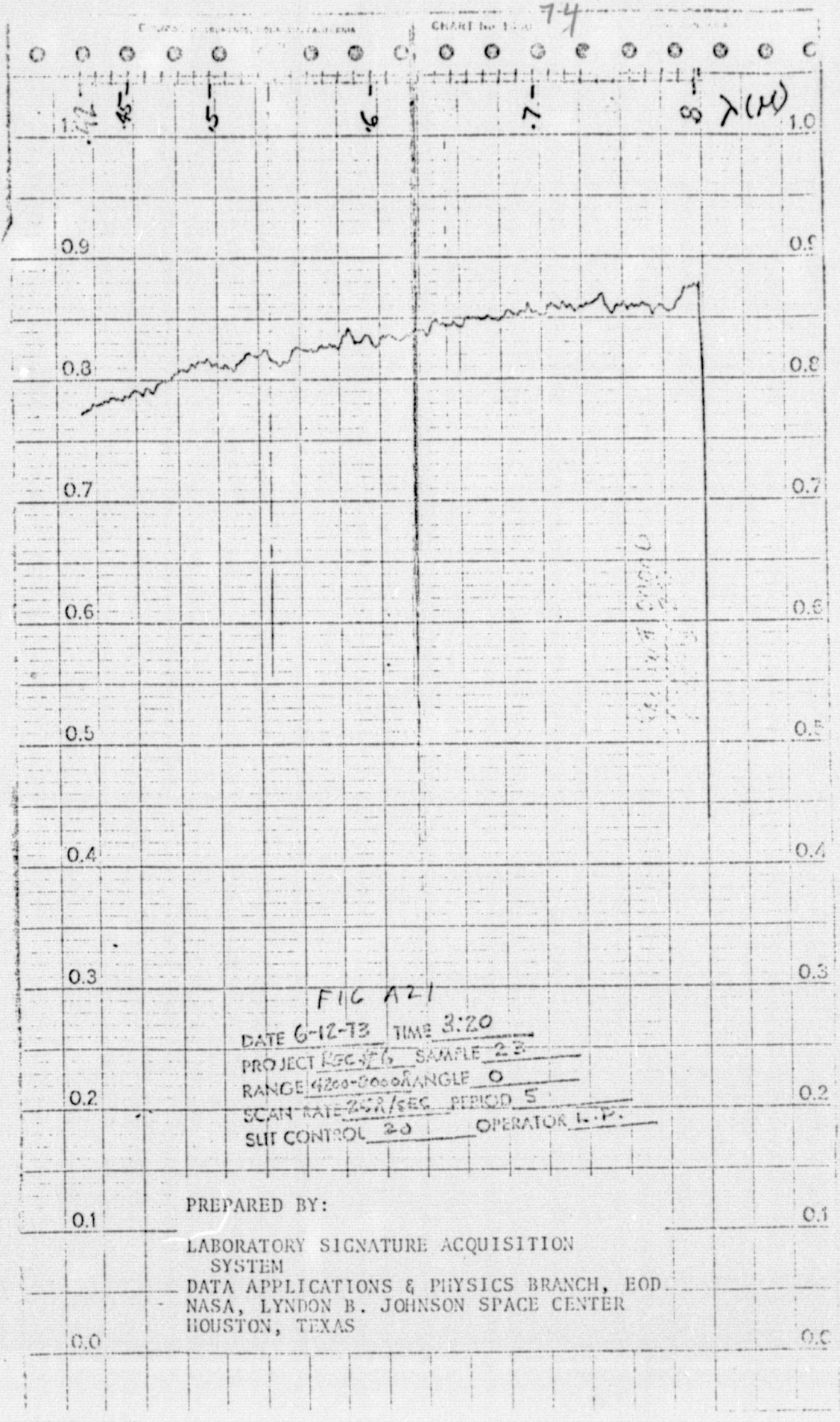
CHART No. 1-10
1.0
0.9
0.8
0.7
0.6
0.5
0.4
0.3
0.2
0.1
0.0
λ(μ)
4.5
5
6
7
8
DATE 6-12-73 TIME 3:20
PROJECT RGCSE SAMPLE 23
RANGE 4200-8000Å ANGLE 0
SCAN RATE 2Å/SEC PERIOD 5
SLIT CONTROL 20 OPERATOR L.P.
PREPARED BY:
LABORATORY SIGNATURE ACQUISITION SYSTEM
DATA APPLICATIONS & PHYSICS BRANCH, EOD
NASA, LYNDON B. JOHNSON SPACE CENTER
HOUSTON, TEXAS

FIG A21

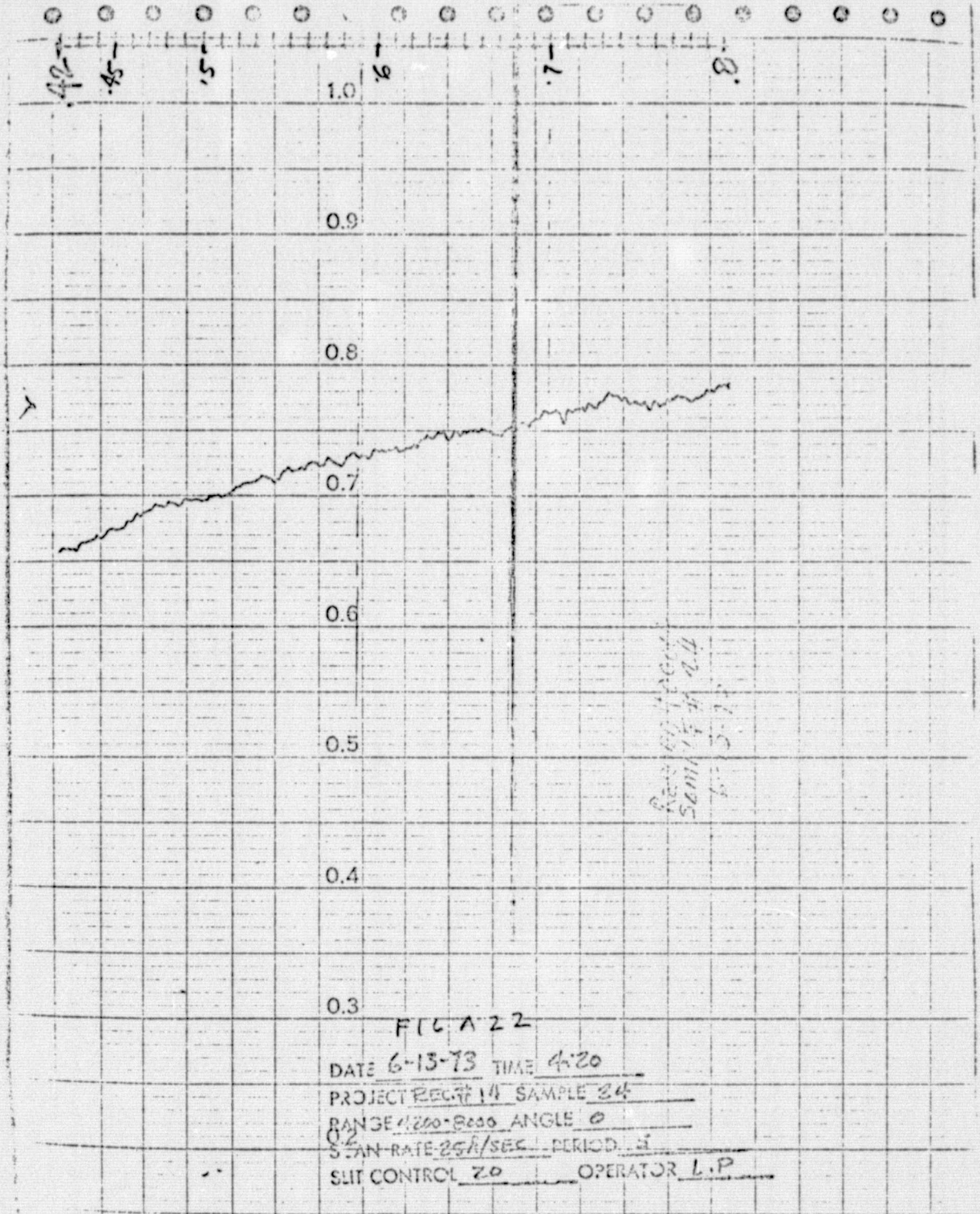


FIL A22

DATE 6-13-73 TIME 4:20

PROJECT REC #14 SAMPLE 24

RANGE 4200-8000 ANGLE 0

SCAN RATE 25A/SEC PERIOD 3

SLIT CONTROL 20 OPERATOR L.P

PREPARED BY:

LABORATORY SIGNATURE ACQUISITION SYSTEM
DATA APPLICATIONS & PHYSICS BRANCH, EOD
NASA, LYNDON B. JOHNSON SPACE CENTER
HOUSTON, TEXAS

ORIGINAL PAGE IS
OF POOR QUALITY

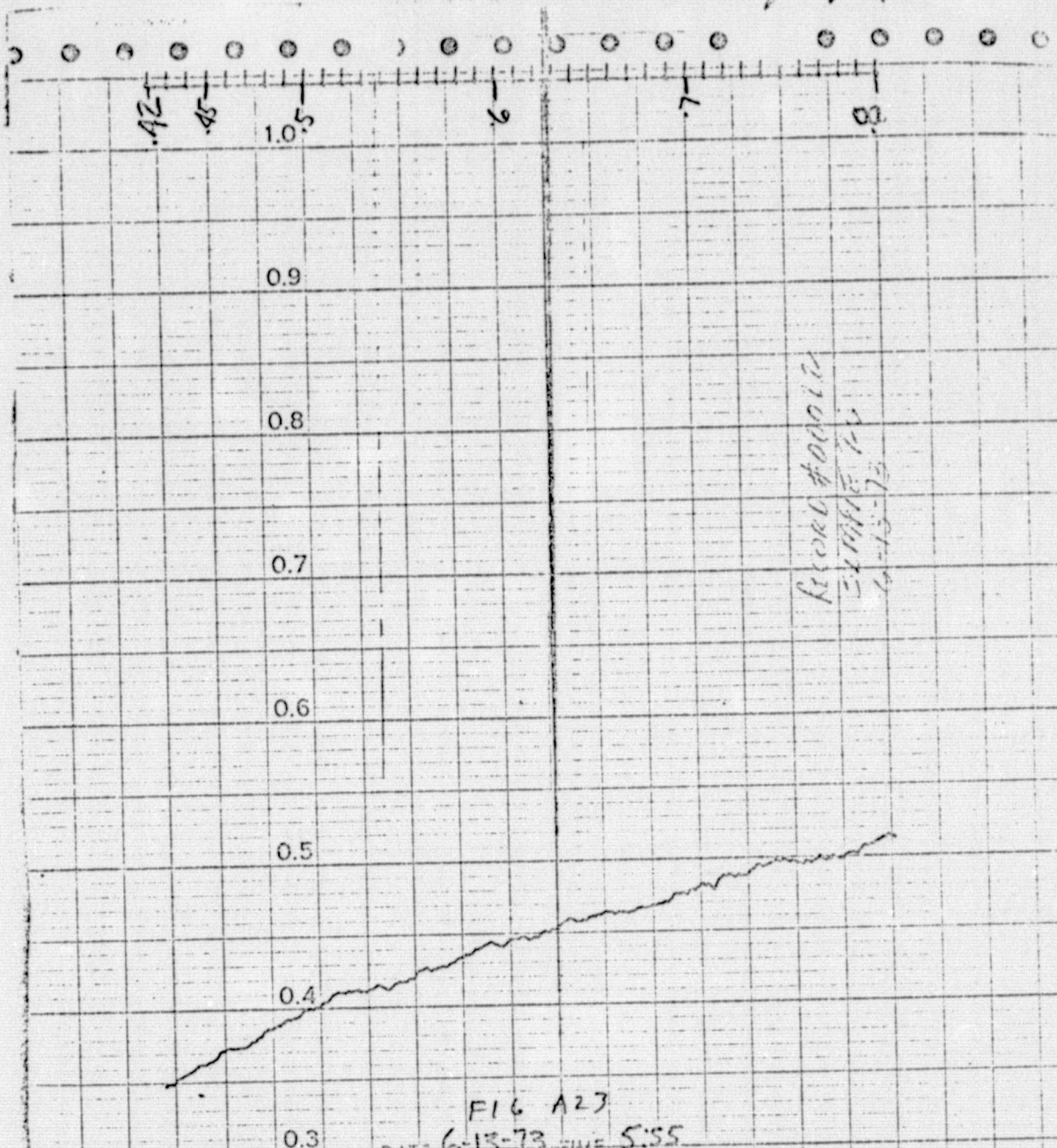


FIG A23

DATE 6-13-73 TIME 5:55
PROJECT Rec # 22 SAMPLE 26
RANGE 4200-8000 ANGLE 0
SCAN RATE 25X/SEC PERIOD 5
SLIT CONTROL 20 OPERATOR L.P.

PREPARED BY:

LABORATORY SIGNATURE ACQUISITION SYSTEM
DATA APPLICATIONS & PHYSICS BRANCH, EOD
NASA, LYNDON B. JOHNSON SPACE CENTER
HOUSTON, TEXAS

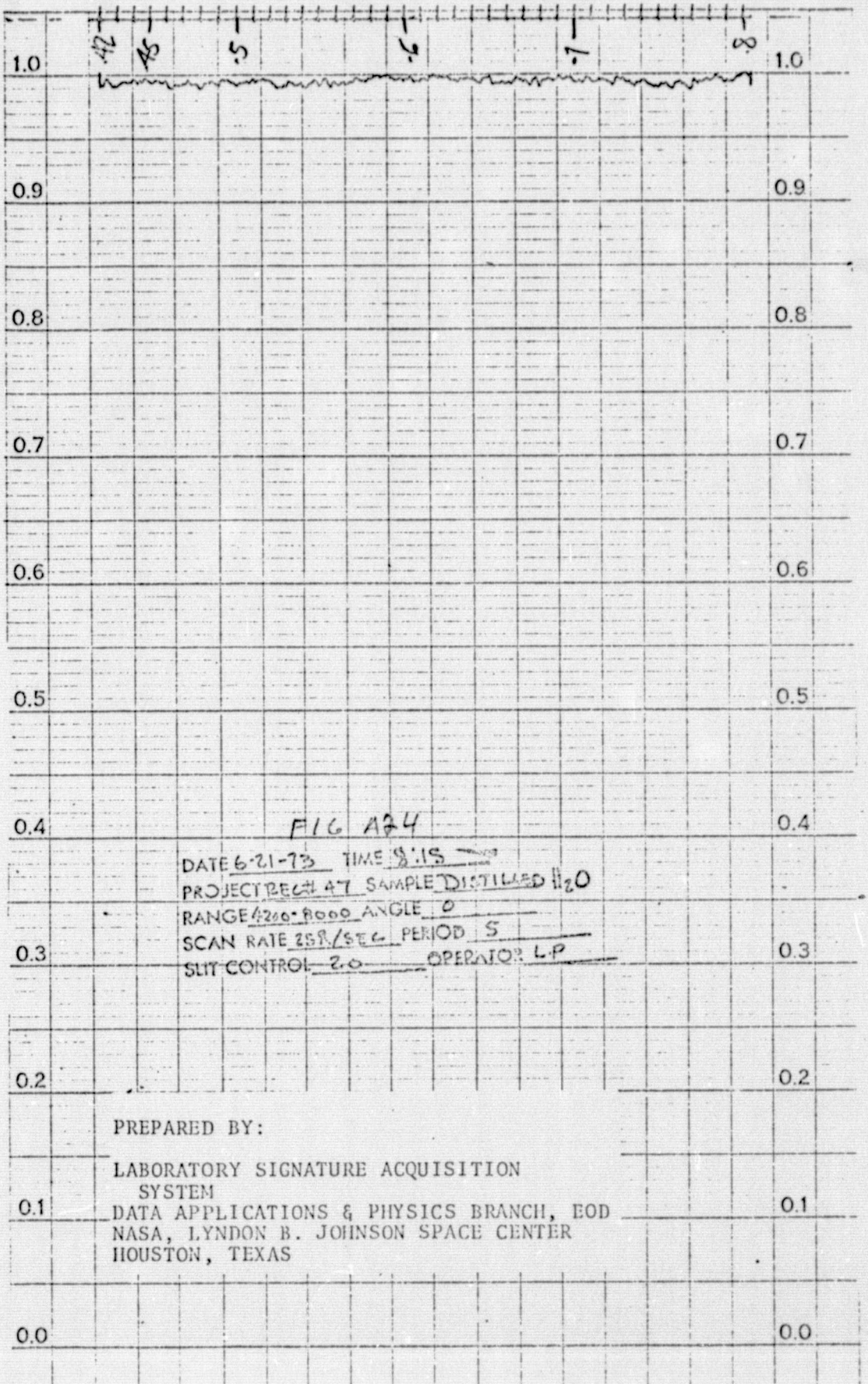
1.0
.42
.45
.5
.6
.7
.8
0.9
0.8
0.7
0.6
0.5
0.4
0.3
0.2
0.1
0.0
FIG A24
DATE 6-21-73 TIME 8:15
PROJECT REC# 47 SAMPLE DISTILLED H2O
RANGE 4200-8000 ANGLE 0
SCAN RATE 25R/SEC PERIOD 5
SLIT CONTROL 2.0 OPERATOR L.P
PREPARED BY:
LABORATORY SIGNATURE ACQUISITION SYSTEM
DATA APPLICATIONS & PHYSICS BRANCH, EOD
NASA, LYNDON B. JOHNSON SPACE CENTER
HOUSTON, TEXAS

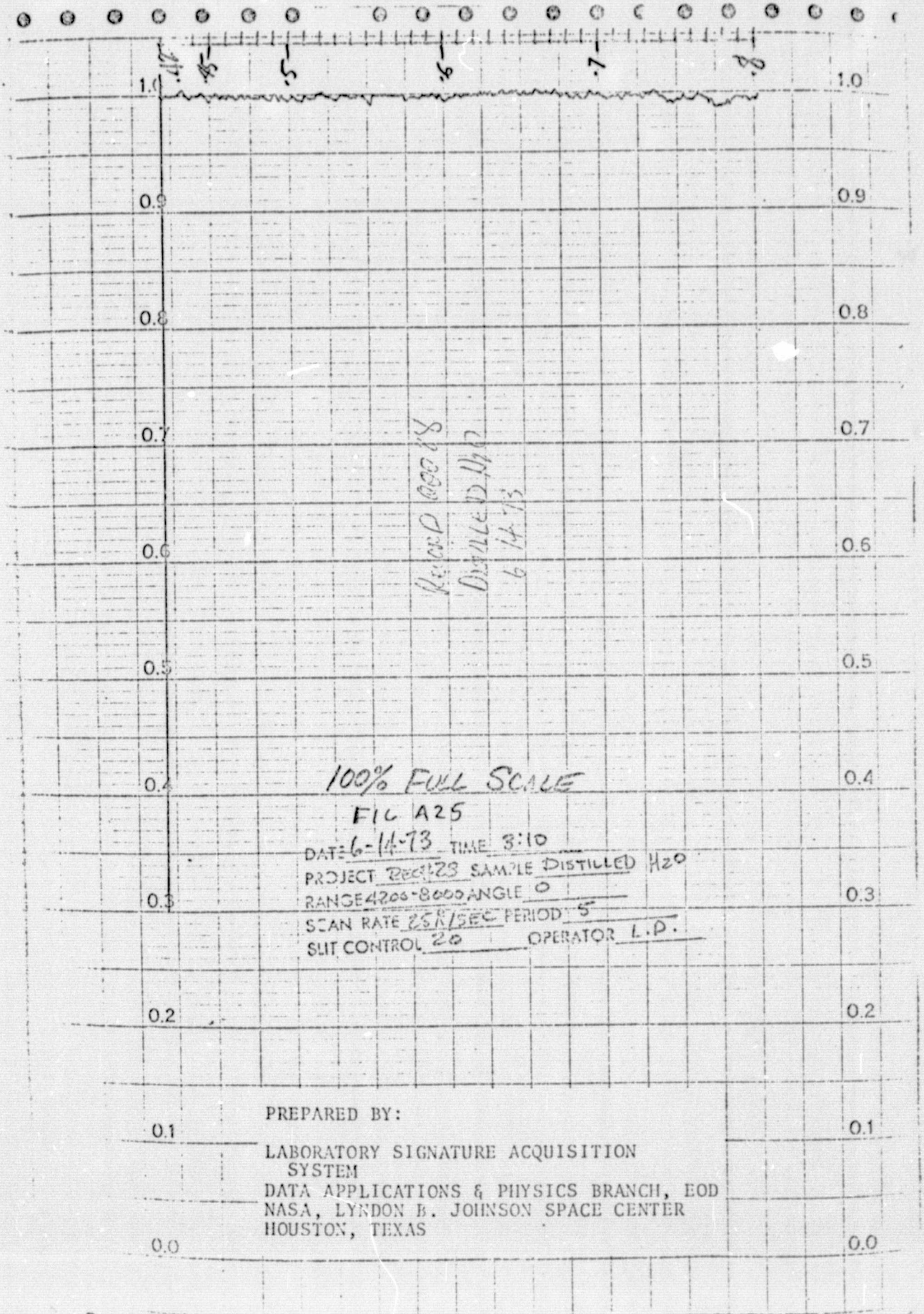
4
5
6
7
8
1.0
0.9
0.8
0.7
0.6
0.5
0.4
0.3
0.2
0.1
0.0
RECORD 0000 18
DISTILLED H2O
6 14 73
100% FULL SCALE
FIG A25
DATE 6-14-73 TIME 3:10
PROJECT Rec#23 SAMPLE DISTILLED H2O
RANGE 4200-8000 ANGLE 0
SCAN RATE 25A/SEC PERIOD 5
SLIT CONTROL 20 OPERATOR L.D.
PREPARED BY:
LABORATORY SIGNATURE ACQUISITION SYSTEM
DATA APPLICATIONS & PHYSICS BRANCH, EOD
NASA, LYNDON B. JOHNSON SPACE CENTER
HOUSTON, TEXAS

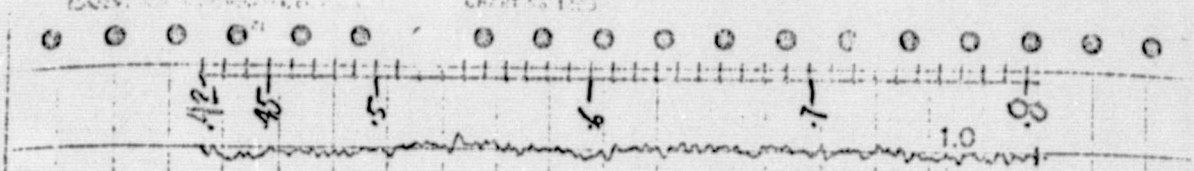


0.9

0.8

DISTILLED H2O
FROM FAUCET
6-14-73

0.7

0.6

0.5

100% FULL SCALE

0.4

FIG A26

DATE 6-14-73 TIME 8:54

PROJECT EECT 211 SAMPLE DISTILLED H20

RANGE 4200-8000 ANGLE 0

SCAN RATE 25Å/SEC. PERIOD 5"

SUT CONTROL 20 OPERATOR L.P.

0.3

0.2

PREPARED BY:

0.1

LABORATORY SIGNATURE ACQUISITION SYSTEM
DATA APPLICATIONS & PHYSICS BRANCH, EOD
NASA, LYNDON B. JOHNSON SPACE CENTER
HOUSTON, TEXAS

0.0

REPRODUCIBILITY OF THE
ORIGINAL PAGE IS POOR

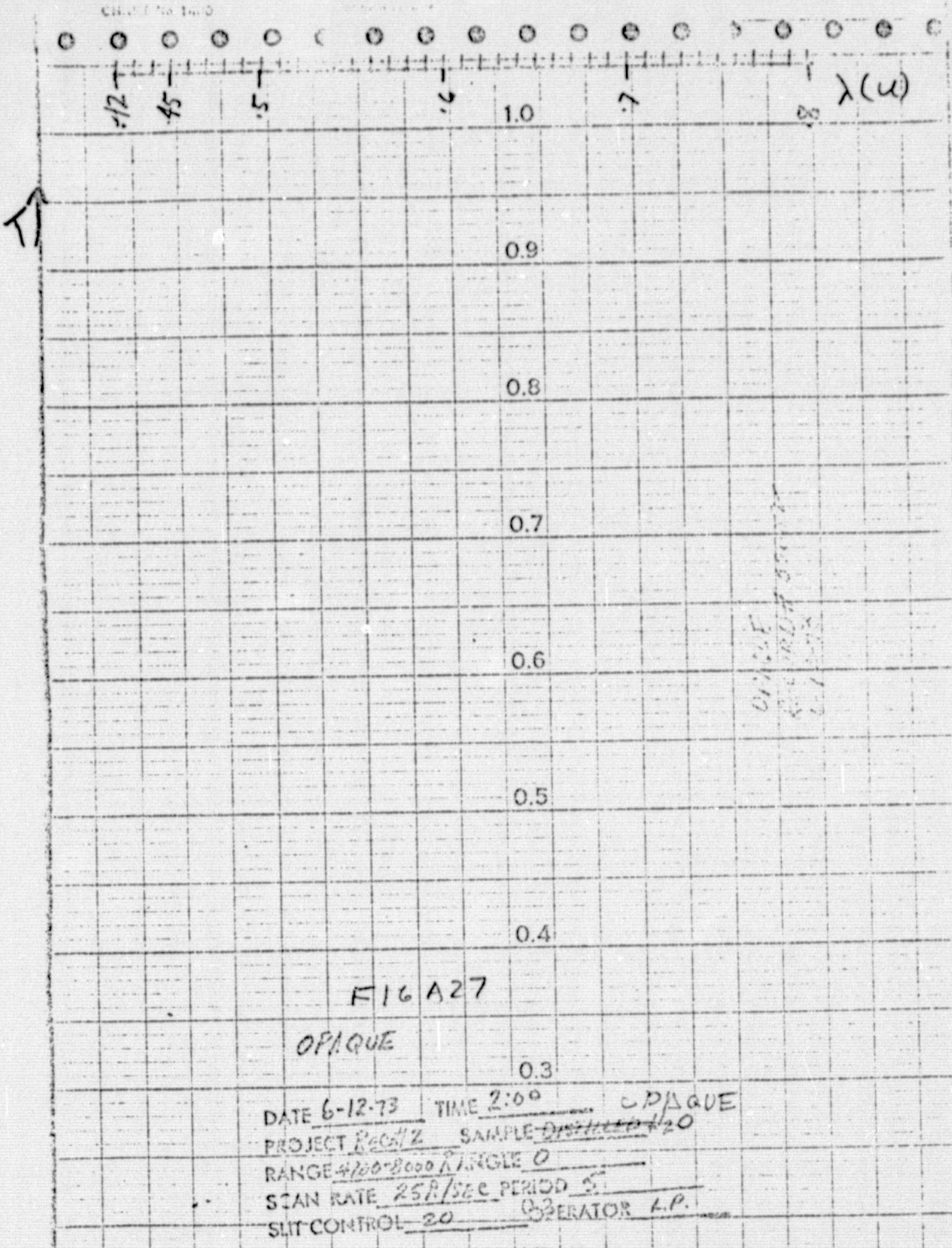


FIG A27

OPAQUE

DATE 6-12-73 TIME 2:00 OPAQUE

PROJECT Beach SAMPLE ~~Distilled H2O~~ H2O

RANGE 4000-8000 ANGLE 0

SCAN RATE 25A/SEC PERIOD 2

SLIT CONTROL 20 OPERATOR L.P.

PREPARED BY:

LABORATORY SIGNATURE ACQUISITION SYSTEM
DATA APPLICATIONS & PHYSICS BRANCH, EOD
NASA, LYNDON B. JOHNSON SPACE CENTER
HOUSTON, TEXAS

The results of mission 4 are given in Tables III and IV and in Figures B1 through B9. This mission was conducted on 9/16/73 approximately 120nm off the coast of Port O'Connor, Texas. Table III gives the position coordinates and time associated with each site. Table IV gives the measured values of chlorophyll concentration, turbidity, and water temperature which were found at each site.

As is shown in Table IV, the values of chlorophyll concentration were in the range of 0.16 to 0.48 $mg/m^3$ for the more distant sites 1 through 4, and a value as high as 1.53 $mg/m^3$ was found at site 5 which was measured about 35 nm out of Port O'Connor on the return trip. The values of turbidity found were in the range of 0.15 to 0.50 JTU. The range of ocean temperatures measured varied from 28.6°C to 29.4°C.

A comparison of the chlorophyll and turbidity levels found in the offshore waters of mission 4 (Table IV) with those found in the coastal and bay waters of mission 2 (Table II) indicates that the levels of chlorophyll and turbidity occuring in the offshore waters of the Gulf of Mexico are between one and two orders of magnitude lower than those found in the coastal waters. Also, it may be observed from Table IV, that there is no evident correlation of turbidity and chlorophyll values for the offshore regions as was found in the coastal regions.

TABLE III

SITE NUMBER, LATITUDE, LONGITUDE AND TIME FOR GROUND TRUTH DATA COLLECTION ON SEPTEMBER 16, 1973, IN THE VICINITY OF 120 nm OFF THE COAST OF PORT O'CONNOR, TX

| SITE | LATITUDE | LONGITUDE | TIME |
|---|---|---|---|
| 1 | 27°15' | 94°35' | 8.10 |
| 2 | 27°10' | 94°41' | 10.10 |
| 3 | 27°09' | 94°42' | 10.42 |
| 4 | 27°19' | 94°54' | 12.20 |
| 5 | 28°04' | 95°52' | 16.50 |

TABLE IV

TURBIDITY, CHLOROPHYLL, AND TEMPERATURE OF OCEAN GROUND TRUTH SITES ON SEPTEMBER 16, 1973, IN THE VICINITY OF 120 nm OFF THE COAST OF PORT O'CONNOR, TX

| SITE | TURBIDITY (JTU) | CHLOROPHYLL ($mg/m^3$) | TEMPERATURE ($^oK$) |
|---|---|---|---|
| 1 | 0.47 | 0.16 | 28.6 |
| 2 | 0.50 | 0.36 | |
| 3 | 0.15 | 0.48 | 29.3 |
| 4 | 0.32 | 0.24 | 29.4 |
| 5 | 0.17 | 1.53 | 29.3 |

Spectral transmission curves of the water samples which were collected during mission 4 are shown in Figures B1 through B9. For these laboratory measurements, the total transmission of the water samples were measured rather than making a ratio measurement as was done previously. The spectrum of distilled water is shown in Figure B1 for comparison purposes. As is shown in these figures, the molecular absorption spectrum of water dominates the overall spectrum with relatively high transmission in the visible portion of the spectrum, 4000 to 6500A°, and strong absorption features in the near infrared located near 7600A°, 9800A°, and beyond 11,500A°. For most sites, two water samples were taken and the spectral curves for different samples from the same site generally show agreement to within 5%. A spectrum of a water sample which contained kelp is shown in Figure B6. As may be seen from this figure, the spectrum is dominated by strong absorption in the blue and green portions of the spectrum.

A problem encountered in making laboratory analyses of water samples which contain living organisms is the time delay between acquiring the water samples and performing the laboratory analyses. In the case of the spectral analsis which we performed, this time delay was between one and two weeks. In order to preserve the water samples, they were refrigerated during the return trip and then frozen until the laboratory measurements could be started. It is likely, however, that changes

Figures B1 through B9

The transmission of a 10 cm sample of ocean water as a function of wavelength for the spectral region from 4000 to 10,000 A° including effects of cell transmittance.

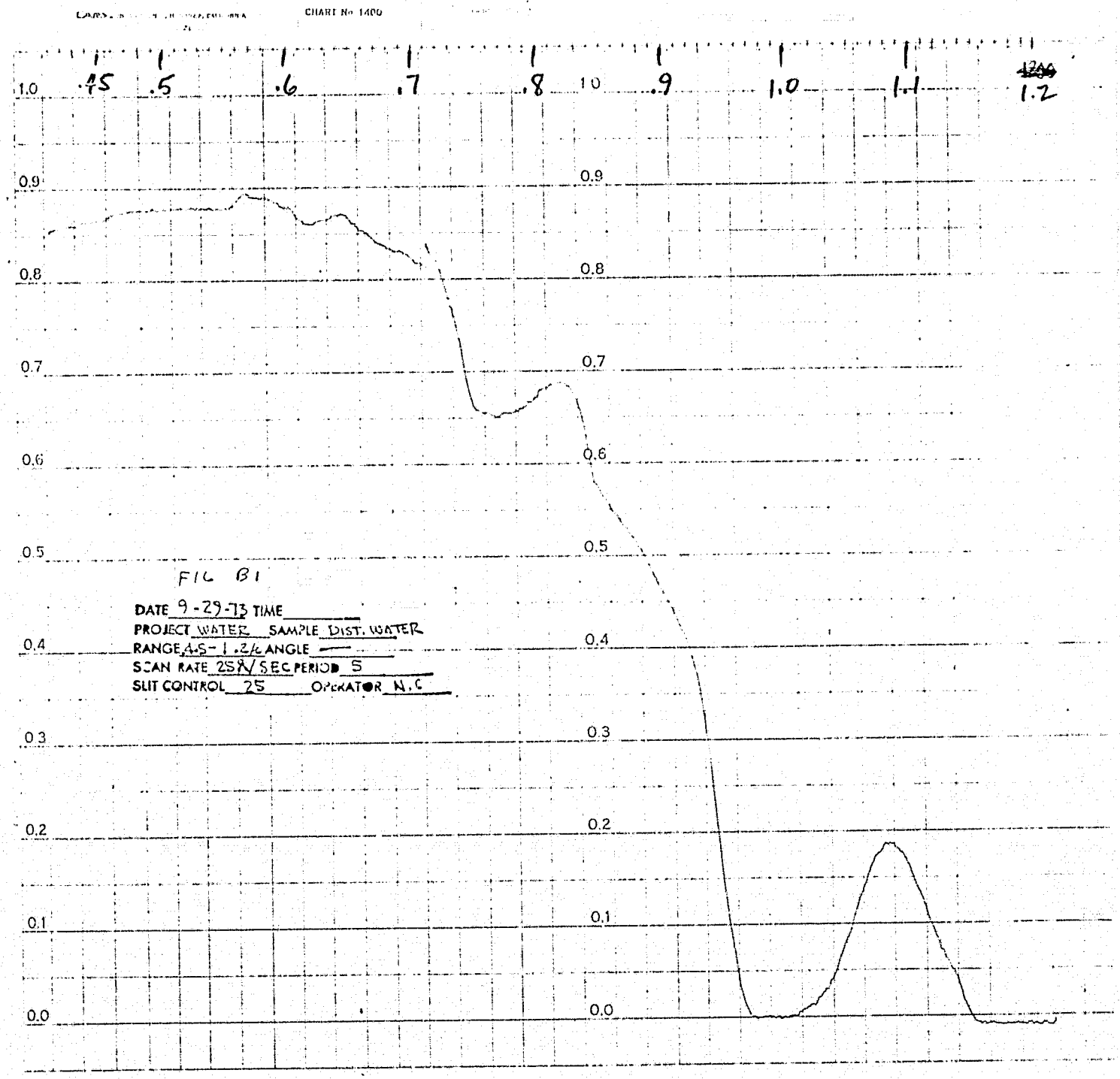


REPRODUCIBILITY OF THE
ORIGINAL PAGE IS POOR

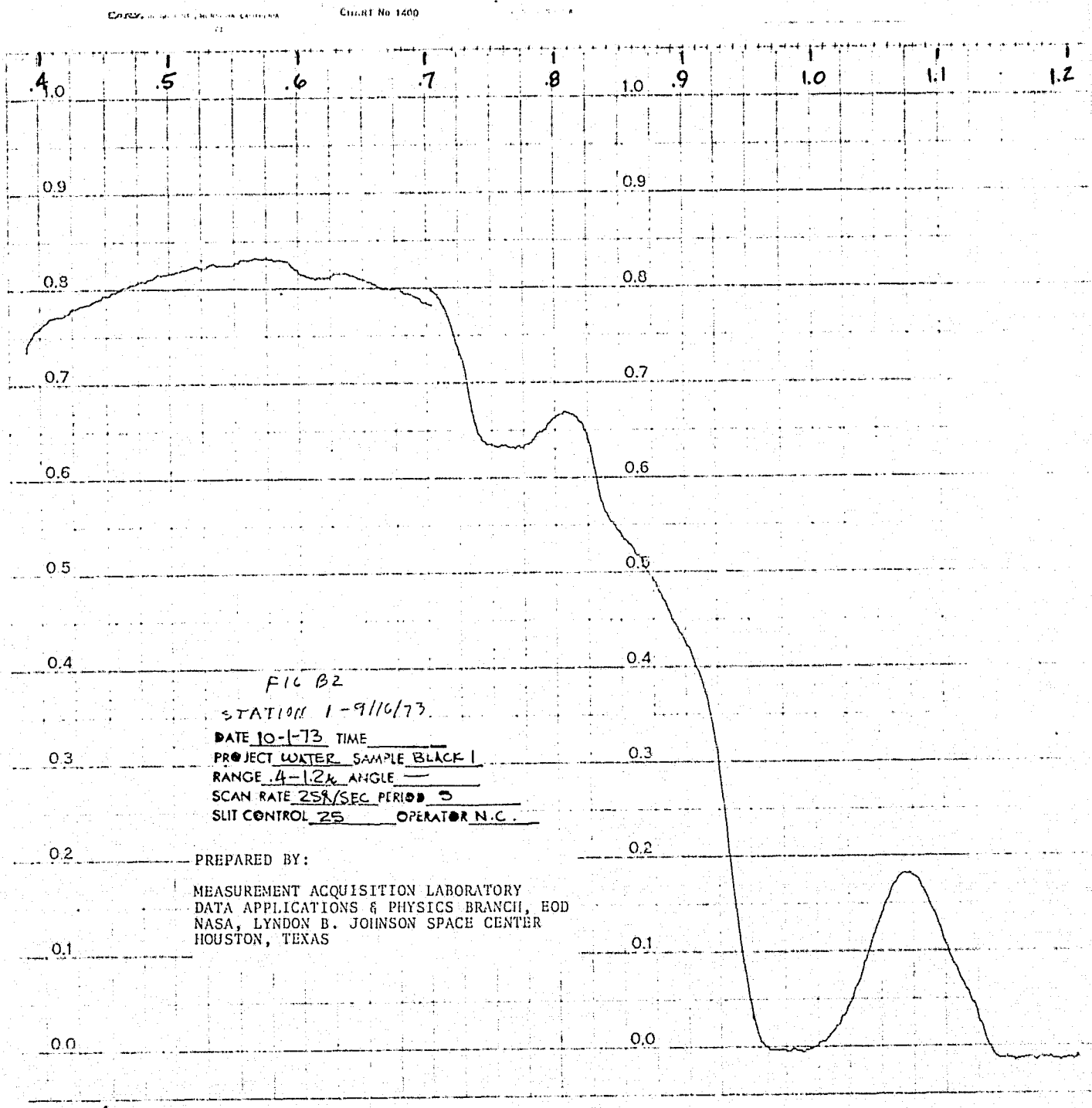
.4
.5
.6
.7
.8
1.0
.9
1.0
1.1
1.2
0.9
0.8
0.7
0.6
0.5
0.4
0.3
0.2
0.1
0.0
FIG B2
STATION 1-9/10/73.
DATE 10-1-73 TIME
PROJECT WATER SAMPLE BLACK 1
RANGE .4-1.2μ ANGLE —
SCAN RATE 25R/SEC PERIOD 5
SLIT CONTROL 25 OPERATOR N.C.
PREPARED BY:
MEASUREMENT ACQUISITION LABORATORY
DATA APPLICATIONS & PHYSICS BRANCH, EOD
NASA, LYNDON B. JOHNSON SPACE CENTER
HOUSTON, TEXAS

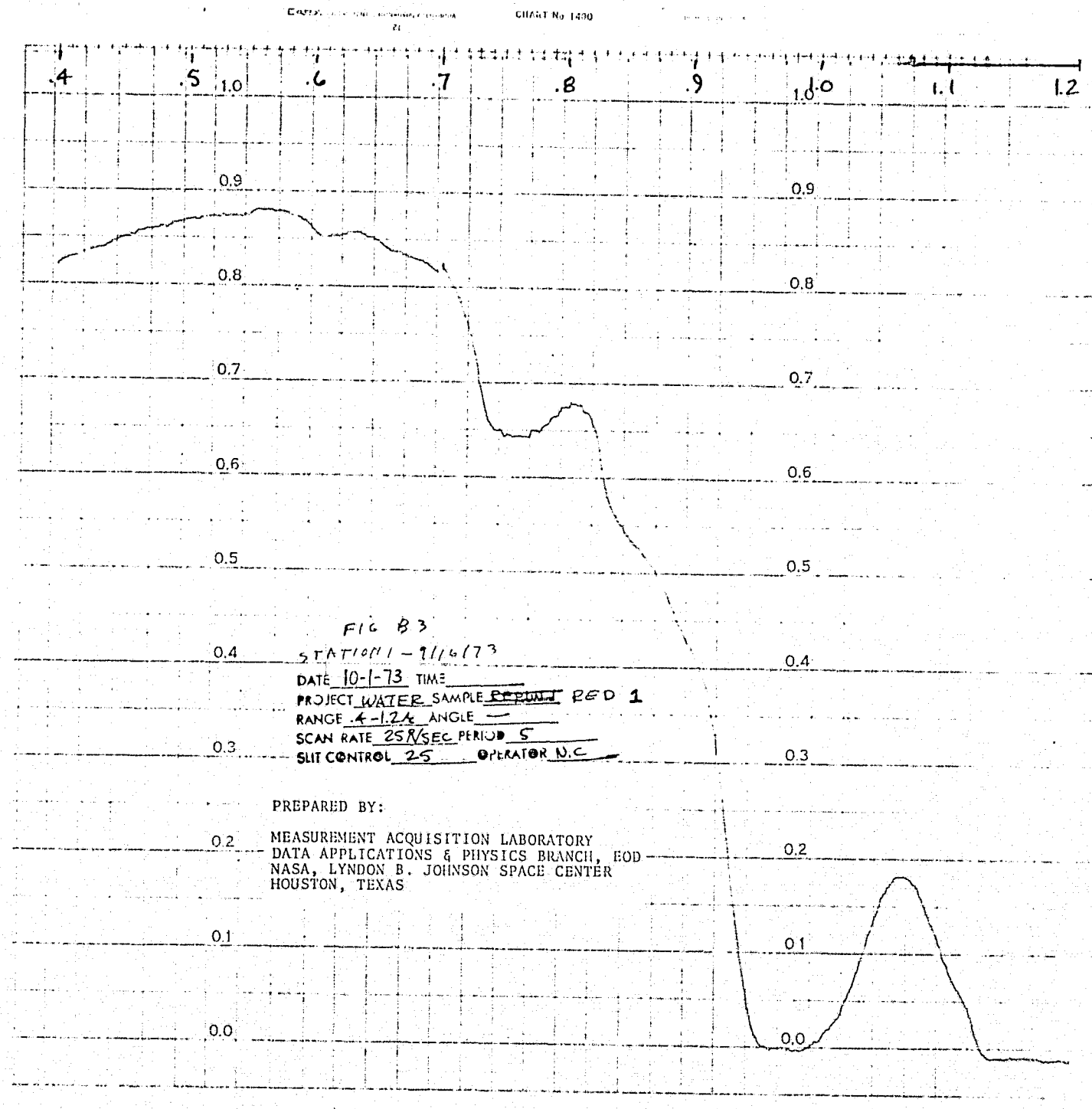
CHART No. 1400
.4
.5
1.0
.6
.7
.8
.9
1.0
1.1
1.2
0.9
0.8
0.7
0.6
0.5
0.4
0.3
0.2
0.1
0.0
FIG B3
STATION 1 - 9/16/73
DATE 10-1-73 TIME
PROJECT WATER SAMPLE REFLUX RED 1
RANGE .4-1.2μ ANGLE —
SCAN RATE 25R/SEC PERIOD 5
SLIT CONTROL 25 OPERATOR N.C
PREPARED BY:
MEASUREMENT ACQUISITION LABORATORY
DATA APPLICATIONS & PHYSICS BRANCH, EOD
NASA, LYNDON B. JOHNSON SPACE CENTER
HOUSTON, TEXAS

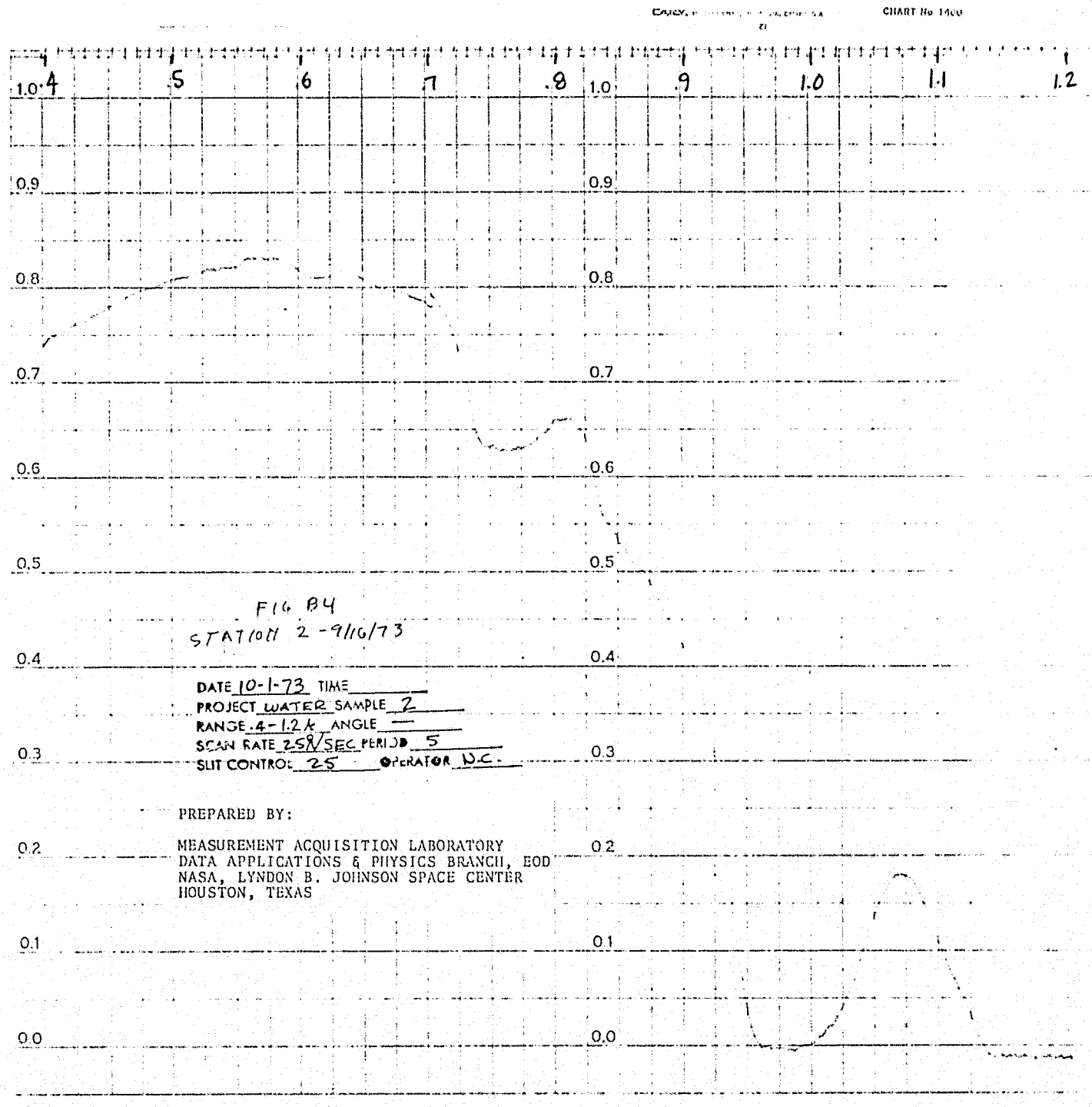
CHART No 1400
1.0 .4 .5 .6 .7 .8 1.0 .9 1.0 1.1 1.2
0.9
0.8
0.7
0.6
0.5
0.4
0.3
0.2
0.1
0.0
FIG B4
STATION 2 - 9/16/73
DATE 10-1-73 TIME
PROJECT WATER SAMPLE 2
RANGE .4-1.2 μ ANGLE —
SCAN RATE 25 SEC PERIOD 5
SLIT CONTROL 25 OPERATOR D.C.
PREPARED BY:
MEASUREMENT ACQUISITION LABORATORY
DATA APPLICATIONS & PHYSICS BRANCH, EOD
NASA, LYNDON B. JOHNSON SPACE CENTER
HOUSTON, TEXAS

CARY CHART No. 1400

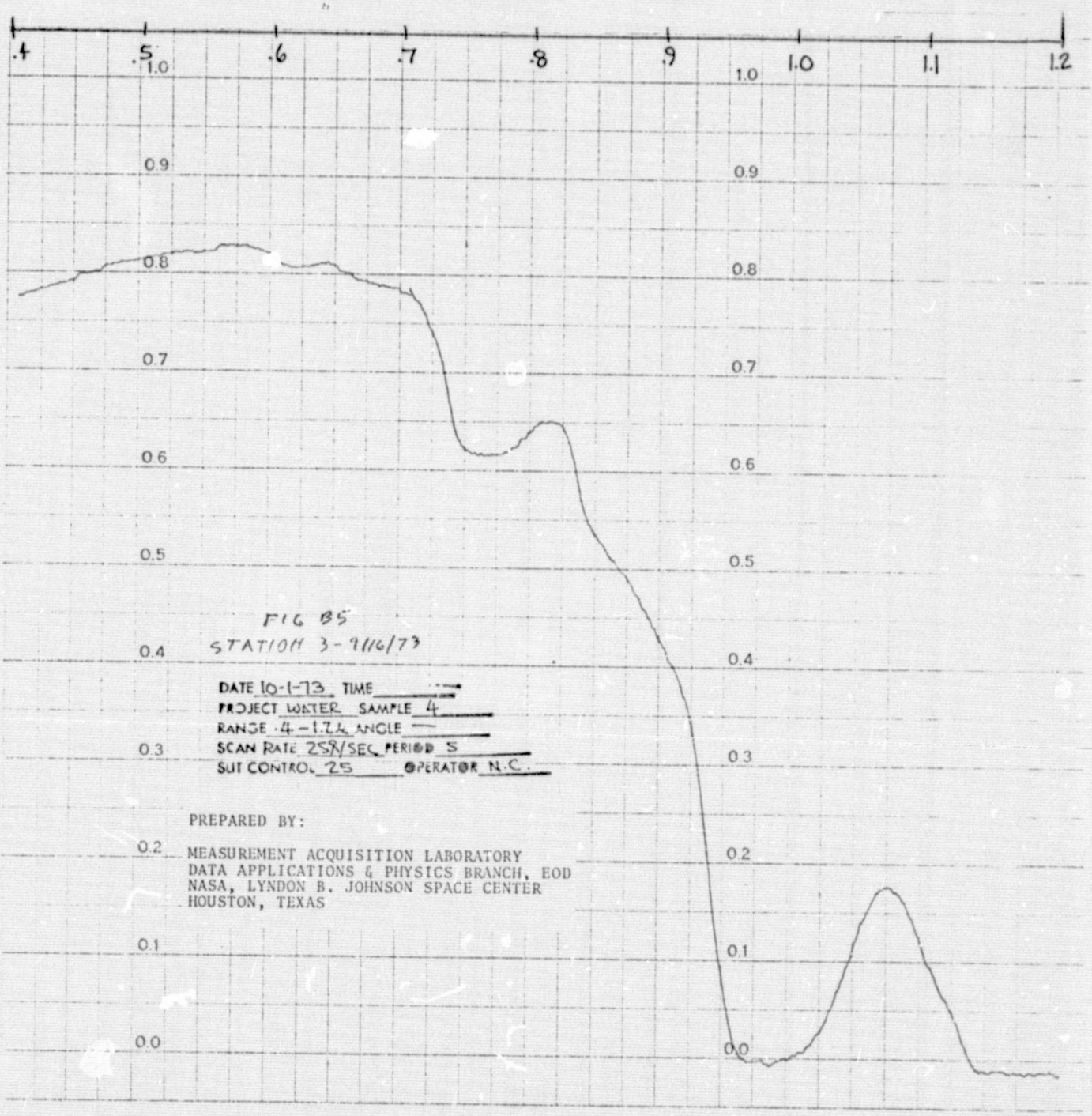


FIG B5
STATION 3 - 9/16/73

DATE 10-1-73 TIME
PROJECT WATER SAMPLE 4
RANGE .4 - 1.2 ANGLE —
SCAN RATE 2SS/SEC PERIOD 5
SUT CONTROL 25 OPERATOR N.C.

PREPARED BY:

MEASUREMENT ACQUISITION LABORATORY
DATA APPLICATIONS & PHYSICS BRANCH, EOD
NASA, LYNDON B. JOHNSON SPACE CENTER
HOUSTON, TEXAS



REPRODUCIBILITY OF THE
ORIGINAL PAGE IS POOR

1400

EARTH

.4 .5 1.0 .6 .7 .8 .9 1.0 1.1 1.2

0.9 0.9

FIG BG

0.8 STATION 3 - 9/16/73 0.8
KELP IN SAMPLE
DATE 10-1-73 TIME
PROJECT WATER SAMPLE 5
RANGE .4-1.2 μ ANGLE —
SCAN RATE 25Å/SEC PERIOD 5
SLIT CONTROL 25 OPERATOR

0.7 0.7

PREPARED BY:

0.6 MEASUREMENT ACQUISITION LABORATORY 0.6
DATA APPLICATIONS & PHYSICS BRANCH, EOD
NASA, LYNDON B. JOHNSON SPACE CENTER
HOUSTON, TEXAS

0.5 0.5

0.4 0.4

0.3 0.3

0.2 0.2

0.1 0.1

0.0 0.0

92

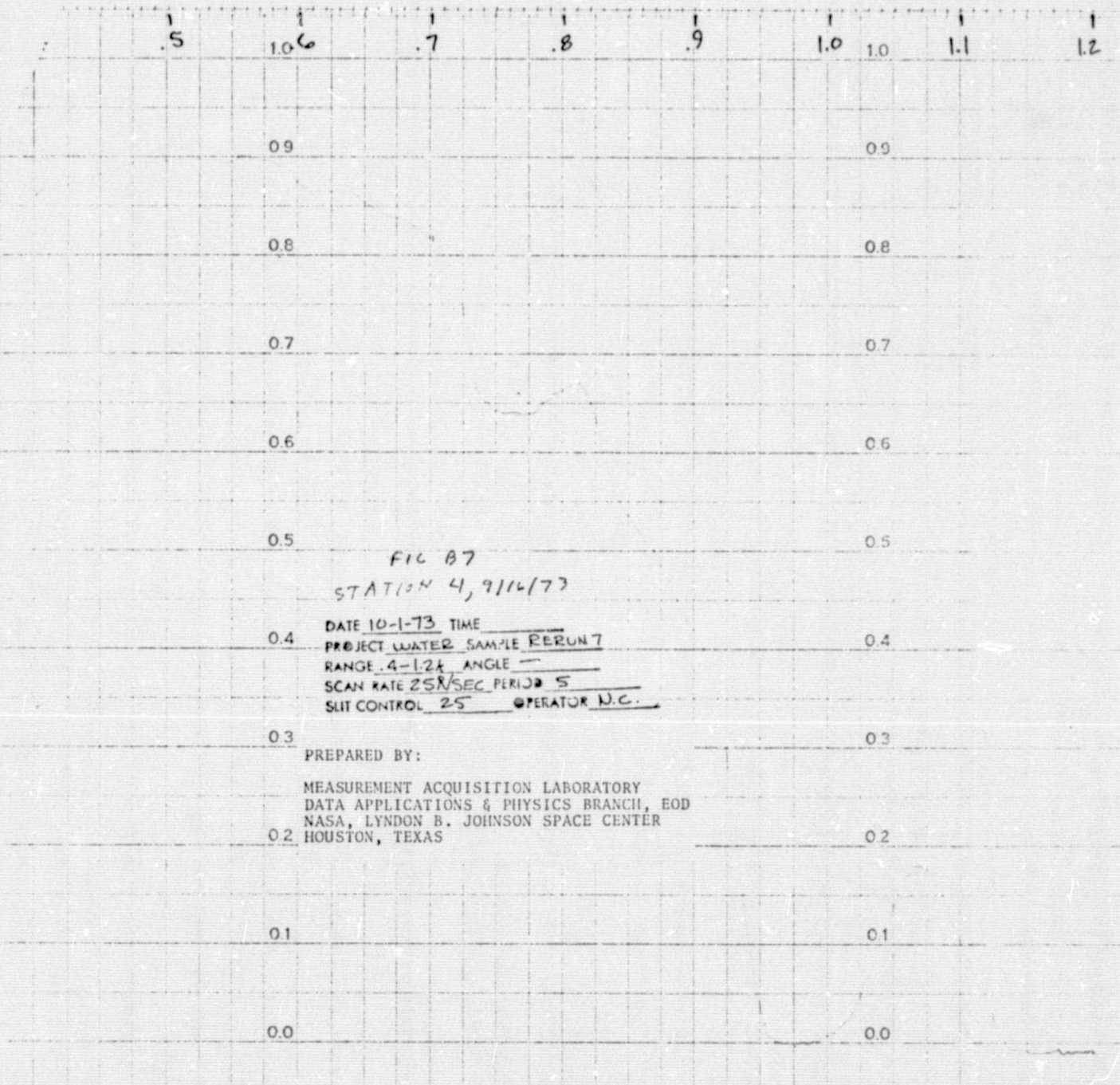


25

ORIGINAL PAGE IS
OF POOR QUALITY

CAREY CHART No 1409

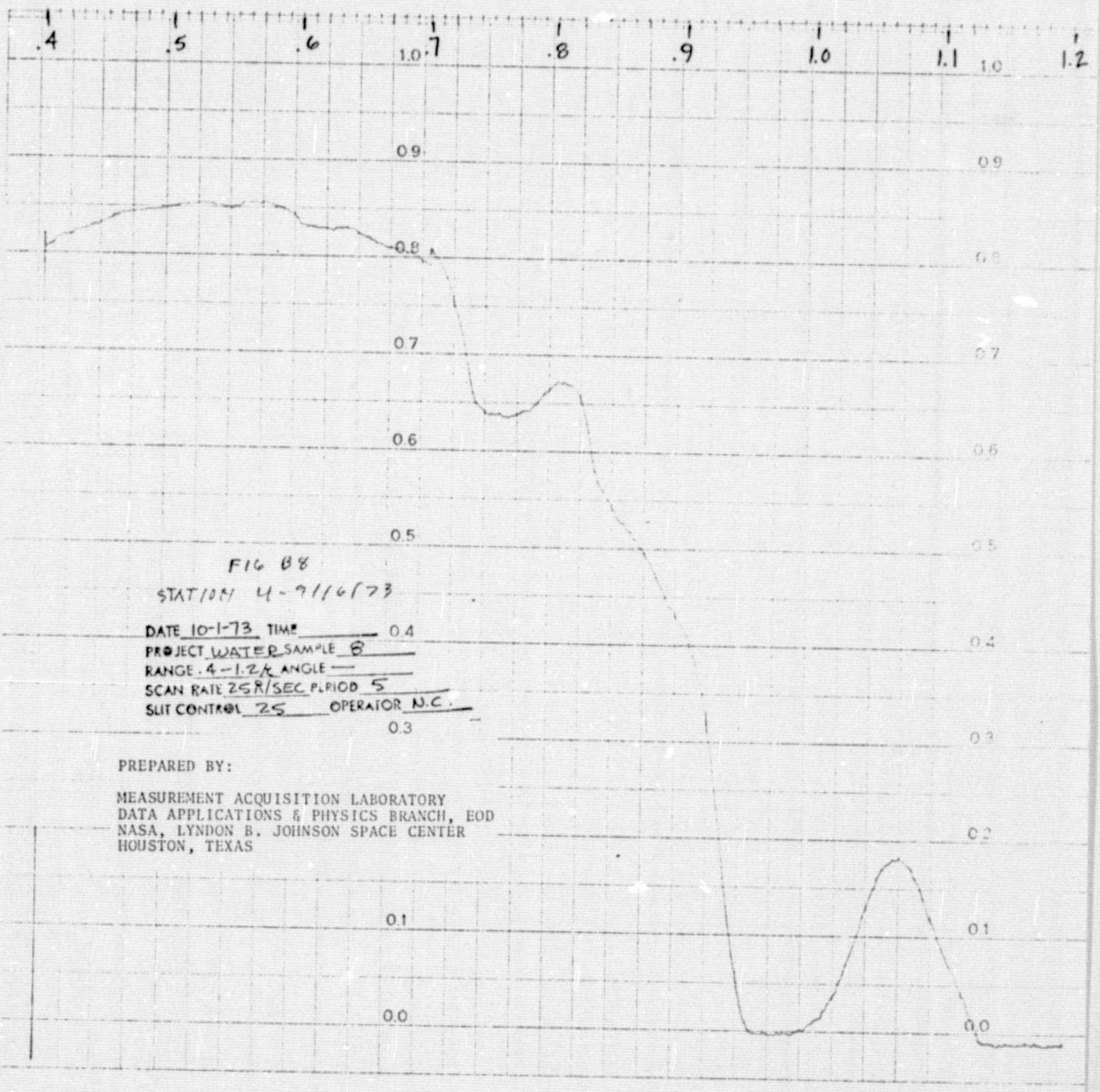


FIG B8

STATION 4-9/16/73

DATE 10-1-73 TIME _____

PROJECT WATER SAMPLE B

RANGE .4-1.2μ ANGLE —

SCAN RATE 25R/SEC PERIOD 5

SLIT CONTROL 25 OPERATOR N.C.

PREPARED BY:

MEASUREMENT ACQUISITION LABORATORY
DATA APPLICATIONS & PHYSICS BRANCH, EOD
NASA, LYNDON B. JOHNSON SPACE CENTER
HOUSTON, TEXAS

CHART No. 1400

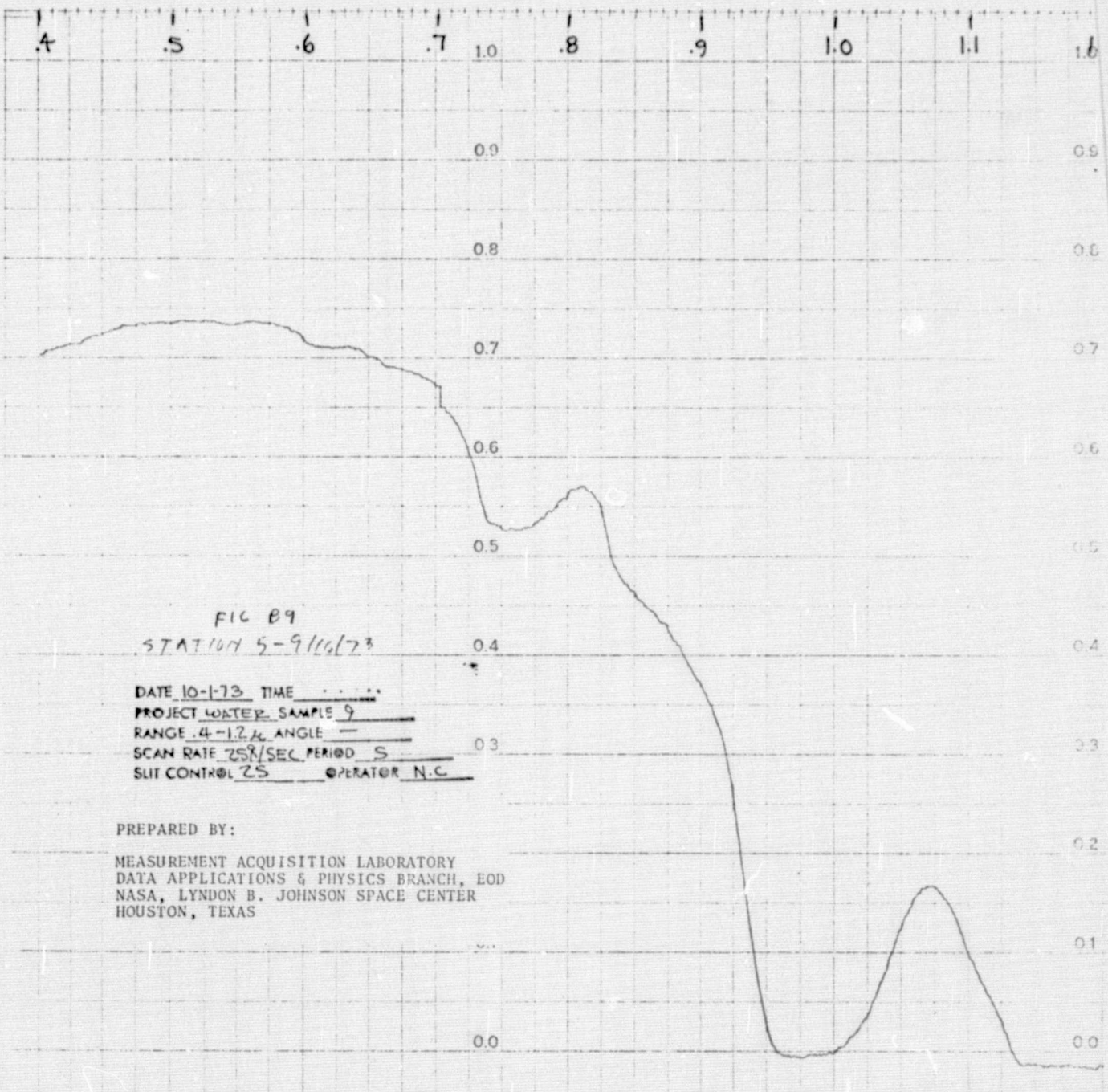


FIG 89

STATION 5-9/16/73

DATE 10-1-73 TIME . . . .

PROJECT WATER SAMPLE 9

RANGE .4-1.2μ ANGLE —

SCAN RATE 25R/SEC PERIOD 5

SLIT CONTROL 25 OPERATOR N.C

PREPARED BY:

MEASUREMENT ACQUISITION LABORATORY
DATA APPLICATIONS & PHYSICS BRANCH, EOD
NASA, LYNDON B. JOHNSON SPACE CENTER
HOUSTON, TEXAS



REPRODUCIBILITY OF THE
ORIGINAL PAGE IS POOR

took place in the biological composition of the water samples during the holding period and thus the measured spectral transmitances are not the same as would have been observed if the measurements had been made in situ.

A considerable effort was made during the course of this investigation to develop a technique for measuring the scattering properties of the water samples. In order to perform these measurements, a Science Spectrum Light Scattering Photometer was rented from the manufacturer. The instrument was capable of making qualitative measurements of the shape of the scattering properties of liquid samples over the angular range from approximately 1 to 170°. A number of difficulties were encountered, however, in attempts to obtain quantitative data. These problems were in the areas of instrument noise which generated large spurious peaks in the scattering measurements; highly nonlinear amplification electronics which required the development of a new calibration technique in order to compensate for this effect; and, spurious scattering which was caused by the introduction of neutral density filters which were needed to attenuate the intense signal which occurs for small scattering angles. The primary instrument problems were fixed and calibration techniques for using the light scattering photometer were developed over the period from August to December, 1973. However, by the time the photometer could be put into operation, the

water samples which had been acquired over the course of the missions had deteriorated.

## CONCLUSIONS

High values of chlorophyll and turbidity were measured in the vicinity of Matagorda Bay, Texas, and the associated offshore coastal waters. Values of chlorophyll were found to be in the range of 1.0 to 14.5 $mg/m^3$ and the values of turbidity were in the range from 0.9 to 25.0 JTU. A correlation coefficient was calculated for the chlorophyll and turbidity data which yielded a value of 0.68. This indicates that the levels of chlorophyll and turbidity were correlated at a confidence level of greater than 99% for the bay and near coastal data. This result, if it is generally characteristic of coastalregions, would have important implications for studies concerned with the remote sensing of chlorophyll in these regions. It may be noted that high levels of turbidity can be identified easily from remote sensing data. Therefore, if a relationship between turbidity and chlorophyll exists such as was found in our data, then the presence of high turbidity levels in remote sensing data could be used to infer the presence of correspondingly high values of chlorophyll.

Measured values of chlorophyll and turbidity were also obtained for the offshore region approximately 120 nm off

the coast of Port O'Connor. For this distant offshore region, the values of chlorophyll were in range from 0.16 to 0.48 $mg/m^3$ and the values of turbidity were in the range from 0.15 to 0.50 JTU. For the relatively low values of chlorophyll and turbidity occuring in these offshore waters, there was no significant correlation between the values of chlorophyll and turbidity.
For the offshore area and also for the coastal data previously discussed, sea surface temperatures were measured and found to lie within a narrow ranges of less than $2^{o}C$. No important correlation was found between sea surface temperature and chlorophyll.